8-3-2017

Quantifying Forearm Soft Tissue Motion and Shock Attenuation following Hand Impacts Consistent with Forward Falls using Massless Skin Surface Markers

Danielle Linda Gyemi
University of Windsor

Quantifying Forearm Soft Tissue Motion and Shock Attenuation following Hand Impacts
Consistent with Forward Falls using Massless Skin Surface Markers

By

Danielle Gyemi

A Thesis
Submitted to the Faculty of Graduate Studies
through the Department of Kinesiology
in Partial Fulfillment of the Requirements for
the Degree of Master of Human Kinetics at the
University of Windsor

Windsor, Ontario, Canada

2017

Quantifying Forearm Soft Tissue Motion and Shock Attenuation following Hand Impacts
Consistent with Forward Falls using Massless Skin Surface Markers

By

Danielle Gyemi

APPROVED BY:

_____

W. Altenhof

Department of Mechanical, Automotive and Materials Engineering

_____

P. van Wyk

Department of Kinesiology

_____

D. Andrews, Advisor

Department of Kinesiology

June 15, 2017

DECLARATION OF ORIGINALITY

I hereby certify that I am the sole author of this thesis and that no part of this thesis has been published or submitted for publication.

I certify that, to the best of my knowledge, my thesis does not infringe upon anyone's copyright nor violate any proprietary rights and that any ideas, techniques, quotations, or any other material from the work of other people included in my thesis, published or otherwise, are fully acknowledged in accordance with the standard referencing practices. Furthermore, to the extent that I have included copyrighted material that surpasses the bounds of fair dealing within the meaning of the Canada Copyright Act, I certify that I have obtained a written permission from the copyright owner(s) to include such material(s) in my thesis and have included copies of such copyright clearances to my appendix.

I declare that this is a true copy of my thesis, including any final revisions, as approved by my thesis committee and the Graduate Studies office, and that this thesis has not been submitted for a higher degree to any other University or Institution.

ABSTRACT

The purpose of this thesis was twofold: 1) quantify planar (2D) displacement and velocity of, and the amount of shock attenuated by, the forearm soft tissues following a forward fall impact; and 2) compare two massless skin surface marker designs with different uniformity and visual contrast (i.e., single layer, uniform (SLU) design; stacked, non-uniform (SNU) design) in terms of how well they can be tracked over varying skin pigmentation using automated motion capture software. Simulated forward fall impacts were performed by two groups of participants (skin pigmentation: light – 9F, 8M; dark – 9F, 6M) using a torso-release apparatus, in which a high speed camera (5000 f/s) captured planar motion of the right forearm. Automated motion tracking software (ProAnalyst®) was used to quantify displacement, velocity, and shock attenuation capacity of the forearm soft tissue from manually digitized markers. Overall, the greatest mean peak soft tissue displacement (1.47 cm) and velocity (112.8 cm/s) occurred in the distal direction in proximal regions of the forearm where more soft tissue is distributed. Soft tissue displacement and velocity exhibited similar trends, increasing from distal to proximal regions of the forearm, while impact shock accelerations were not attenuated in the forearm, but instead increased by 76%. Apart from proximal rebound distance, soft tissue kinematics between females and males did not significantly differ ($p > 0.05$). Conversely, the effects of specific tissue masses (i.e., bone mineral content, fat mass, lean mass, and wobbling mass) on tissue kinematics varied between the sexes. Significant differences were found between marker designs for displacement, rebound distance, and velocity ($p \leq 0.05$), wherein the SLU design consistently produced higher values than the SNU design.

DEDICATION

To each and every person who has made a positive impact on my life, no matter how big

or small.

ACKNOWLEDGEMENTS

First and foremost, I would like to express my sincerest gratitude to my Master's thesis advisor, Dr. Dave Andrews. Your ability to bring out the best in your students and help foster their potential for success, even at times when they may doubt it, is a quality I truly admire. I am very thankful to have had the opportunity to work with and learn from you over the past couple years and cannot tell you how much I have come to appreciate your unparalleled guidance and support.

To my committee members, Dr. William Altenhof and Dr. Paula van Wyk, thank you for the time and resources you have invested towards the preparation, execution, and completion of this thesis. Your insights and advice during this process have been invaluable and I hold both of you in the highest regard.

A special thank you to Don Clarke, without whom this thesis project would not have been possible. Your willingness to not only assist with numerous aspects of this study, but also take the extra time to entertain my curiosity and answer my questions, no matter how small or seemingly obvious, is greatly appreciated.

Thank you to the past and present faculty and staff in the Department of Kinesiology for their kindness and support throughout my graduate degree, as well as my fellow grad students and lab mates for listening to my frustrations and always offering encouragement to persevere through many challenging and stressful times. You have all contributed to making this experience an enjoyable one.

To my each of my friends who lent a helping hand during the many trials and tribulations of my thesis project, regardless of the extent of the efforts, I am fortunate to be surrounded by such generous and caring people.

Finally, I wish to thank my family, including my parents and sisters, for their unwavering love and support throughout my life.

TABLE OF CONTENTS

LIST OF TABLES

LIST OF FIGURES

LIST OF APPENDICES

LIST OF ABBREVIATIONS

BMC – bone mineral content

CT – computed tomography

DIC – digital image correlation

FM – fat mass

ISO – International Organization for Standardization

LEDs – light emitting diodes

LM – lean mass

MRI – magnetic resonance imaging

PULARIS – Propelled Upper Limb fall ARrest Impact System

SLU – single layer, uniform

SNU – stacked, non-uniform

STA – soft tissue artifact

UV – ultraviolet

WM – wobbling mass

GLOSSARY

Anisotropic – Having a physical property that is directionally dependent and exhibits different values when measured in different directions.

Anterior (displacement) – The downward motion of the forearm soft tissue perpendicular to the long axis of the forearm following forward fall impact.

Attenuation – Weakening or reduction in force, intensity, or value that occurs as a result of absorption, spreading, or distance.

BMC (bone mineral content) – The amount of bone material or mineral in a specific bone site (measured in grams).

Calibration – The process of checking the experimental readings of a device or instrument against a known standard to determine the correctness of its quantitative measurements.

Contrast – The ratio to which adjacent areas of an image differ in brightness.

Deformation – The action or process of changing in shape through the application of mechanical loads.

Digital Image Correlation (DIC) – A non-contact optical technique that employs tracking and image registration practices to acquire 2D and/or 3D measurements of deformation, displacement, and strain on the surface of a specimen.

Displacement – A vector value that refers to the change in position of a moving body from an initial to final position in a given direction.

Displacement Field – A region in a body for which the displacement of all points is defined.

Distal (**displacement**) – The motion of the forearm soft tissue towards the wrist joint following forward fall impact.

Distal Upper Extremity – The furthermost section of the upper extremity relative to the trunk, consisting of the forearm and hand.

Fall – (of a person) downward movement from a loss of balance, typically rapidly and freely without control, resulting in impact with the ground or other lower level.

FM (fat mass) – The total mass of the adipose tissue in the body or segment.

Impact – A transient event in which a high force or shock is applied when two or more bodies collide.

In-plane motion – The motion of a body such that all its points move within (parallel to) some fixed plane.

In Vitro – The study of biological tissues outside of their living biological context.

In Vivo – The study of biological tissues within a living body.

LM (lean mass) – The total mass of all body tissues that does not contain fat (i.e., muscle).

Out-of-plane motion – The motion of a body such that its points move in additional planes outside of the fixed plane of motion.

Pendulum – A body suspended from a fixed point that has the ability to swing freely back and forth under the action of gravity.

Photogrammetry – The science of making measurements from photographs; high-speed imaging is often employed to detect, measure, and record the exact positions of surface reference points on any moving object to quantify 2D and 3D motion fields.

Posterior (displacement) – The upward motion of the forearm soft tissue perpendicular to the long axis of the forearm following forward fall impact.

Proximal (**displacement**) – The motion of the forearm soft tissue towards the elbow joint following forward fall impact.

Shape Permutations – One of several possible variations in shape.

Shock (mechanical) – A sudden, transient acceleration of a system caused by an abrupt change in force application, such as an impact event.

Shock attenuation – A reduction in the amplitude of the impact force that occurs as the shock wave propagates through the tissues of the body.

Shock wave – The propagation of a stress wave through a medium such as the soft tissues of the human body.

Soft Tissue – A generic term for tissues that are not bone that connect, support, or surround various structures and organs of the body. This includes muscle, fat, skin, tendons, blood vessels, etc.

Spatial Resolution – The capacity of an imaging system to distinguish between small details of adjacent points; it is dependent on the number of independent pixel values available per unit length.

Stereo-photogrammetry – An extension of photogrammetry that uses the process of triangulation to estimate 3D points on the surface of an object using measurements made in two or more photographic images taken from different positions.

Strain – A measure of deformation that represents the displacement between particles in a deformed body relative to the same particles in a reference (undeformed) body.

Strain Field – A region in a body for which the strain of all points is defined.

Subset – A defined set consisting of elements within a larger, inclusive set.

Triangulation – The process of determining the location of a point by measuring the angles relative to its position from known reference points at either end of a fixed baseline.

Viscoelastic – Having a combination of both viscous and elastic properties when undergoing deformation.

WM (wobbling mass) – The non-rigid tissues of the body (lean and fat masses) that are attached to underlying bony structures.

1. INTRODUCTION

A common reaction to a fall resulting from a loss of balance during recreational and daily activities is to land on the hand of an outstretched arm to protect your head and trunk from injury (Hsiao & Robinovitch, 1998; O'Neill et al., 1994). Forces sustained by the distal upper extremity from this type of fall arrest impact have the potential to jeopardize the structural integrity of the wrist, forearm, and elbow joint, leading to severe injuries such as sprains, dislocations, and fractures (Nevitt & Cummings, 1993; Oskam et al., 1998; Palvanen et al., 2000; Sasaki et al., 1999).

Forward falls and direct impacts to the hand and wrist have been highlighted in the literature as being particularly problematic due to the high incidence of upper extremity injury associated with them (Idzikowski et al., 2000; Nevitt & Cummings, 1993; Palvanen et al., 2000; Vellas et al., 1998). Among older adults, Vellas et al. (1998) found that approximately 50% of falls occurred in the forward direction. Of those falls, the hands were the part of the body that were impacted most frequently. Palvanen et al. (2000) found that the majority of elderly patients sustaining a fracture to the upper extremity (i.e., proximal humerus fracture: ~47%; elbow fracture: ~66%; wrist fracture: ~45%) reported that the fall occurred in a forward or forward oblique direction. Seventy six percent of patients with a wrist fracture in this sample reported the main impact to be directed straight to the hand and wrist, a finding which supports previous work by Nevitt and Cummings (1993) for elderly women. In addition, young adults engaged in recreational activities such as snowboarding (Idzikowski et al., 2000) and rollerblading (Mirhadi et al., 2015) are also often subjected to forward falls involving impacts that result in upper extremity injuries. For example, Idzikowski et al. (2000) found that 92%

of all snowboarding upper extremity injuries were due to a fall, with 53.6% occurring in the forward direction.

It has been estimated that the direct medical costs for non-fatal fall-related injuries to the upper extremity among adults aged 65 years and older in the United States in 2000 was approximately $3 billion (Stevens et al., 2006). In Canada, falls were the leading cause of all injury-related hospitalizations (55%) and emergency room visits (30%) in 2010, accounting for $8.7 billion or 34% of the total injury costs that year; this included $6.7 billion and $2 billion in direct and indirect costs, respectively (Parachute, 2015). Considering that the baby boomer population is expected to grow exponentially over the next two decades (Parachute, 2015), and high-risk sporting activities like snowboarding are continuing to rapidly grow in popularity each passing year (Canadian Ski Council, 2014), this raises major concerns for potentially significant increases in healthcare costs associated with forward fall-related injuries. Therefore, given the magnitude of the negative health outcomes linked to forward fall-related injuries and the economic burden that they place on healthcare systems, if the mechanism by which rigid and soft tissues interact to attenuate impact shock as it propagates through the hand and forearm can be identified, improved injury prevention strategies, such as age-specific fall arrest strategies and modified wrist guard designs, may then be realized.

Prior research concerning the injury mechanisms of a fall on the hand of an outstretched arm has focused largely on the in vitro impact response of the distal radius (i.e., bone) (Burkhart et al., 2012a; Muller et al., 2003; Myers et al., 1991), since it is a very common fracture site for both young and older adult populations. Comprising one-sixth of all fractures seen in the emergency department (Bonafede et al., 2013; Kilgore et

al., 2009), distal radius fractures are often due to high-energy trauma from sporting activities and relatively low-energy trauma from accidental falls (Krishnan, 2002). Although these studies demonstrate the capacity of the distal radius to dissipate high levels of mechanical energy from dynamic impact loads, rigid tissues (bone) do not act independently to protect the human body from injury. There is much evidence to support that the response of soft tissues (muscle, fat, skin) relative to bone also plays an important protective role in mitigating the potentially injurious effects of impact through shock attenuation (Cole et al., 2006; Gittoes et al., 2006; Pain & Challis, 2001; Pain & Challis, 2002; Pain & Challis, 2006), despite often being viewed as error (or soft tissue artifact – STA) that needs to be removed from biomechanical analyses (Peters et al., 2010). To date, impact events involving the lower extremity (e.g., running, drop landings) have received the most attention due to the frequency of their occurrence in everyday human movement (Cole et al., 2006; Gittoes et al., 2006; Pain & Challis, 2006). However, Pain and Challis (2002) demonstrated that soft tissue deformation of the forearm following a downward hand striking task could account for approximately 70% of the dissipated energy lost during these impacts.

The contribution of active mechanisms (i.e., muscle activation and joint angle) as well as passive structures (soft and rigid tissue masses) for impact shock attenuation in the body has been well documented for various foot impacts (Chu & Caldwell, 2004; Coventry et al., 2006; Dufek et al., 2009; García-Pérez et al., 2014; Mercer et al., 2003; Mercer et al., 2010; Schinkel-Ivy et al., 2012; Zhang et al., 2005). In contrast, with respect to hand impacts, only the influence of active mechanisms has been examined (Burkhart & Andrews, 2010b; DeGoede & Ashton-Miller, 2002; Pain & Challis, 2002);

3

the role of different tissue masses, such as bone mineral content (BMC), fat mass (FM), lean mass (LM), and wobbling mass (WM), for passive energy dissipation, has yet to be assessed. Following controlled heel impacts with a human pendulum, Schinkel-Ivy et al. (2012) were able to show that increases in absolute leg tissue masses corresponded to decreases in tibial acceleration responses, with LM and BMC having the most significant contributions. Therefore, quantifying soft tissue motion in the distal upper extremity may help identify how the different tissue types, and amounts of specific tissue masses between individuals, influence the motion of soft tissue following a forward fall impact.

Review of the literature has shown that a broad spectrum of motion tracking techniques has been employed to quantify soft tissue motion (predominantly in the lower extremity) for human movement analysis, each with their own set of limitations. Three-dimensional (3D) optoelectronic systems (Fuller et al., 1997; Gao & Zheng, 2008; Wolf & Senesh, 2010) as well as Magnetic Resonance Imaging (MRI) (Akbarshahi et al., 2010; Sangeux et al., 2006) involve the use of complex and expensive equipment that often requires the assistance of a trained professional to operate, whereas radiological methods such as X-ray and video fluoroscopy can expose the participant to potentially harmful radiation (Akbarshahi et al., 2010; Kuo et al., 2011; Sati et al., 1996; Südhoff et al., 2007; Wrbaškić & Dowling, 2007). Consistent with each of these methods is also the requirement for externally mounted devices (e.g., accelerometers, active or passive skin surface markers, etc.) to be attached to the body segment in order to track soft tissue motion; an action that has been found to alter the natural physiological movement of the underlying soft tissue (Leardini et al., 2005; Stefanczyk et al., 2013). Consequently, if soft tissue motion and shock attenuation during an impact event is to be accurately

measured using motion tracking techniques, eliminating the need to affix external devices to the participant is key in order to avoid any non-physiological tissue responses following impact. Photogrammetric motion tracking methods that utilize massless skin surface markers (e.g., paint, marker pens) would thus be a preferred non-contact, non-invasive, and radiology-free measurement tool to document and assess soft tissue motion during dynamic loading.

One such method, digital image correlation (DIC), is a non-contact, optical technique that is used to understand the deformation behavior of a wide range of materials. Traditionally, DIC is used in the field of experimental solid mechanics to assess the mechanical properties of inanimate structural materials (e.g., wood [Betts et al., 2010; Samarasinghe & Kulasiri, 2004], concrete [Choi & Shah, 1997; Shih & Sung, 2013], and metals [Backman et al., 2006; Bewerse et al., 2013]). To date, the use of this method for quantifying soft tissue motion in vivo during human movement analysis is very limited. Instead of using discrete surface markers, DIC works by tracking unique, stochastic details (i.e., random speckle patterns) on the surface of the specimen when in a non-deformed and deformed state to provide full-field measurements of displacement and strain (Sutton et al., 2009). With no mechanical interaction with the specimen required, the capacity of DIC to provide accurate results is directly dependent on the quality of the speckle pattern on the surface of the specimen, as it is the sole carrier of the deformation information (Crammond et al., 2013; Hua et al., 2011; Lecompte et al., 2006; Pan et al., 2010). Therefore, when a suitable textured pattern is not naturally present on the specimen being evaluated, a high-quality artificial speckle pattern must be created in order to obtain valid DIC results.

Unfortunately, the feasibility of successfully implementing DIC for in vivo human soft tissue motion and shock attenuation impact analysis is limited by several factors. Primarily, methodological inconsistencies and insufficient procedural information in the literature regarding speckle pattern application methods (i.e., application tools and strategies) and compositions (i.e., substance(s) applied and background contrast) make it difficult to discern an optimal approach for creating a high-quality speckle pattern on any surface, let alone a surface with physical properties as complex as human skin. In addition, the expense associated with acquiring DIC equipment and software, along with the tools necessary for applying a speckle pattern on human skin, such as complete airbrush kits, is very costly. Time efficiency is also another limitation, as the proper use of DIC requires extensive training, and being able to consistently achieve a desired speckle pattern during specimen preparation has been shown to require a tedious "trial-and-error" process (Betts et al., 2010; Lecompte et al., 2006; Yavari et al., 2013).

A study by Brydges et al. (2015) demonstrated the success of an alternative method in which position and velocity data of leg soft tissue motion following heel impacts (i.e., pendulum, drop landing) could be quantified using a motion capture system with automatic feature tracking capabilities (ProAnalyst®; Xcitex, Cambridge, MA, USA). An appealing element of the marker system presented in this work was the use of massless skin surface markers, wherein a flexible plastic stencil was used to apply a grid of circular black surface markers onto the leg with a permanent black marker pen. Since no supplementary external devices were attached to the body segment, the risk of interfering with the natural physiological impact response of the soft tissue was entirely

removed. Furthermore, compared to more traditional motion capture systems, software systems with the capacity to perform automatic feature tracking, such as ProAnalyst®, are relatively inexpensive and compatible with a variety of camera video formats. More specifically, the use of ProAnalyst® to analyze high-speed camera images has been validated against optical displacement transducers with respect to the measurement of vertical wheel displacements of heavy mining vehicles, illustrating a maximum difference of 4.05% between the two methods (Tonkovich et al., 2012). The adaptability of the system also lends itself to a range of applications, as the number of markers that can be used is specific to the research objectives (with a minimum of one marker needed to measure tissue motion), and thus, can be expanded to investigate soft tissue motion of other body segments (e.g., the distal upper extremity).

Despite the many advantages of using this experimental set-up for recording and tracking soft tissue motion, it is not without its limitations. Position measurements were reported to have good within- and between-measurer reliability; however, velocity measurements were found to be slightly less reliable (Brydges et al., 2015). Although this was shown to have a relatively small impact on the differences between the measured kinematic variables (between-measurer: <0.8 cm for position, <3.7 cm/s for velocity; within-measurer: <0.5 cm for position, <2.6 cm/s for velocity), modifications can be made to improve both the accuracy and reliability of this method. For example, with respect to marker contrast and shape, changes can be made to account for different participant skin pigmentations and enhance the accuracy of automated tracking, respectively.

Therefore, utilizing the research methods conducted by Brydges et al. (2015) to examine the impact response of forearm soft tissue following a forward fall on the hand of an outstretched arm will provide the most authentic insight into how soft tissue motion attenuates impact energy in the upper extremity. Taking into consideration the tissue composition of the distal upper extremity will also better our understanding of the individual role that each tissue mass (e.g., FM, LM, WM, and BMC) plays in dissipating impact shock, which will help drive biomechanical modelling efforts. Additionally, testing the use of a novel massless surface marker design with improved contrast and shape variation on participants of varying skin pigmentation will benefit the automated motion tracking process and broaden the inclusivity of this motion tracking technique.

Therefore, the purposes of this thesis are to:

1) quantify planar (2D) displacement and velocity of, and the amount of shock attenuated by, the soft tissues of the forearm following a forward fall impact;

2) assess if there are differences in soft tissue motion and impact shock attenuation due to sex, or as a function of the region of the forearm measured;

3) identify the relationship between the displacement, velocity, and shock attenuation capacity of the forearm soft tissues and their individual tissue masses (BMC, FM, LM, and WM);

4) determine if a stacked, non-uniform (SNU) marker design (non-uniform, ~0.5 cm diameter black dots overlaid on top of a grid of contrasting ~1 cm diameter white dots; 2 cm inter-marker distance) produces significantly different kinematic results and improves automated marker tracking across different skin

pigmentations compared to the single layer, uniform (SLU) marker design (grid of

uniform, 0.5 cm diameter black dots; 2 cm inter-marker distance) previously

established by Brydges et al. (2015).

1.1. Hypotheses

It is hypothesized that:

1)   it will be possible to quantify planar (2D) displacement and velocity of,

        and the amount of shock attenuated by, the soft tissues of the forearm following a

        forward fall impact through a combination of photogrammetric motion tracking

        techniques and massless skin surface markers;

2a)   males will have greater soft tissue displacements and velocities, and attenuate a

        greater amount of shock following impact than females because, on average,

        males have greater amounts of WM in the arms compared to females (Mazess et

        al., 1990);

2b)   WM in the proximal region of the forearm will demonstrate greater displacement

        than the distal region, and WM in the anterior region will be greater than the

        posterior region, respectively, since greater amounts of WM are distributed

        proximally and anteriorly in the forearm;

3)   the amount of impact shock attenuated by passive soft tissue movement will be

        positively correlated with the absolute magnitude of the estimated forearm tissue

        masses (FM, LM, WM, and BMC), similar to the results found by Schinkel-Ivy et

        al. (2012) for the influence of leg soft tissue composition on tibial acceleration

        responses following impact. Furthermore, magnitudes of FM, LM, and/or WM

will be positively correlated with the displacement and velocity of soft tissue in the proximal-distal direction, but have no significant correlations in the anterior-posterior directions.

4) the SNU marker design will produce similar kinematic results to the SLU marker design for the light skin pigmentation group, but significantly different results for the dark skin pigmentation group. This is because the SNU marker design will improve the automated marker tracking process by 1) adding a localized white background against the black dot marker to provide consistently high contrast for marker detection across all skin pigmentations (especially those individuals with darker skin pigmentations), and 2) using non-uniformly shaped markers to enhance discrete marker recognition and tracking by providing a more unique fingerprint for each marker.

2. REVIEW OF LITERATURE

2.1. Soft Tissue Motion Analysis

2.1.1. Soft Tissue Artifact

In studies of human motion analysis using skin-based systems, the movement of surface markers on the skin relative to the underlying bone that they are intended to represent is a phenomenon commonly referred to as "soft tissue artifact" (STA) (Peters et al., 2010). The occurrence of STA is the result of soft tissue deformation associated with skin movement and inertial effects, especially around the joints (Cappozzo et al., 1996), as well as muscular contractions (Leardini et al., 2005). It has also been shown that the amount of STA observed is dependent on multiple factors, such as differing physical characteristics between individuals (Holden et al., 1997), the location of surface markers on the body (Schwartz et al., 2004), and the nature of the task being performed (Fuller et al., 1997; Leardini et al., 2005; Manal et al., 2003).

Ultimately, STA is viewed as a major source of error in human movement analysis that limits the ability to accurately quantify skeletal system kinematics and detailed joint movements. For example, during a natural cadence walking task, Manal et al. (2003) demonstrated that the movement of bone compared to soft tissue on the proximal tibia had average differences of 7.4, 3.7, and 2.1 mm along the X (medial-lateral), Y (anterior-posterior), and Z (superior-inferior) axes, respectively. Across a variety of tasks (i.e., stationary bicycling, squatting, normal gait, voluntary swing movement), Fuller et al. (1997) observed larger differences overall, in which magnitudes of 20 mm were reached for skeletal pin versus skin mounted marker arrays. In addition,

calculated joint angles were found to have significantly different values from those that were expected due to soft tissue motion. Consequently, many solutions have been proposed in the literature to minimize the error related to STA when analyzing human movement that involve a variety of complex estimation algorithms and skin marker set techniques (e.g., point cluster technique) in an attempt to more accurately model the motion of the underlying bone (Alexander and Andriacchi 2001; Cappello et al., 1997; Cappello et al., 2005; Gao et al., 2007; Soderkvist & Wedin, 1993). However, with regard to human impact analysis, measuring soft tissue motion is critical to understanding the mechanisms by which the complex structure and non-linear, viscoelastic mechanical behaviour of soft tissues work with rigid tissue to prevent injury through impact shock attenuation. Therefore, removing soft tissue motion from biomechanical analyses would eliminate an important contributor to how the human body attenuates shock during impacts (Pain and Challis, 2002).

2.1.2. Stereo-photogrammetry

The combination of stereo-photogrammetry and skin markers is one of the most commonly used measurement methods for 3D motion analysis of human movement (Akbarshahi et al., 2010; Cappozzo et al., 2005; Fuller et al., 1997; Holden et al., 1997; Houck et al., 2004; Leardini et al., 2005; Manal et al., 2003; Stagni et al., 2005). This motion tracking technique utilizes the process of triangulation and photogrammetry to estimate 3D coordinates of specific reference points on the surface of a moving object from measurements based on two or more images taken from different, fixed positions. In order to track soft tissue movement, researchers need only to place skin surface

12

markers along the length of the body segment being analyzed; therefore, making stereo-photogrammetry an appealing alternative without the limitations of other motion tracking techniques, such as the highly invasive nature of intra-cortical pins and percutaneous skeletal trackers, potentially harmful radiological exposure of X-ray and fluoroscopy, and limited static or quasi-static investigations of MRI (Peters et al., 2010).

2.1.2.1. Optoelectronic Systems

Depending on the type of marker that is applied, different stereo-photogrammetry based motion capture systems and software can be used to track and measure soft tissue motion. Optoelectronic (3D) camera systems work by means of light detection, and involve the use of two basic types of systems (Figure 1): active, which use infrared light emitting diodes (LEDs) as markers that actively emit light themselves (Ball, 2011; Fuller et al., 1997; Houck et al., 2004; Scholz, 1989), and passive, which use retro-reflective markers that passively reflect light off their surface (Akbarshahi et al., 2010; Chu et al., 2010; Dufek et al., 2009; Gao & Zheng, 2008; Holden et al., 1997; Manal et al., 2003; Pain & Challis, 2002; Stagni et al., 2005; Telfer et al., 2010). Single markers allow variables such as displacement, velocity, and accelerations to be analyzed, whereas marker triads can be used to acquire measures of rotation and translation of the skin surface (Gao & Zheng, 2008). Each optoelectronic system uses multiple motion position sensors or cameras to record and track 3D marker movement, with upwards of 12 cameras used for experimental setups in certain cases (Dufek et al., 2009).

Despite the progressions made by optoelectronic camera systems in human motion analysis research, a limitation of these types of systems is that the motion tracking

13
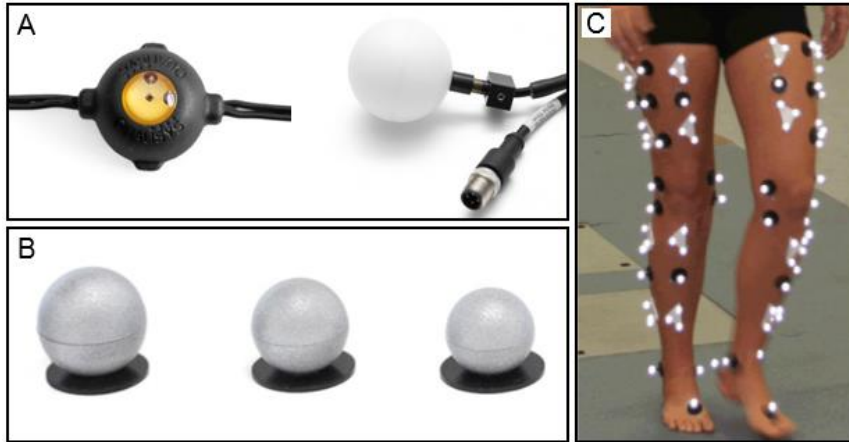
Figure 1. Different optoelectronic camera system markers and formations: A) active light emitting markers; B) passive reflective markers; C) single markers and marker triads (Modified from Gao & Zheng, 2008; Qualisys, 2016a, 2016b, 2016c).

capabilities are reliant on external devices (i.e., active or passive markers) typically mounted to the skin using double-sided adhesive tape (Fuller et al., 1997; Gao & Zheng, 2008; Houck et al., 2004) or straps (Fuller, et al., 1997; Manal et al., 2003). A recent investigation by Stefanczyk et al. (2013) found that the attachment of a 4 g accelerometer to the distal lower extremity just distal to the knee joint using only a thin Velcro® strap significantly altered the natural physiological motion of the underlying soft tissues of the leg after heel impacts, especially in the proximal regions of the segment, closer to the knee where the strap was fashioned. Moreover, affixing an external device to a body segment can interfere with soft tissue motion by way of their mass (e.g., 4–7 g), size (e.g., 10 mm diameter), and/or shape (Gao & Zheng, 2008). Therefore, when using optoelectronic systems to quantify soft tissue movement following impact, researchers cannot be certain that the true motion of soft tissue will remain undisrupted.

Another limitation of these optoelectronic systems is that the frame rate for data collection decreases as the total number of markers used increases, and thus, are

commonly only able to capture images at relatively low frame rates. This can prove to be problematic in terms of acquiring detailed kinematic data regarding soft tissue motion from impact events, such as forward falls, due to the impulsiveness associated with these events. Using the Optotrak Certus System (Northern Digital Inc., Waterloo, Canada) as an example, if soft or rigid tissue movement were to be monitored, the sample rate would be limited by the total number of markers, as calculated by Equation 1 (Northern Digital Inc., 2016):

$$\text{Sample rate} = 4600/(N + 1.3) \text{ Hz} \qquad\qquad \text{(Eq. 1)}$$

where N = number of markers.

Considering that prior investigations of shock attenuation in the distal upper extremity following hand impacts has used as many as 28 reflective surface markers on the forearm to measure soft tissue motion (Pain & Challis, 2002), using Equation 1, a maximum sampling rate for this marker array would only be approximately 157 Hz. With deceleration of the hand and arm following a forward fall observed to begin as quickly as 20 ms after initial hand impact (Chiu & Robinovitch, 1998), a sampling rate of this magnitude is not sufficient to collect a comprehensive view of the soft tissue response that occurs during this time. Additionally, the expense associated with optoelectronic systems is another limitation that must be taken into account as asymmetrical or highly dynamic tasks may require the use of multiple cameras, in addition to the active and passive marker sets, to optimally track the area of interest (Chu et al., 2010; Dufek et al., 2009; Gao & Zheng, 2008).

2.1.2.2. Digital Image Correlation

Digital image correlation is a non-contact, optical method that employs tracking and image registration techniques to measure full-field 2D or 3D surface displacement, strain, and deformation of a specimen undergoing mechanical loading (Sutton et al., 2009). A major advantage of this method is that no mechanical interaction with the specimen is required, and thus, the need for external devices to measure kinematic variables is eliminated. The basic principle of DIC involves identifying, matching, and correlating target subsets from a recorded image of a specimen in a deformed state relative to the corresponding subsets in an undeformed reference image (Reu, 2012a). Typically, if the natural texture of the specimen does not have sufficient grey intensity variation, this process is accomplished with the aid of an artificial speckle pattern applied to the surface of the specimen. As a result, the resolution and accuracy of any DIC analyses are conditional on the quality of the speckle pattern, whether naturally occurring or artificially applied (Crammond et al., 2013; Hua et al., 2011; Lecompte et al., 2006; Pan et al., 2010). Unfortunately, a general lack of practical instruction combined with a limited number of references in the literature regarding artificial speckle pattern application on the surface of biological soft tissues (e.g., human skin) in vivo make it difficult to discern an optimal approach for utilizing DIC to track soft tissue motion. Table 1 provides an overview of speckle pattern approaches that have been used on human skin in vivo to date.

Table 1. Overview of speckle pattern approaches used on biological soft tissue in vivo.

Speckle Pattern	Source	Test Specimen	Composition	Application Method
Zinc powder background with black marker speckles	Omkar et al. (2013)	Human skin on the anterior surface of the forearm	*Background*: zinc powder *Speckles*: Black marker	Anterior forearm coated with zinc powder prior drawing on black speckles with a marker
Aqueous black ink speckles	Ito et al. (2015)	Human skin on the dorsolateral and medial surface of the foot	*Background*: None *Speckles*: Aqueous black ink	N/P
Black and white water-based face paint speckles	Blenkinsopp et al. (2012)	Human skin on the dorsolateral and medial surface of the foot	*Background*: None *Speckles*: Black and white water-based face paint	N/P
No stain, powder or paint	Marcellier et al. (2001)	Non-surgical scar on the forearm	*Background*: None *Speckles*: None	N/A
	Staloff et al. (2008a)	Human skin on back of hand		N/A
	Staloff et al. (2008b)	Human skin on face		N/A

Note: N/A = Not applicable; N/P = Not provided

The use of painted speckle patterns has been observed in two recent studies that utilized 3D DIC to assess the deformation of the human foot while running (Blenkinsopp et al., 2012) and walking (Ito et al., 2015), respectively. Blenkinsopp et al. (2012) reported that water-based face paint was used to produce a contrasting black and white speckled pattern on the dorsal surface of the foot, whereas Ito et al. (2015) only used speckles of aqueous black ink. The notion of using varying combinations of black and white paint to create artificial speckle patterns is strongly supported in other experimental domains, such as experimental solid mechanics and in vitro biological soft tissue DIC studies (Figure 2), in which the most frequently used patterns include: black paint speckles (Abanto-Bueno & Lambros, 2002; Choi & Shah, 1997; Gerhardt et al., 2012; Mates et al., 2012; Moerman et al., 2009; Ni Annaidh et al., 2012; Zhang et al., 2002), a

combination of black and white paint speckles (Samarasinghe & Kulasiri, 2004), and black paint speckles over a solid base coat of white paint (Betts et al., 2010; Shih & Sung, 2013; Backman et al., 2006; Zhang & Arola, 2004; Libertiaux et al., 2011; Bruck et al., 1989; Lan et al., 2014).
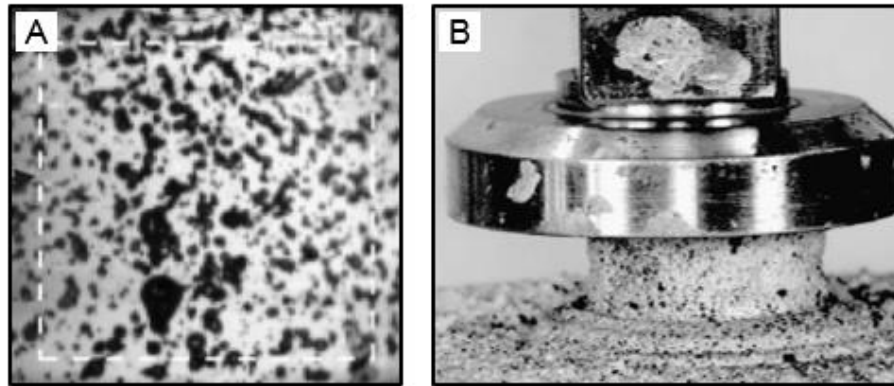
Figure 2. Examples of black and white paint combinations used to create speckle patterns for DIC analyses: A) black paint speckles with no background applied to a biomimetic elastomer; B) black paint speckles with a white painted background applied to swine brain tissue (Modified from Libertiaux et al., 2011; Mates et al., 2012).

Although painted speckle patterns are capable of acting as virtually massless marker systems for tracking soft tissue motion that (compared to external devices) allow underlying tissues to move freely without interruption, notable limitations with this approach are still present. First, in spite of evidence presented by Barranger et al. (2010) supporting the superior accuracy of painted over powder speckle patterns at lower strains (10%–50%), paint was still found to be susceptible to DIC measurement error following the eventual occurrence of cracks within the patterns at strains greater than 50%, which diminished their quality. Moreover, since this study used a flat, transparent silicone specimen for testing, the findings may not be indicative of the additional complications that the unique mechanical properties of human skin in vivo may pose under similar

loading conditions. Second, while other motion tracking techniques, such as optoelectronic systems, only measure localized points designated by discrete markers, DIC software calculates global measures (i.e., full-field displacement and strain maps), and thus, requires that the entire area of interest be covered in a speckle pattern. As a result, it must be ensured that the applied speckle pattern does not alter the mechanical properties of the soft tissue (e.g., increased stiffness and/or dehydration). Libertiaux et al. (2011) used displacement-driven compression tests to demonstrate that the application of a painted speckle pattern caused no significant statistical difference in the mechanical response of brain tissue samples; the implications for human skin in vivo may be very different.

Aside from painted speckle patterns, only two other speckle pattern approaches have been used on human skin in vivo to execute DIC analyses. In an attempt to better understand the etiology of carpal tunnel syndrome, Omkar et al. (2013) used a unique speckle pattern approach to measure the strain of the superficial muscles and tendons in the anterior compartment of the forearm during wrist extension in vivo, in which zinc powder was coated on the surface of the right anterior forearm to improve the contrast against a random black speckle pattern applied with a marker (Figure 3). However, since no further detail was provided in the methods on this specimen preparation process (e.g., brand of zinc powder, ease of application, cost, exposure time, etc.), the reproducibility of this approach and its appropriateness for in vivo DIC research remains questionable, especially given the notable adverse side effects associated with zinc-based powders (Centers for Disease Control and Prevention [CDC], 1994).
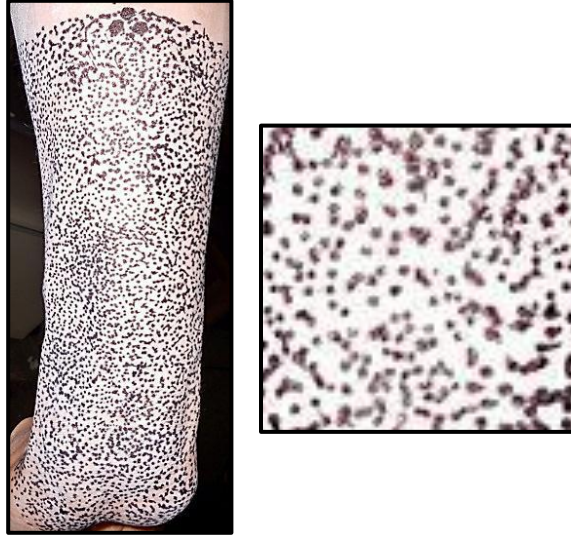
Figure 3. Zinc powder and black marker speckle pattern used on the anterior surface of the human forearm for in vivo DIC analysis of wrist extension (Modified from Omkar et al., 2013).

Alternatively, there have also been DIC studies on human skin that involve no speckle pattern treatment, suggesting that the pores intrinsic to the skin form an ideal set of markers for assessing its mechanical properties (Marcellier et al., 2001; Staloff et al., 2008a; Staloff et al., 2008b). While this is an enticing option that would theoretically provide the truest representation of soft tissue motion after impact without any form of image artifact, each of these studies only tested very confined areas of the skin in which the applied skin deformation was kept very subtle (e.g., wrinkles near the corner of the eye when closing the eye lid) on participants with relatively light skin pigmentation. Thus, further assessment of this technique would be necessary to determine if the contrast would be sufficient for large impact deformations of the skin characteristic of entire body segments, as well as individuals with darker skin pigmentations.

2.2. ProAnalyst® Motion Analysis Software

ProAnalyst® is a motion analysis software package that employs photogrammetric techniques to perform non-contact motion tracking analyses on a moving object. The software allows users to measure and compute many kinematic variables associated with specified reference points on the surface of the object throughout its motion pathway, including position, velocity, acceleration, size, and location, in addition to other characteristics. With both manual and automatic tracking capabilities, users have the option to track reference points manually by continuously selecting the same feature frame by frame, or automatically by selecting a feature in the initial video frame and then using the automatic tracking tool within the software to locate and track the motion of that feature in subsequent frames. ProAnalyst® is compatible with virtually any video camera and format; however, it is often paired with high speed imaging systems to document the motion pathway of an object for 2D or 3D analysis, depending on the version being used. In addition, the comprehensive capabilities of this motion analysis software make it a highly versatile tool that can be applied in laboratory simulations as well as real-life tasks and activities across numerous fields of research (e.g., automotive, ballistics, biomechanics, etc.). It is also worth noting that, as commercially available premium motion analysis software, a large portion of the research performed with ProAnalyst® software is conducted by companies that do not publish their findings to the scientific community (e.g., NASA).

Although ProAnalyst® can be used for markerless motion tracking, in which specific regions on the object of interest (e.g., edge length or diameter in the x-axis) are selected as reference points during post-processing of the video data (Alsakarneh et al.,

2012; Audysho et al., 2013), researchers have also used a variety of surface markers in combination with the motion analysis software to aid the automated marker tracking process (see Table 2 for an overview of the different surface markers used with ProAnalyst®). Reflective markers have been used with rats to track limb positions for assessing locomotor compensation after peripheral nerve lesion (Bennet et al., 2012) and to compute head rotational and lateral translational displacements in the coronal plane for investigations on the pathology of diffuse axonal injury (Li et al., 2010). Neto and Magni (2007) reported the use of high contrast markers affixed to the lateral surface of participants' forearms (2 cm apart) from elbow to wrist to analyze the kinematic characteristics of Kung Fu Yau-Man palm strikes without impact. Furthermore, Facchinello et al. (2015) reported that rigid markers were attached to vertebral bodies to test the stabilization capacity of monolithic spinal rods with different flexural stiffness and anchoring arrangement.

As opposed to using externally mounted surface markers, recent studies have also been performed in which massless surface markers have been used. O'Neill et al. (2015) applied nontoxic, water-soluble white paint markers over specific anatomical landmarks to assess the kinematics of the chimpanzee pelvis and hindlimb during bipedal walking. Similarly, white paint dots were also utilized in a study by Tonkovich et al. (2012) to investigate tyre deformation behaviour on heavy mining vehicles. In contrast, Crowley et al. (2015) reported the use of black ink to track the limb position of specific anatomical landmarks on rats in relation to the effect of intrathecal neurochemical excitation of thoracic propriospinal neurons on locomotion performance. Finally, a recent study by Brydges et al. (2015) utilized a grid pattern of circular black dots (0.5 cm diameter, 2 cm

inter-marker distance) applied with a permanent marker pen to track and measure soft

tissue motion of the leg following heel impacts (Figure 4).

Table 2. Overview of surface markers used with ProAnalyst® motion tracking software.

Surface Marker	Source	Marker Type	Research Application
Externally mounted surface markers	Bennet et al. (2012)	Reflective markers	Track forelimb and hindlimb positions in rats to assess locomotor compensation after peripheral nerve lesion
	Li et al. (2010)	Reflective markers	Compute head rotational and lateral translational displacements in the coronal plane to assess the pathology of diffuse axonal injury in rats
	Neto and Magni (2007)	High contrast markers	Analyze forearm kinematic characteristics of Kung Fu Yau-Man palm strikes without impact
	Facchinello et al. (2015)	Rigid markers	Test the stabilization capacity of monolithic spinal rods with different flexural stiffness and anchoring arrangement
Massless surface markers	Brydges et al. (2015)	Grid of circular black dots applied with a black permanent marker	Track soft tissue motion of the leg following pendulum and drop heel impacts
	O'Neill et al. (2015)	Nontoxic, water-soluble white paint dots applied on specific anatomical landmarks	Compare kinematics of the chimpanzee pelvis, hip, knee, and ankle during bipedal walking to those values of humans walking
	Crowley et al. (2015)	Black ink marks applied over specific anatomical landmarks	Track limb positions in rats with spinal hemisections to examine the effect of intrathecal neurochemical excitation of thoracic propriospinal neurons on locomotion performance
	Tonkovich et al. (2012)	White paint dots applied in a strategic pattern on the tyre surface	Track local tyre deformation behaviour on heavy mining vehicles under static and quasi-static loading, and compare against optical displacement transducers
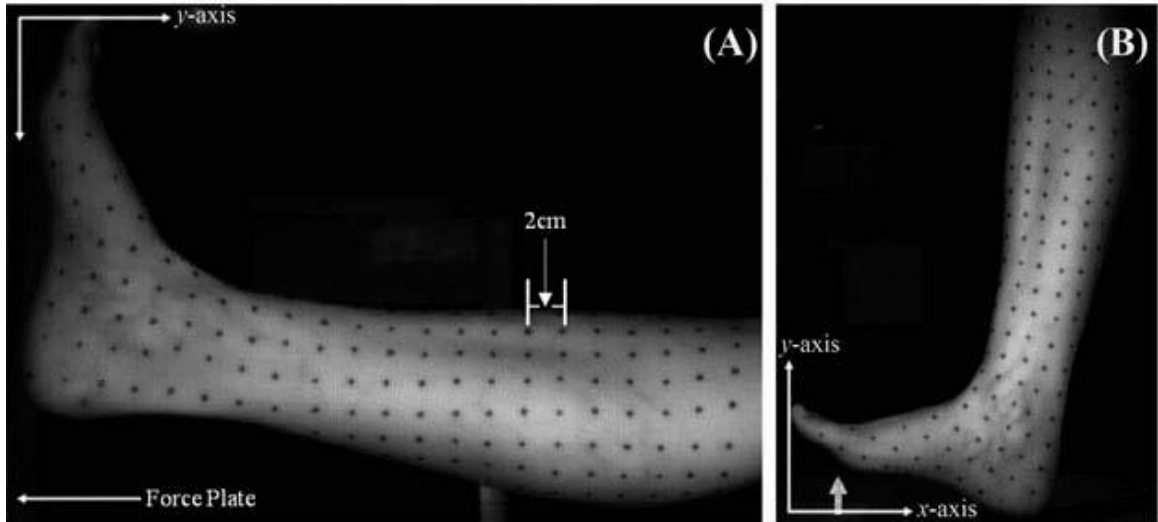
Figure 4. Square grid of uniform circular markers used for tracking soft tissue motion on the distal lower extremity (Modified from Brydges et al., 2015).

2.3. Massless Surface Markers

The use of photogrammetric techniques together with massless markers (e.g., paint, permanent marker pen) on the surface of the skin to measure soft tissue motion is a fairly novel concept. Although not a conventional approach for soft tissue motion analysis, a primary benefit of massless skin surface markers is their capacity to provide researchers with the most authentic view of the kinematics associated with soft tissue movement, especially with tissue motion pertaining to impact shock attenuation.

To date, apart from a few studies that have quantified the deformation and strain of human soft tissue in vivo using 3D DIC (Blenkinsopp et al., 2012; Ito et al., 2015; Omkar et al., 2013), Brydges et al. (2015) have conducted the only other investigation involving the use of massless skin surface markers for tracking soft tissue movement. Designed for the purpose of measuring leg and foot soft tissue position and velocity data

24

following heel impacts, the square grid of circular black markers (0.5 cm diameter; inter-marker distance of 2 cm) used in this study was simply created with a flexible, clear plastic stencil and a black permanent marker pen. The practical advantages of this particular massless marker approach (e.g., cost and time efficiency, minimal training, etc.) make it an attractive option for soft tissue motion analysis; however, modifications to specific marker parameters, such as the shape and contrast, could help further improve its accuracy and reliability.

2.3.1. Marker Contrast

Consistent with all photogrammetric motion tracking techniques is the need for high contrast markers to enhance marker detection and tracking capabilities; for instance, increasing the contrast between the speckles and the background of a speckle pattern during DIC analyses maximizes the intensity gradient (and thus information content) of the recorded images so that the noise levels and measurement error can be kept to a minimum (Reu, 2012b; Sutton et al., 2009). However, unlike optoelectronic camera systems that utilize different forms of light detection (i.e., active or passive markers) to ensure adequate contrast when documenting soft tissue motion, massless surface markers rely solely on the colouration of the marker against the surface of the skin to which it is applied. Consequently, taking into consideration the wide range of possible skin pigmentations that can make up the background of the body segment to be examined, the task of consistently maintaining a high level of contrast across multiple participants with this technique may prove to be challenging.

To date, the influence of skin pigmentation variability on the precision of soft tissue motion tracking using massless surface markers has not been addressed. In the study performed by Brydges et al. (2015), each of the massless surface markers applied to the leg of every participant were exclusively black in colour. Although no indication was made if contrast discrepancies between the skin pigmentations of the participants influenced the precision of automated motion tracking, during the data analysis it was reported that additional image filters were used to improve the contrast between the marker and background (i.e., skin). Thus, it is fair to assume that strictly using black surface markers limits this approach since more tracking errors would theoretically occur as the contrast between the marker and background is reduced for increasingly darker skin pigmentations. One potential solution may be to use a combination of contrasting pigmentations, similar to the black and white speckle pattern implemented by Ito et al. (2015), in order to create a more universally distinct marker that can be used on varying skin pigmentations; however, further research on this is needed to address this question.

2.3.2. Marker Shape

One of the main issues discovered by Brydges et al. (2015) during data analysis was that the use of uniformly shaped circular markers actually weakened the accuracy of the automated marker tracking process. Due to the identical shape of each marker, several instances occurred in which ProAnalyst® had difficulty identifying specific markers that were manually selected in the initial video frame for automatic tracking. This resulted in poorer marker detection in some cases, which forced researchers to revert back to manual tracking. Therefore, it was proposed that utilizing a set of more unique

markers may help to improve the accuracy and reliability of this method for tracking movement of soft tissue by allowing the motion analysis software to better discriminate between individual markers.

The notion of using greater shape variation with massless surface markers has been found to be advantageous for other motion tracking techniques, such as DIC. For example, Crammond et al. (2013) demonstrated that in comparison to spray painted speckle patterns, airbrushed speckle patterns often contain speckles with higher shape permutations that ultimately produce a more defined texture for enhanced tracking capabilities. In addition, although there is currently no information regarding an optimal marker shape for massless motion tracking techniques, a study by Haddadi and Belhabib (2008), which tested the error related to five different types of speckle patterns for DIC (Figure 5), provided evidence of what shape not to use, as speckle patterns consisting of either small (B) or large (C) circular black spots corresponded to high DIC measurement error compared to patterns with randomly shaped speckles.
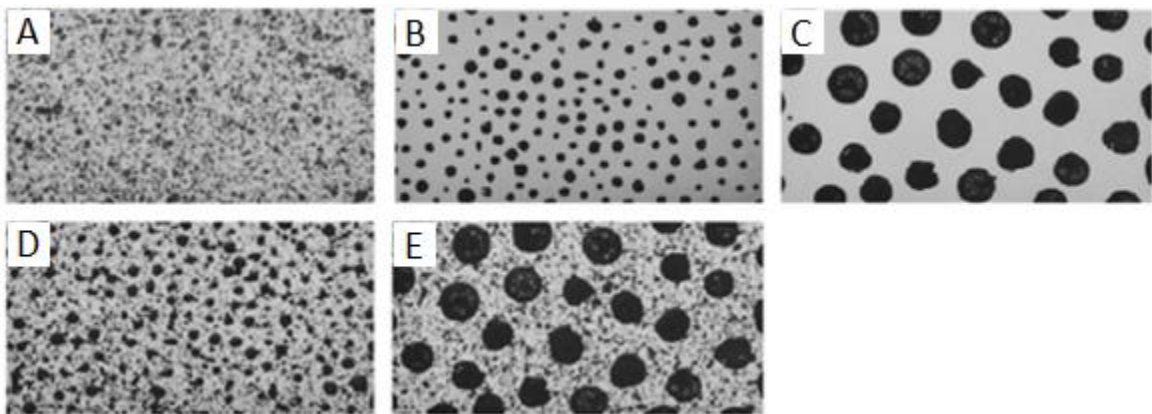
Figure 5. Different types of speckle patterns: A) random speckle; B) small black spots; C) large black spots; D) small black spots and random speckle; E) large black spots and random speckle (Modified from Haddadi and Belhabib, 2008).

27

2.4. In Vivo Test Specimen

2.4.1. Forearm Tissue Composition

Through the direct measurement of cadaver forearms using a water displacement method, the total tissue composition of the human forearm has been shown to be made up of approximately 8.6% skin, 13.7% bone, 6.1% tendon, 8% fat (including fat, fascia, nerves and blood vessels), and 63.6% muscle by volume (Cooper et al., 1955). In a more recent study by Maughan et al. (1984) that utilized computed tomography (CT) scans to determine the composition of the human forearms in healthy young adults (20 to 35 years of age), further evidence was provided in support of these previously reported values, as muscle was found to account for approximately 65.5% of total limb volume overall.

From the same study, significant differences in forearm tissue volumes were observed between sexes, in which males demonstrated higher muscle volume (72%) than females (59%), while females had nearly double the fat volume (29.3%) compared to males (15%) (Maughan et al., 1984). Total bone volume of the male forearms was found to be more than that of the female forearms as well, however, in terms of percentage composition, it was determined that bone content in relation to the total forearm volume was fairly constant between females (12%) and males (13%). Therefore, it was concluded that the variability observed with forearm tissue composition between sexes was due to the differences in the proportion of muscle and fat (Maughan et al., 1984).

In addition, there is also evidence to support the notion that significant differences in tissue composition of the forearm do exist between dominant and non-dominant limbs. In a separate study by Maughan et al. (1986), CT scans were once again used to demonstrate that the dominant arms of individuals, both trained (33 ± 10 years of age),

28

and untrained (26 ± 5 years of age), possess greater total forearm volume than the non-dominant arm. Higher percentages of forearm muscle volume in the dominant arm were found to be one of the main factors contributing to this difference, with muscle accounting for 75.4% and 71.4% of the total forearm volume in the trained and control group, respectively.

2.4.2. Human Skin

Human skin is a complex, multi-layered membrane covering almost the entire external surface of the human body that has been shown to possess viscoelastic, anisotropic, and non-linear stress-strain mechanical properties (Flynn et al., 2011; Khatyr et al., 2004; Pailler-Mattei et al., 2007; Silver et al., 2001). Also referred to as the cutaneous membrane, the skin consists of two primary layers: the epidermis and the dermis (Jablonski & Chaplin, 2004; Tortora & Nielsen, 2014). The epidermis is the thinner, most superficial layer of the skin that is composed of stratified squamous epithelial tissue. Aside from the presence of hair and the pores of sweat glands, the surface of the epidermis is relatively smooth. The dermis is the thicker, deeper layer composed of papillary and reticular regions that contain several types of connective tissue. An additional layer deep to the dermis, but not part of the skin, is the subcutaneous layer (also known as the hypodermis), which is comprised of loose connective tissue (Tortora & Nielsen, 2014). The general structure of human skin is illustrated in Figure 6.

The broad spectrum of skin pigmentation observed in humans, both within and between populations (Jablonski, 2004), has been determined to be the result of genetics

(Strum et al., 1998) as well as adaptations to many environmental factors associated with geographical location, such as ultraviolet (UV) light exposure (Tadokoro et al., 2005). Melanin is the pigment responsible for providing much of the coloration in human skin (Uyen et al., 2008). The quantity, size, distribution pattern, and type of melanin within the epidermis have been shown to be some of the main intrinsic factors influencing skin pigmentation variation (Thong et al., 2003).
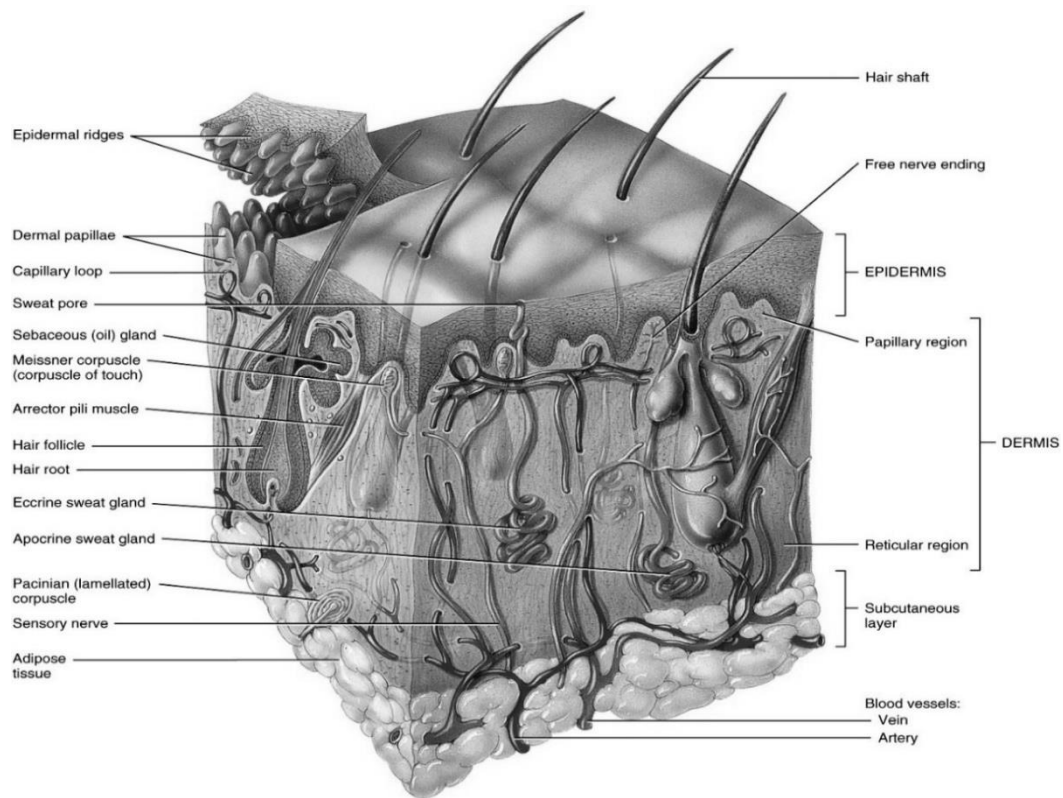
Figure 6. Cross-section of human skin and subcutaneous layer (Modified from Tortora & Nielsen, 2014).

2.5. Forward Fall Impacts

The basic mechanics of a forward fall on the hand of an outstretched arm typically involves a compressive (axial) load (i.e., parallel to the long axis of the forearm) applied

to a hyperextended wrist at impact (Figure 7) (Brügger & Michel, 2015; Burkhart et al., 2012a; Whiting & Zernicke, 2008). Although there are many contributing factors that can influence the outcome of this impact event, such as soft tissue thickness over the palm (Choi & Robinovitch, 2011) or the energy-absorbing capacity of the surface impacted (Choi et al., 2014), two key factors that are central to forward fall-related impacts include both the direction and magnitude of the impact loads.
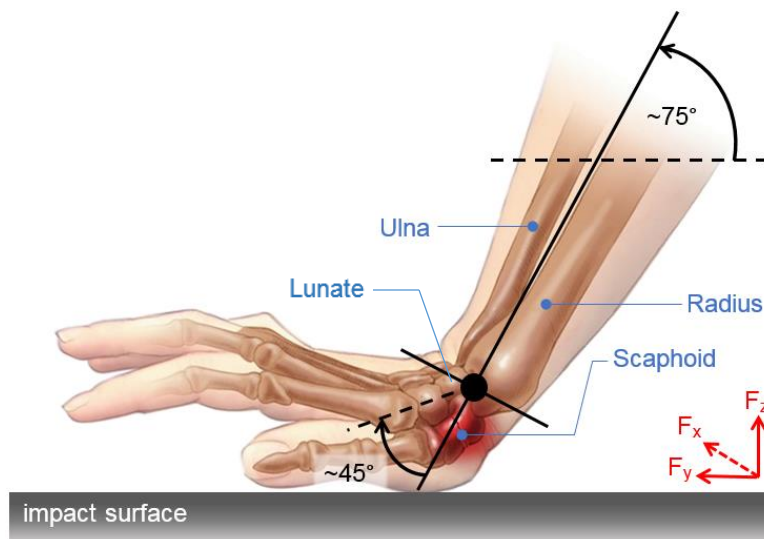
Figure 7. Schematic diagram representing the hand, wrist, and forearm biomechanics associated with a forward fall impact on the hand of an outstretched arm.

In the literature the most commonly reported angle that the forearm makes in relation to the impact surface (or ground) during a forward fall is 75° (Burkhart et al., 2012a; Burkhart et al., 2014; Greenwald et al., 1998; Myers et al., 1991; Troy & Grabiner, 2007a), with the wrist positioned at approximately ~30 to ~45° of extension (Burkhart et al., 2012a; Burkhart et al., 2014; Greenwald et al., 1998; Troy et al., 2005). As a result of this orientation of the distal upper extremity at the moment of impact, the point of force application is naturally distributed over the scaphoid and lunate carpal

bones (th.e weakest part of the palm), which directly articulate with and transmit force to the distal radius (Gitajn & Rodriguez, 2011).

With respect to the impact loads sustained by the distal upper extremity during a forward fall on the hand of an outstretched arm, dynamic impact experiments performed by Burkhart et al. (2012a) using human cadaveric radii found a consistent pattern of directional loading of the distal radius in which the F_z vector component stood out as the dominant contributor to the resultant impact reaction force, on average directing 96% along the long axis of the radius. Review of the literature has shown that the critical (i.e., fracture) level of these impact loads tends to occur at magnitudes upwards of 2100 N (Burkhart et al., 2012a; Greenwald et al., 1998; Troy & Grabiner, 2007b).

2.5.1. Shock Wave Attenuation

Forces created upon impacting the ground with the hands during a forward fall on outstretched arms are usually transmitted through the palm of the hand, into the wrist joint, and then proximally along the forearm toward the elbow joint. The resultant accelerations and decelerations of the tissues in the body stemming from these impact forces can be analyzed and observed as waves (Shorten & Winslow, 1992). The term "shock" refers to an abrupt change of force application in which the equilibrium of a system is disrupted temporarily before returning to its resting state (Nigg et al., 1995). Therefore, a "shock wave" can be described as a stress wave propagating through the tissue of the human body. The reduction in the amplitude of the shock wave, from the impact force, as it propagates through the body is thus known as shock (wave) attenuation. This can be accomplished by both passive and active mechanisms. Shock

wave attenuation can occur passively through the independent movement of soft tissue (fat, muscle, skin) relative to bone. Pain and Challis (2002) demonstrated the significance of this phenomenon in the distal upper extremity following hand impacts as the soft tissue of the forearm during the loose condition (i.e., when the muscles of the forearm were relaxed) was found to dissipate impact energy considerably. Active impact mechanisms, such as fall arrest strategies that reduce extension of the elbow prior to impact (DeGoede & Ashton-Miller, 2002) and altering forearm muscle activation (Burkhart & Andrews, 2010b; Pain & Challis, 2002), have been shown to significantly contribute to attenuating shock waves from impacts to the distal upper extremity as well.

In addition to these mechanisms, there are also several external factors that influence shock attenuation in forearm soft tissue during a fall on the hand of an outstretched arm. Protective devices such as wrist guards have been shown to have a significant dampening effect on impact shock in the hand and forearm (Burkhart & Andrews, 2010a; Maurel et al., 2013). Furthermore, the stiffness of the surface that the hands contact during a forward fall has been found to affect the attenuation of impact force. Robinovitch and Chiu (1998) demonstrated that even a relatively small decrease in the stiffness of the contact surface by adding a simple foam pad (thickness of 1.3 cm and compressibility of about 0.3 cm) can significantly attenuate the transient peak impact force at the hand by reducing, as well as delaying, the peak velocity generated across the damping components of the wrist.

Quantifying shock attenuation through the body's musculoskeletal system has been accomplished using Equation 2 (Chu and Caldwell, 2004; Dufek et al., 2009; Zhang et al., 2005),

$$\text{Shock attenuation} = \left[1 - \left(\frac{a_{\text{proximal}}}{a_{\text{distal}}}\right)\right] \times 100 \qquad \text{(Eq. 2)}$$

where:

a_{proximal} is the peak acceleration of the proximal segment

a_{distal} is the peak acceleration of the distal segment

Since the majority of shock attenuation research has focused on lower extremity impacts (e.g., running and jumping), these peak acceleration values are typically measured at the anteromedial surface of the distal tibia and the head, with the use of skin-mounted accelerometers (Brizuela et al., 1997; Coventry et al., 2006; Dufek et al., 2009; Mercer et al., 2003; Mercer et al., 2010). However, given that the basis of the equation is founded on an acceleration ratio (Voloshin et al., 1981), in theory, it could also be applied to show the attenuation between the distal and proximal aspects of a given segment for a variety of impact events, including the shock-attenuating capacity of the forearm following a forward fall on the hand of an outstretched arm using peak accelerations at, or near, the elbow and wrist.

2.5.2. Impact Apparatuses

To date, numerous experimental methods have been designed to simulate impacts to the distal upper extremity that are consistent with a forward fall on the hand of an outstretched arm. However, due to the need to maintain the severity of the impact force at a safe level for participants, in vivo forward fall simulation methods have been limited to highly controlled laboratory-based experiments. Troy and Grabiner (2007a) employed

a simple motor task to simulate the descent phase of a fall in which participants leaned forward in the sagittal plane from an upright kneeling position until their hands impacted a force plate. Other studies have designed variations of torso-release methods where a participant's body weight is initially supported in a forward-directed lean from either an upright kneeling or standing position with a sling, tether, or cable prior to being released, to impact a force plate with their hands (Chiu & Robinovitch 1998; DeGoede & Aston-Miller, 2002a; Hwang et al., 2006; Kim & Ashton-Miller, 2003; Robinovitch & Chiu, 1998). Forward falls have also been simulated using different types of pendulum apparatus for accurate control of impact consistency. To study the influence of varying elbow angles on resultant impact force to the upper extremity, DeGoede et al. (2002) impacted the hands of stationary seated participants using a weighted pendulum. In contrast, Burkhart and Andrews (2010a, 2010b) employed a seated human pendulum method where participants were released from a predetermined resting position to impact vertically mounted force plates with their hands. Lastly, with the goal of improving kinematic and kinetic data that can be obtained from forward fall simulation methods, Burkhart et al. (2012b) developed the Propelled Upper Limb fall ARrest Impact System (PULARIS); an innovative system that better represents the initial dynamic movement as well as the hip and extremity postures adopted during the real world mechanisms of a forward fall event.

From a feasibility standpoint, the simple motor task employed by Troy and Grabiner (2007a) ranks the highest among the forward fall simulation methods with regard to its simplicity and cost efficiency. However, with the participant in full control of the impact protocol (e.g., self-initiated falls from an upright kneeling position), this

method does not accurately represent the true events surrounding a forward fall on the hand of an outstretched arm, since factors such as preparation time before fall initiation and potential learning effects can influence the validity and reliability of the impact force, both within and between participants. On the other hand, more complex forward fall simulation methods like the PULARIS (Burkhart et al., 2012b) and different variations of the pendulum apparatus (Burkhart and Andrews; 2010a, 2010b; DeGoede et al. 2002) may provide better authenticity and consistency when testing forward fall mechanisms, respectively, but are much more challenging to implement. Many resources need to be considered for these methods, including: cost of the equipment; time and personnel required to construct, test, and validate the safety of the apparatus; and training of personnel to operate the apparatus.

In comparison to the other forward fall simulation methods, torso-release methods (Chiu & Robinovitch, 1998; DeGoede & Aston-Miller, 2002a; Hwang et al., 2006; Kim & Ashton-Miller, 2003) offer a balance between feasibility and accuracy when attempting to replicate distal upper extremity impacts associated with a forward fall on the hand of an outstretched arm. The many variations of this method and low cost of equipment set-up give the researcher flexibility in terms of the experimental design in different lab environments. Additionally, the release time can be randomized in order to reduce any anticipatory effects of participants. The relatively short time it takes to reset the participant and apparatus in-between trials reduces the time of data collection as well.

2.5.3. Hand Impact Force

When simulating the forces sustained by the distal upper extremity during a forward fall on the hand of an outstretched arm, multiple studies in the literature have shown that a bimodal pattern is often observed in relation to the ground reaction force profile during impact to the hand (Figure 8) (Chiu & Robinovitch, 1998; DeGoede & Ashton-Miller, 2002; Hwang et al., 2006; Kim & Ashton-Miller, 2003).
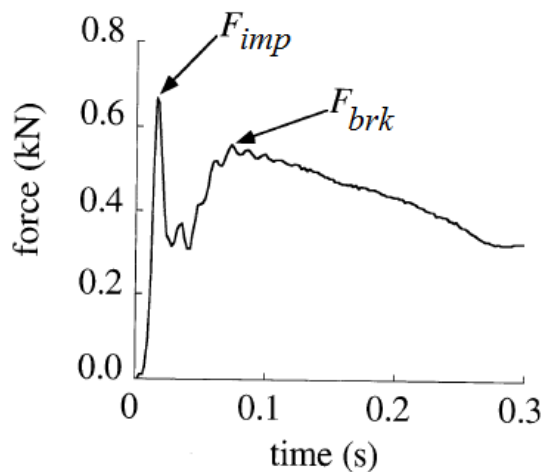
Figure 8. Bimodal shape of the measured ground reaction force on the hand during forward fall arrests with two force peaks: peak impact force (F_{imp}) and peak braking force (F_{brk}) (Modified from Chiu & Robinovitch, 1998).

Despite the use of different forward fall impact apparatus, this pattern is consistently characterized by two distinct force components: a primary peak impact force (F_{imp}) shortly followed by a secondary peak braking force (F_{brk}). Studies have defined F_{imp} as the consequence of the sudden impact of the heel of the hand with the ground representing the short period of passive impact response, whereas F_{brk} is the result of the active contraction of the muscles of the upper extremity to gradually decelerate the forward motion of the body (Hwang et al., 2006; Kim & Ashton-Miller, 2003). The uniqueness of their origins contributes to the different spectral distributions of each force

peak (Hwang et al., 2006), leading Chiu and Robinovitch (1998) to describe this impact phenomenon as a high-frequency transient force followed by a low-frequency oscillation.

The bimodality of this ground reaction force profile on the hand is consistent with other human activities involving collision with the ground, such as impacts to the foot when jumping (Dufek & Bates, 1991; Özgüven & Berme, 1988), and is thought to be attributable to the slight delay in the reaction of the upper extremity musculature to the sensory signal from the initial hand contact (Kim & Ashton-Miller, 2003). The overall timing of the two force peaks is very brief, with F_{imp} occurring between a range of about 20 to 60 ms after hand impact and F_{brk} typically appearing in under 200 ms (Chiu & Robinovitch, 1998; Hwang et a., 2006; Kim & Ashton-Miller, 2003).

Various factors have been shown to affect the magnitude of the two force peaks. Kim & Ashton-Miller (2003) demonstrated that increases in falling distance during torso-release forward fall simulations corresponded to statistically significant increases in both F_{imp} and F_{brk}. Similar results were found by Chiu and Robinovitch (1998) with increases in fall height; however, a much more marked effect was observed for F_{imp} than F_{brk}. In contrast, Chiu and Robinovitch (1998) also found that increases in body mass more strongly correlated to increases in the magnitude of the F_{brk} compared to the F_{imp} component of hand impact force.

3. METHODS

3.1. Participants

3.1.1. Sample Size

Due to the relative novelty of using an automated motion tracking technique (i.e., ProAnalyst®) to measure soft tissue movement and shock attenuation of forearm soft tissue in vivo, prior information on which to base sample size calculations was minimal. In a related experiment by Pain and Challis (2002), it was noted that the mean (±SD) displacement of markers on the forearm along the long axis of the radius following a hand impact task was 1.7 (± 0.3) cm. Using these values in combination with Equation 3 (listed below), it was determined that an approximate sample size of 36 participants was needed to execute the study with a desired power of 0.8 (80%), at a significance level in which alpha (α) equals 0.05 (95%), and with a margin of error of only 0.1 cm.

$$ E = z\alpha_{/2} \cdot \frac{\sigma}{\sqrt{n}} \qquad \Longrightarrow \qquad n = \left[\frac{z\alpha_{/2} \cdot \sigma}{E}\right]^2 \qquad \text{(Eq. 3)} $$

*Rearranging the formula

where:

E is the margin of error (the maximum difference between the sample mean $\bar{x}$ and the population mean μ)

$z\alpha_{/2}$ is the known critical value

σ is the population standard deviation (estimated from Pain and Challis (2002))

n is the sample size

39

However, taking into consideration the scope of the project (e.g., availability of the equipment, duration of data collection process, etc.), a reduced sample size was also considered to accommodate feasibility concerns for completing the project. Given that the project was building on the methodologies from a prior study (Brydges et al., 2015), it was anticipated that the minimum sample size be equivalent to the number previously used (twenty participants: 9 male, 11 female).

3.1.2. Participants

A total of 32 healthy, young adults (18 female, 14 male) with an overall mean (±SD) age, height, and body mass of 22.3 (2.8) years, 1.73 (0.09) m, and 71.2 (14.0) kg, respectively, were recruited (from the University of Windsor student population) to participate in the study (Table 3).

Table 3. Mean (±SD) age, height, and body mass of all participants.

Participants	Age (years)	Height (m)	Body Mass (kg)
Female (n=18)	22.2 (2.7)	1.68 (0.07)	63.3 (8.8)
Male (n=14)	22.4 (2.9)	1.80 (0.07)	81.2 (13.0)
Overall (n=32)	22.3 (2.8)	1.73 (0.09)	71.2 (14.0)

Participants were then categorized into one of two groups based on their skin pigmentation (light and dark) using a modified Fitzpatrick Skin Type Questionnaire (Appendix A); a numerical classification system for human skin color that was founded on two components: 1) genetic disposition, and 2) reaction of different skin types to ultraviolet light (Fitzpatrick, 1988). The Fitzpatrick Skin Type Questionnaire is a self-report questionnaire and consists of six skin types that range from Type I (pale white) to

Type VI (deeply pigmented dark brown or black). To establish more general parameters for differentiating skin pigmentation, participants' skin types were split into either a light (Type I–III: 9 female, 8 male) or dark (Type IV–VI: 9 female, 6 male) group.

In addition, considering that body composition (and thus soft tissue composition) is unique to each individual as a result of multiple factors such as age (Baumgartner, 2000; Horber et al., 1997), sex (Daniels et al., 1997; Horber et al., 1997), and activity level (Guo et al., 2015), and that a progressive decline of skin elasticity has been shown with age (Luebberding et al., 2014; Sumino et al., 2004), an effort was be made to match participants between the light and dark skin pigmentation groups according to their height (cm), body mass (kg), age (17–30 years), and sex in order to limit differences between groups as a result of these variables. Ensuing analyses demonstrated that there were no statistically significant differences between the two skin pigmentation groups for any of the aforementioned variables when compared overall, and when split into females and males ($p > 0.05$).

3.1.3. Exclusion Criteria

Only right hand dominant individuals were considered for the study in an attempt to limit any possible soft tissue variations between dominant and non-dominant arms (Maughan et al., 1986). Participants also had to be within 17 and 30 years of age in order to meet the age parameters of the tissue mass prediction equations that were subsequently used in the study to determine the soft and rigid tissue composition of participants' forearms (Arthurs et al., 2009). Lastly, each participant completed a pre-test general health questionnaire (Appendix B) to determine if there were any possible issues with the

participants' upper limbs (i.e., hand, wrist, forearm, elbow, shoulder) and skin, or if they had any general health conditions which may have excluded them from participation. If a participant answered "yes" to any of the questions, the investigator and participant would then discuss the extent of the violation before a final decision was made concerning their exclusion from the study, at the discretion of the investigator.

3.1.4. Consent

All methods for this study were approved by the Research Ethics Board of the University of Windsor. Procedures were explained to each participant both verbally and in a written letter of information, and informed consent was obtained from each participant prior to participating in the study.

3.2. Instrumentation and Apparatus

3.2.1. High Speed Camera

A high speed camera (Photron, San Diego, CA, USA, FASTCAM SA4; 5000 frames/s, 1024 x 800 pixels^2 resolution, shutter speed 0.2 ms) was used to record planar (2D) soft tissue motion of the lateral aspect of the pronated right forearm during forward fall simulated impacts. The camera was mounted to a tripod at a fixed height of approximately 150 cm with a downward angle of 15–20° to ensure that the field of view could fully capture the soft tissue motion of the right forearm without interference from the left forearm. Two tungsten lights (ARRI, Munich, Germany, T1 Fresnel; 1000W, 120V) positioned at angles above and below the forearm provided adequate lighting

conditions for capturing the soft tissue motion. Figure 9 shows a schematic diagram of the experimental test set-up.
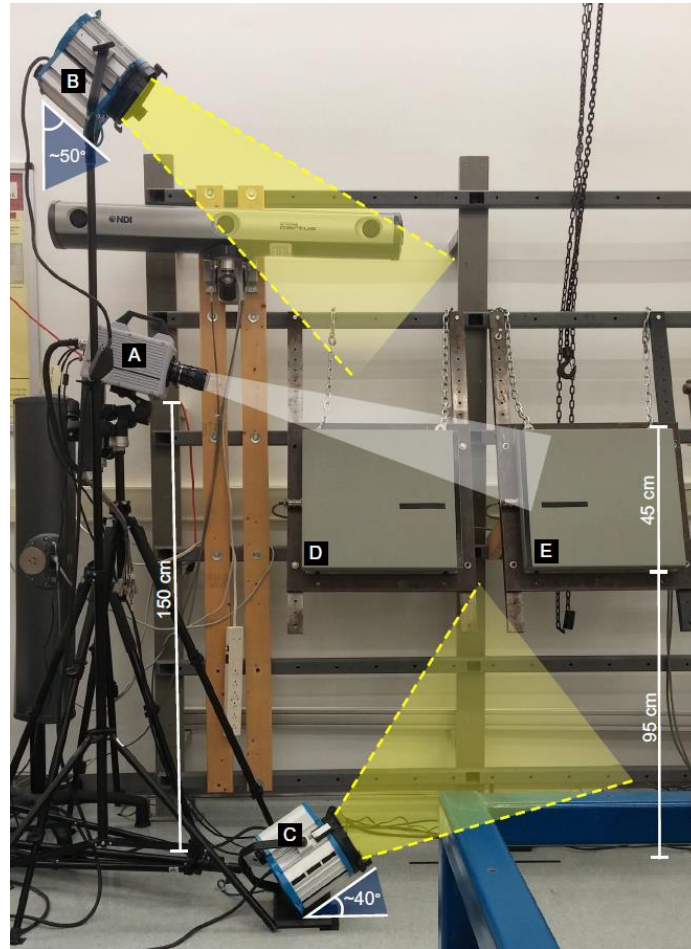
Figure 9. Schematic diagram of the experimental test set-up: A) high-speed camera; B) primary flood light; C) secondary flood light; D) left hand force plate; E) right hand force plate.

3.2.2. Torso-Release Impact Apparatus

A modified version of a torso-release apparatus from previous studies was used to apply bilateral impacts to the right and left hand consistent with forward falls on the hands of outstretched arms (Kim & Ashton-Miller, 2003; Hwang et al., 2006) (Figure 10). Participants stood in an upright position and were fitted with a safety-harness
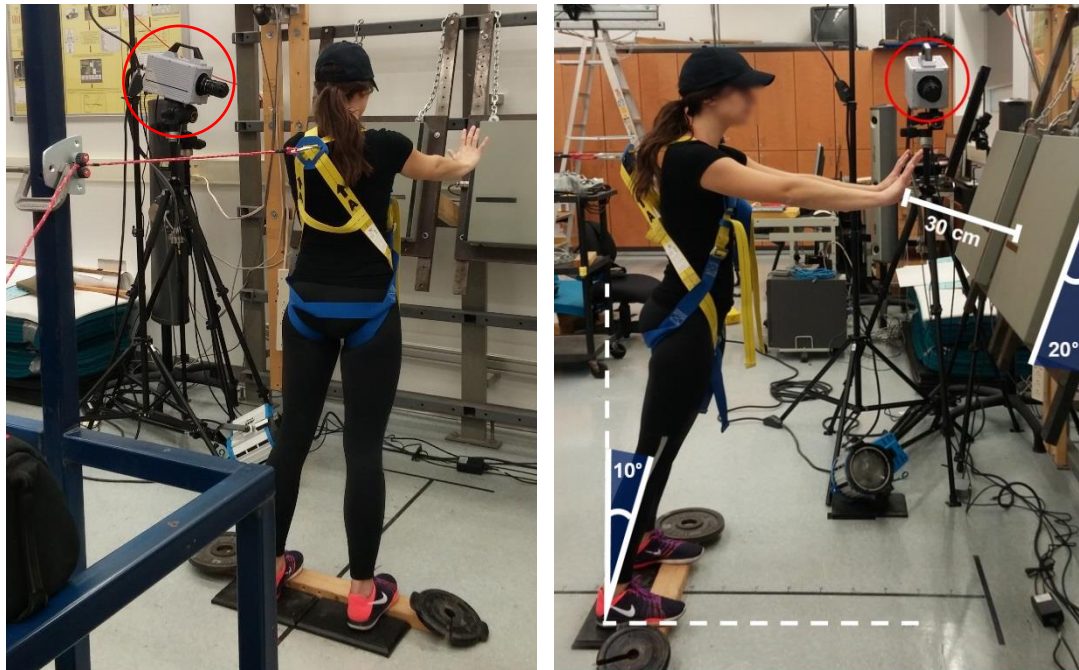
Figure 10. Schematic diagram of the torso-release apparatus and the location of the high speed camera and force plates: A) sagittal view; B) posterior view.

(McCordick Glove & Safety Inc., Cambridge, ON, Canada) around their trunk that was connected to a support cable. A manually-controlled quick release device securely affixed to a heavy, steel frame with a C-clamp (located 2 m from the force plates) acted as the attachment point for the support cable to hold the participant's body weight prior to initiating the forward fall simulation. The practical configuration of the quick release device allowed for its height to be easily adjusted along the length of the steel frame to account for the varying heights of the participants so that the support cable remained level with the ground and was not pulling the harness on an angle. Two force plates were rigidly mounted beside one another in front of the participant at an incline of approximately 20° to the vertical to aid in simulating the angles of the wrist (~30° to 45° extension) and forearm (~75° with respect to the ground) characteristic of the hand and forearm positions adopted when impacting the ground during a forward fall (Myers et al.,

44

1991; Greenwald et al., 1998; Troy et al., 2005; Burkhart et al., 2012a; Burkhart et al., 2014). Participants started each trial supported in a forward lean position just outside their base of support at approximately 10° with respect to the vertical and with a hand distance of approximately 30 cm from the force plates.

The main focus of the current study was to quantify planar (2D) displacement and velocity data, and shock attenuation capacity, of forearm soft tissue following hand impacts consistent with a forward fall on outstretched arms. Therefore, using a fall simulation technique that accommodated the requirements of our experimental set-up while also providing a reputable representation of real-life forward fall events was an important consideration when selecting an impact method. A key advantage of using this torso-release apparatus to generate impacts for automated motion tracking with ProAnalyst® was its ability to isolate the forward fall impact event in such a way that the camera and lighting used could be properly configured without being obstructed by the apparatus or participant. In addition, the capability of this impact method to produce consistent impact loads without the need of complex equipment, made it a feasible option with regard to repeatability, as well as cost and assembly in any laboratory.

3.2.3. Force Plates

The two force plates (AMTI, A-Tech Instruments Ltd, Scarborough ON, Canada, AMTI-OR6–6-1000; 1000 Hz natural frequency) that participants impacted were mounted side-by-side at an angle of 20° to the vertical on a steel grid frame anchored to the laboratory wall and floor. A black horizontal line was applied to the surface of each force plate to provide a clear target for participants to contact with the heel of their right

and left palms when arresting the forward fall (Figure 11). The 3D impact reaction forces (F_x, F_y, and F_z) from the plates were measured at a sampling rate of 1000 Hz and then normalized to each participant's body mass (Hwang et al., 2006; Kim & Ashton-Miller, 2003).
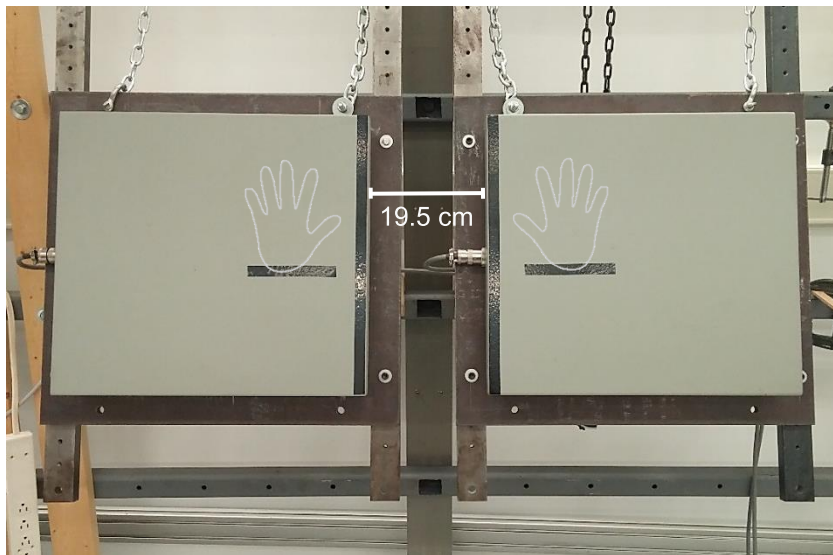
Figure 11. Participant point of view of the force plates mounted side-by-side with impact targets represented.

3.2.4. Laser Displacement Transducer

A non-contact laser displacement transducer (Acuity, Schmitt Measurement Systems Inc., Portland, OR, USA, AR700-50; sampling rate 9 kHz) was used to trigger and synchronize the collection of force and video data during the forward fall impact simulation. The laser displacement transducer was configured along the same plane as the force plates (20° to the vertical) such that the participants' hands would cross the laser beam at a distance of approximately 1 cm from the surface of the force plates, and subsequently trigger the data collection just prior to impact.

In order to reproduce the SLU marker design previously implemented by Brydges et al. (2015) on the distal upper extremity, a flexible plastic stencil (overhead transparency) with holes in a square grid arrangement was wrapped around the posterior, and lateral surface of the forearm. A designated row aligned along the midline of the posterior forearm, with the first marker positioned just lateral to the styloid process of the ulna, was used to ensure consistent marker placement between participants. Once the stencil was correctly positioned, a grid pattern of circular black surface markers (0.5 cm diameter), with a distance of 2 cm between adjacent markers, was then applied to the right forearm of each participant using permanent marker pen (Sharpie®, Newell Rubbermaid, Downers Grove, IL, USA) from the crease of the wrist joint (when in full extension) to just before the crease of the elbow joint (Figure 12). The number of marker columns allocated on each participant depended on the length of their forearm. During marker application, participants were seated with their forearm resting on a table in pronation (i.e., palm facing downward).

To create the SNU marker design on the surface of the forearm, circular white surface markers (~1 cm diameter) were manually drawn directly over top of the existing markers from the SLU marker pattern, creating a grid of white dots with the same inter-marker distance of 2 cm. Within each of these white dots, a contrasting black marker of random shape was also manually drawn, while maintaining an approximate diameter of 0.5 cm. Figure 13 provides a schematic diagram of the SNU marker design applied, demonstrating how this technique helped to standardize contrast across participants with different skin pigmentation. Specialty water-based paint markers (Sharpie®, Newell

Rubbermaid, Downers Grove, IL, USA) were used to apply the SNU marker design.

These markers are acid free and AP (Approved Product) certified that they contain no

materials in quantities that could cause either acute or chronic health problems.

Moreover, they are safe for use by children and require only soap and water to remove.
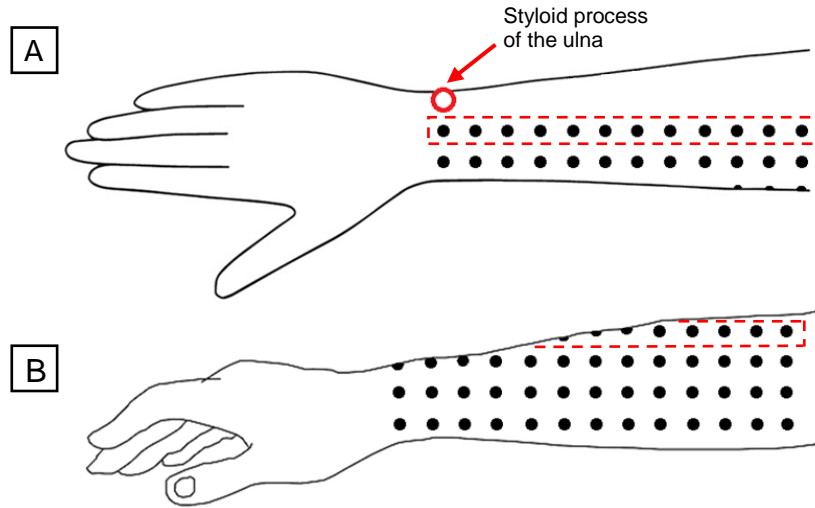
Figure 12. Schematic diagram of the SLU marker design (2 x 2 cm square grid of circular black dots of 0.5 cm diameter) on the forearm from A) posterior and B) lateral views.
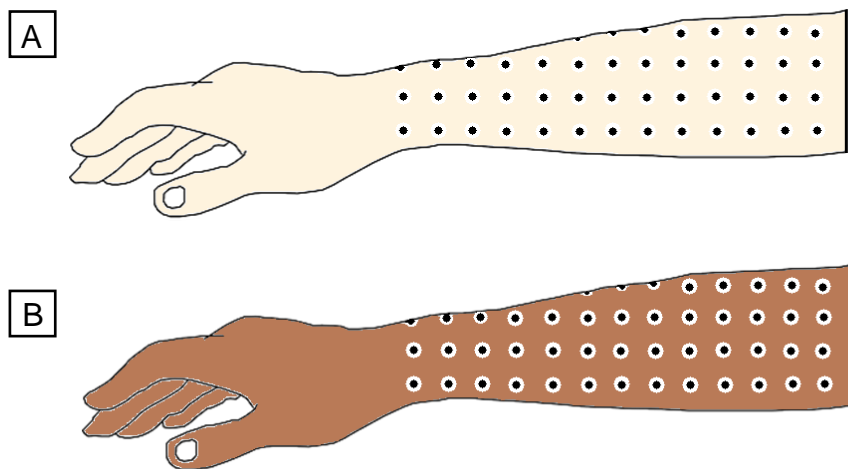
Figure 13. Schematic diagram of the SNU marker design (2 x 2 cm square grid of circular white dots of ~1 cm diameter with random black dots overlaid on top) on the forearm demonstrating the contrast for A) light and B) dark skin pigmentations.

A summary of the procedures followed in the study is provided in Figure 14.

Detailed descriptions of each procedure can be found in a separate section below.

Anthropometric measurements taken
for all participants

⬇

Measurements were input into equations to determine bone mineral content (BMC),
fat mass (FM), lean mass (LM), and wobbling mass (WM) of the forearm segment

⬇

The SLU marker design (grid of uniform, 0.5 cm diameter black dots; 2 cm inter-marker distance) was
applied to the right forearm of each participant (from the wrist joint to the elbow joint) using a black
permanent marker and flexible plastic stencils

⬇

Participants were subjected to three simulated forward fall hand impacts using a torso-
release apparatus with vertically mounted force plates, in which forearm soft tissue
motion was recorded with a high speed camera

⬇

The same impact protocol was repeated for the SNU marker design (non-uniform, ~0.5 cm diameter
black dots overlaid on top of a grid of contrasting ~1 cm diameter white dots; 2 cm inter-marker
distance), which was manually drawn over top of the SLU marker design on the right forearm of each
participant using white and black water-based paint markers.

⬇

All resultant videos (total of 6 impacts per participant) and impact reaction force data
were imported into ProAnalyst® motion analysis software

⬇

Video Analyses

⬇

Data Analyses

Figure 14. Flowchart of the procedures.

3.3.1. Anthropometric Measurements

Prior to marker application, a number of anthropometric measures (Table 4) were taken from the right forearm of each participant. These measures were used to estimate the BMC, FM, LM, and WM (FM + LM) of the right forearm using regression equations developed by Arthurs et al. (2009) for predicting upper extremity tissue masses in healthy, young adults (17–30 years). These tissue mass predictions were later used during data analysis to determine the relationship between the kinematic measures obtained and the individual forearm tissue masses.

Table 4. Prediction equations for bone mineral content (BMC), fat mass (FM), lean mass (LM), and wobbling mass (WM) tissues of the forearm (Modified from Arthurs et al., 2009).

Type of forearm tissue mass	Eq. no.
Bone mineral content mass (BMC) Y^I(forearm) $= -196.308 + 4.343(x4) + 37.94(x2) + 3.037(x1) + 2.333(x5) - 1.14(x6)$	4
Fat mass (FM) Y^I(forearm) $= 148.929 + 10.539(x6) + 1.996(x9) + 11.023(x13) - 180.851(x2)$	5
Lean mass (LM) Y^I(forearm) $= -2193.008 + 49.334(x4) - 24.651(x13) + 21.197(x15) + 26.796(x5) + 76.163(x16) + 339.118(x2) + 45.198(x11)$	6
Wobbling mass (WM) Y^I(forearm) $= -1492.793 + 22.131(x15) + 100.012(x11) + 4.948(x9) + 32.219(x5) + 90.268(x16)$	7

Note: Where: $x1$ = elbow circumference (cm), $x2$ = height (m), $x4$ = styloid circumference (cm), $x5$ = lateral forearm length (cm), $x6$ = posterior forearm skinfold (mm), $x9$ = body mass (kg), $x11$ = sex (0 for F, 1 for M), $x13$ = medial forearm skinfold (mm), $x15$ = mid-forearm circumference (cm), $x16$ = medial/lateral mid-forearm breadth (cm).

A total of seven surface measurements were taken using standard anthropometric measurement equipment (flexible measuring tape, anthropometer - Layfayette Instrument Company, Layfayette, IN, USA), and skinfold calipers (Slimguide®, Creative Health Products, Plymouth, MI, USA). This included one length, three circumferences, one

breadth, and two skinfold thicknesses (Appendix C). Good to excellent reliability has been previously established for these measurements for trained personnel (Burkhart et al., 2008).

3.3.2. Participant Preparation

All participants underwent one session of data collection, during which they were potentially required to shave the lateral and posterior aspect of their right forearm from the wrist to the elbow joint before testing the different massless skin surface marker designs. Data were collected on an SLU marker design involving a grid of uniform, circular black dots (0.5 cm diameter, 2 cm inter-marker distance) and a SNU marker design involving non-uniform black dots (~0.5 cm diameter) overlaid on top of a grid of uniform, circular white dots (1 cm diameter, 2 cm inter-marker distance). The application of both marker patterns was performed by the same investigator for all participants.

Prior to applying the markers, it was ensured that the skin on the participant's forearm was clean and free of any lotions that may have affected the application of the markers. The SLU marker design, utilizing the permanent marker pen to produce the grid pattern of circular black dots, was tested first. This allowed for the most efficient transition between testing the two marker designs, as the SNU marker design could then be applied directly over top of the SLU marker design, removing the need to wash the pattern off in between treatment conditions and, more importantly, eliminating any potential errors associated with the placement of the markers on the participant's forearm between the two impact trials. For the SNU marker design, additional time was permitted

before the impact trials (~5 minutes) to allow for each component of the design (i.e.,

larger white dots and smaller black dots) to properly set on the forearm using the water-

based paint markers. A designated area set-up at a nearby sink served as a washing

station for marker removal. Soap, water, and towels were provided for the participants to

remove the markers once all impact trials for the data collection process were completed.

3.3.3. Impact Protocol

Following the appropriate participant preparation procedures for each of the two

marker designs, each participant underwent a set of three forward fall impacts per design

for a total of six impacts in all. The distance at which participants stood from the force

plates was standardized according to the length of their upper extremity reach from the

force plates at 90° of shoulder flexion with fully extended arms (Hwang et al., 2006).

While maintaining vertical body alignment in this posture, the investigator used a

measurement scale on the floor to record the distance of their feet from the force plates

(Figure 15). From this mark, the position of their feet was moved back an additional 60

cm to determine the final distance the participant would stand from the force plates; this

parameter was determined during preliminary testing of the impact protocol using trial

and error. An elevated platform (72 x 9 x 4 cm) was then placed at this distance and

reinforced with weights (Figure 15). Similar to the torso-release design employed by

Kim & Ashton-Miller (2003), participants stood on the narrow platform in a mid-foot

stance to prevent ankle plantarflexion and participants resisting the forward motion with

the balls of their feet during the fall simulation.

**Figure 15. Picture of the measurement scale used to standardize the distance participants
stood from the force plates on the elevated platform.**

Next, the targets for the location of the heel of the palm were adjusted up or down

on the force plates to match the position at which the participants' forearms were at ~ 75°

with respect to the force plates (i.e., ground) at impact (refer to Figure 11). A hand

distance of approximately 30 cm from the force plates was held constant between all

trials and participants by making slight adjustments to the amount of slack on the support

cable (refer to Figure 10).

Since one of the main objectives of the impact protocol was to acquire consistent

impacts across all trials, the participant was instructed to contact the target on the force

plates with their arms in full elbow extension to control for differences in natural fall-

arrest strategies between participants affecting the impact forces. Moreover, rather than

starting the fall simulation with their arms at their sides, the participants began with their

shoulders flexed and arms extended to remove the need for ballistic arm movements at close distances to stop their forward motion; an action that has been shown to result in significantly different peak impact forces across different age groups (Kim & Ashton-Miller, 2003). Throughout the trial, participants were also asked to imitate the fall of a broomstick by maintaining the vertical alignment of their head, trunk, and lower extremities (Hwang et al., 2006; Kim & Ashton-Miller, 2003). Finally, although upper extremity muscle activation levels were not directly controlled, participants were instructed to keep their upper extremities relatively relaxed prior to the release of the support cable in an attempt to attain a better representation of the initial passive effects of shock wave transmission through the soft tissues during an unintentional forward fall scenario.

Once the torso-release apparatus was properly modified to the appropriate specifications for each participant, and they understood the guidelines for executing the forward fall, practice trials were executed to allow a familiarization period with the impact protocol. During this time, a general idea of the participant's average impact force was determined. Impact trials started in a controlled forward lean of approximately 10° with the cable supporting the participant's body weight. Each impact trial had a randomized release time between 0 and 5 seconds to prevent participants from anticipating the initiation of the fall; this was controlled by the investigator pulling the support cable free from the quick release device.

For each participant, the variability of the impact forces (F_z) on the right hand across all trials had to fall within a 10–15% range of their body weight (BW) in order to help ensure consistent impacts for each marker design; this range was determined during

preliminary testing of the torso release apparatus. If the trial had an impact force within this range, it was recorded and the impact protocol was reset to perform the next trial. Those trials with an impact force outside of this range were most likely attributable to the participant not maintaining proper upper extremity and body postures throughout the impact, specifically at the elbow joint. In the event that this occurred, the participant was given verbal feedback regarding their posture from the investigator as well as the recorded impact trial on a computer monitor (e.g., elbow flexion could clearly be seen on the video record as the forearm would rotate inferiorly after hand impact), and the trial was repeated.

3.3.4. Video Analysis

Videos of forearm soft tissue motion recorded for each impact trail were imported into ProAnalyst® motion tracking software (Xcitex, Cambridge, MA, USA). As per Brydges et al. (2015), prior to analysis, all videos were subjected to the same calibration process to properly calibrate both the scale and coordinate system for automated tracking. First, to convert pixels to centimetres, a 6 cm distance between four adjacent markers in the same row was set as the calibration unit (Figure 16). Second, the planar (2D) axes of the coordinate system were set in two directions: X (parallel with the long axis of the radius and ulna, running in the proximal-distal direction) and Y (perpendicular to the long axis of the radius and ulna, running in the anterior-posterior direction of the forearm).
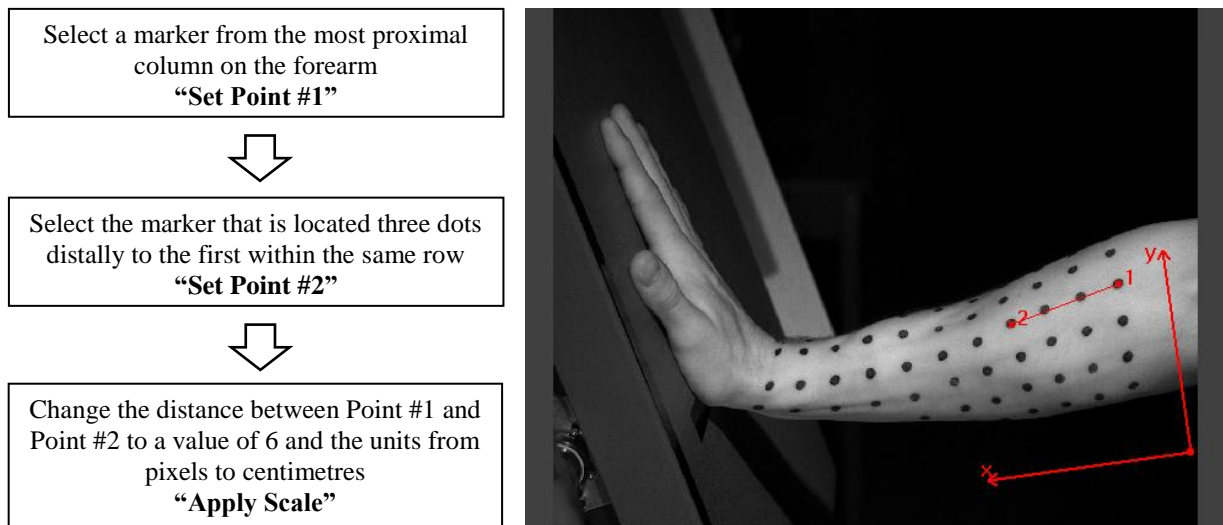
Figure 16. ProAnalyst® calibration process performed for all videos.

A single image filter [Convolve: Sharpening (3 x 3 Center)] was applied to the videos to slightly enhance the overall sharpness of the raw video footage (i.e., contrast and marker edge detection). In addition, the "frames to search after loss" feature provided in the software (determines how many frames to search for a particular marker once the marker has been lost) was set to a low number (i.e., two frames) to optimize the number of markers retained throughout the entire impact duration, as suggested by Brydges et al. (2015). Analysis of the markers began prior to the heel of the palm impacting the force plate at the earliest possible frame where all markers, specifically those located most distally, were visible within the field of view, until the point when soft tissue motion caused by the impact had ceased. A total of between approximately 100 and 230 ms (or approximately 500 and 1150 images) were analyzed for each video across all participants.

The grid of markers on the forearm was segmented into four zones (similar to Brydges et al. (2015) for the leg) during video analysis, wherein two columns of markers

56

(A and B) were selected at 0 %, 25 %, 50 %, and 75 % of the distance from the styloid

process of the ulna to the joint space of the elbow (Figure 17 and Figure 18). Following

appropriate marker selection, automated 2D motion tracking was performed in

ProAnalyst® and the resultant X and Y position coordinates of each selected marker were

outputted. The search parameters were held the same for all markers that were

automatically tracked. The search region multiplier (%) was set to a fairly conservative

value of 125% due to the relative closeness of adjacent markers, especially the larger

diameter SNU markers, and the matching threshold tolerance (0.0–1.0) was kept at the

default value of 0.75.
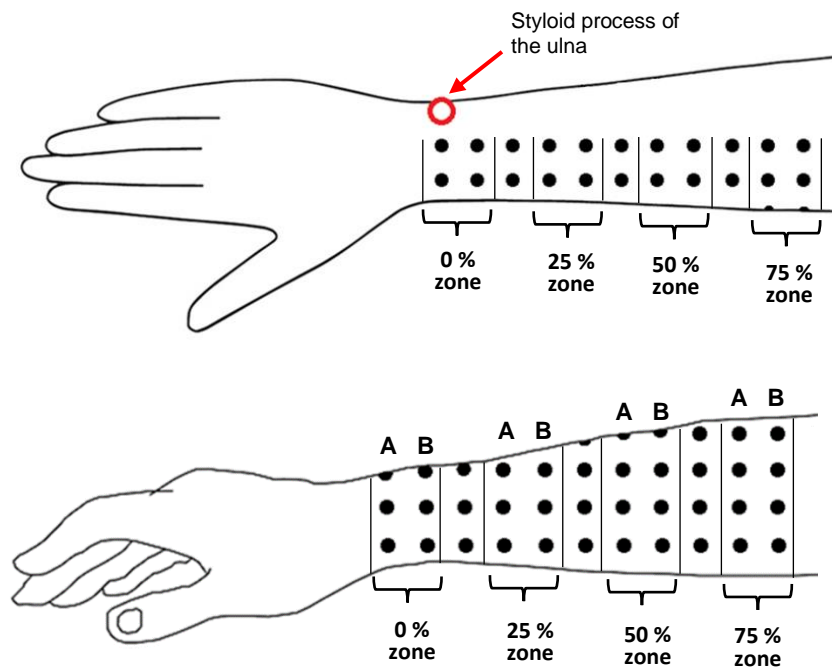
Figure 17. Schematic diagram of the marker grid pattern (2 x 2 cm squares of dots) and the four analysis zones (0%, 25%, 50%, and 75%) on the forearm.
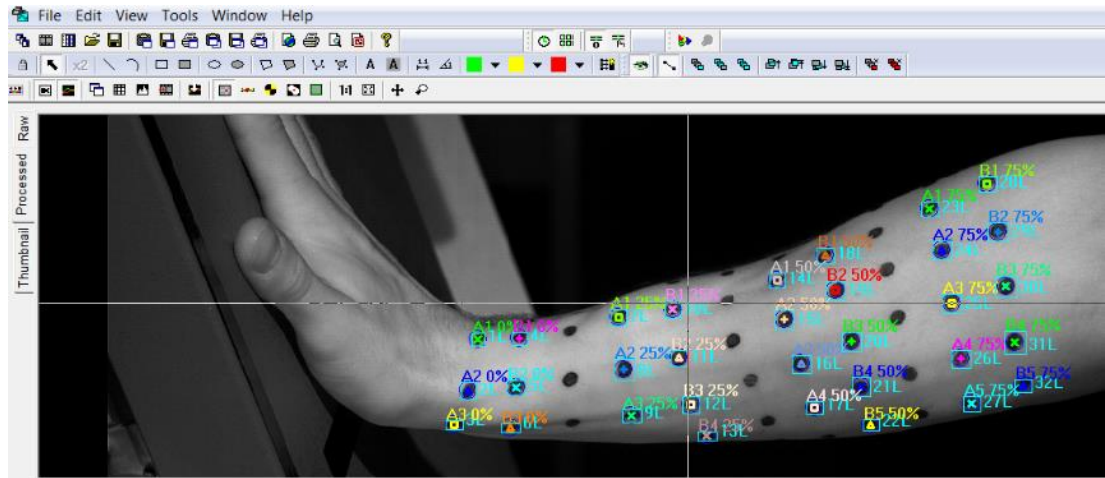
Figure 18. Screenshot from ProAnalyst® (zoomed in) showing the two columns of markers (A and B) selected for the 0%, 25%, 50%, and 75% zones.

3.4. Data Analysis

A total of 10 dependent variables were assessed in relation to the planar (2D) movement of forearm soft tissue following hand impacts consistent with a forward fall on outstretched arms; this included, peak displacement (cm) and velocity (cm/s) in the proximal, distal, anterior, and posterior directions, as well as two additional variables of proximal and posterior rebound distance (cm) from peak displacement in the distal and anterior directions, respectively. To incorporate the potential for differences in these kinematic variables because of soft tissue distribution, each of the four zones (0%, 25%, 50%, 75%) were further split into anterior and posterior regions by visually dividing the forearm in half (Brydges et al., 2015), and ensuring that a relatively equal number of markers were allocated to both sides (Figure 19). Therefore, eight separate regions were established along the forearm to be analyzed. Within each of these regions, a single marker was selected for soft tissue displacement and velocity analyses. Marker selection from each region was random, however, due to the small number of markers within the

0% zone at the wrist, there were a few instances that occurred in which only one marker was available to be selected from region 1 and/or 2.
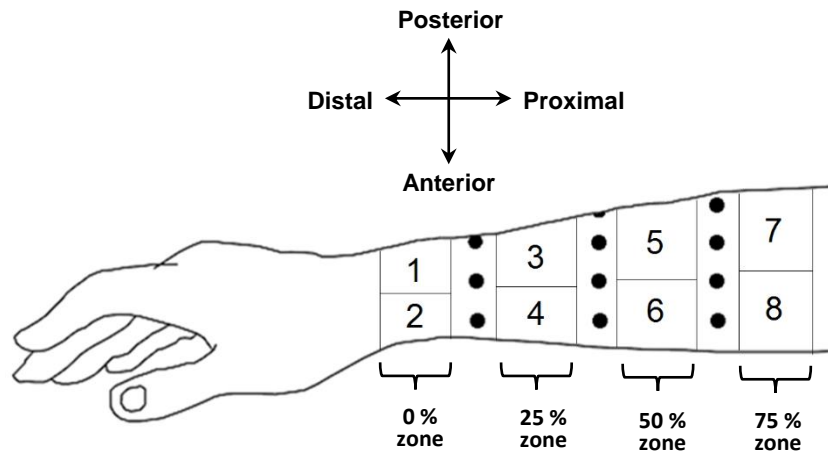
Figure 19. Schematic diagram of the marker grid (2 x 2 cm squares of dots) and the eight regions on the forearm.

Shock attenuation of the forearm soft tissue was also quantified (using Equation 2) based on the mean peak accelerations (cm/s^2) along the proximal-distal axis calculated from two markers located closest to the posterior aspect of the forearm at the most proximal and distal columns near the elbow and wrist joint (Figure 20). Ideally, it was thought that the location of these markers should mimic the placement of accelerometers used in previous studies investigating the acceleration response of the forearm during simulated forward fall impacts (distal accelerometer: posterior surface of the distal forearm, medial to the radial styloid; proximal accelerometer: over the olecranon process of the ulna) (Burkhart & Andrews, 2010a; 2010b). However, this was not entirely feasible given the camera view. Therefore, these specific markers were selected to be as close as possible to these locations, while having a high visibility to ensure that they could be tracked throughout the entirety of the impact without marker drop out.
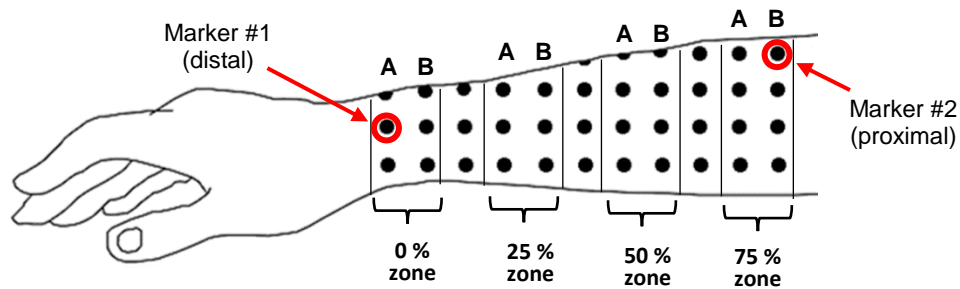
Figure 20. Schematic diagram of the most distal and proximal markers used for calculating shock attenuation in the forearm.

The planar (2D) marker position coordinates from ProAnalyst® were imported into a customized LabVIEW program (LabVIEW® 2016, National Instruments, Austin, TX, USA) where they were converted to displacement data and filtered at a cut-off frequency of 60 Hz using a dual-pass, fourth-order Butterworth lowpass digital filter. As per Winter (2005), a residual analysis was performed in order to determine the cut-off frequency. Filtered displacement data were differentiated using 2nd order central finite differences to calculate velocity and acceleration. The dependent variables were then outputted as Excel (.xlsx) data files for subsequent data analyses.

Establishing a method to isolate forearm soft tissue motion caused by the impact consistently across all trials was an important consideration in the data analysis process. Generally, it was observed that the fingers were the first part of the distal upper extremity to impact the force plate; however, the point of contact varied between participants (i.e., distal phalanx first versus fingers and palm flush with the force plate). Therefore, it was decided that the specific onset point at which to trigger the analysis of the filtered kinematic data should correspond to the moment the heel of the palm fully contacted the force plate and the forearm ceased the "free-fall" phase of the forward fall simulation.

60

In order to determine this onset point, a graphical representation of the filtered kinematic data associated with the X (proximal-distal) axis was used (Figure 21). Specifically, the investigator utilized the velocity curve (in green) to identify the onset point by visually selecting the knee point in the curve where the velocity in the distal direction began to rapidly decrease from a relatively constant value; the point at which the acceleration curve (red) started decelerating from zero. The process used by the investigator for selecting this knee point is further explained in Figure 21. For each participant, the onset point was based on the kinematic data from most distal marker closest to the site of impact (i.e., the heel of the palm), which was then subsequently applied to all remaining markers.
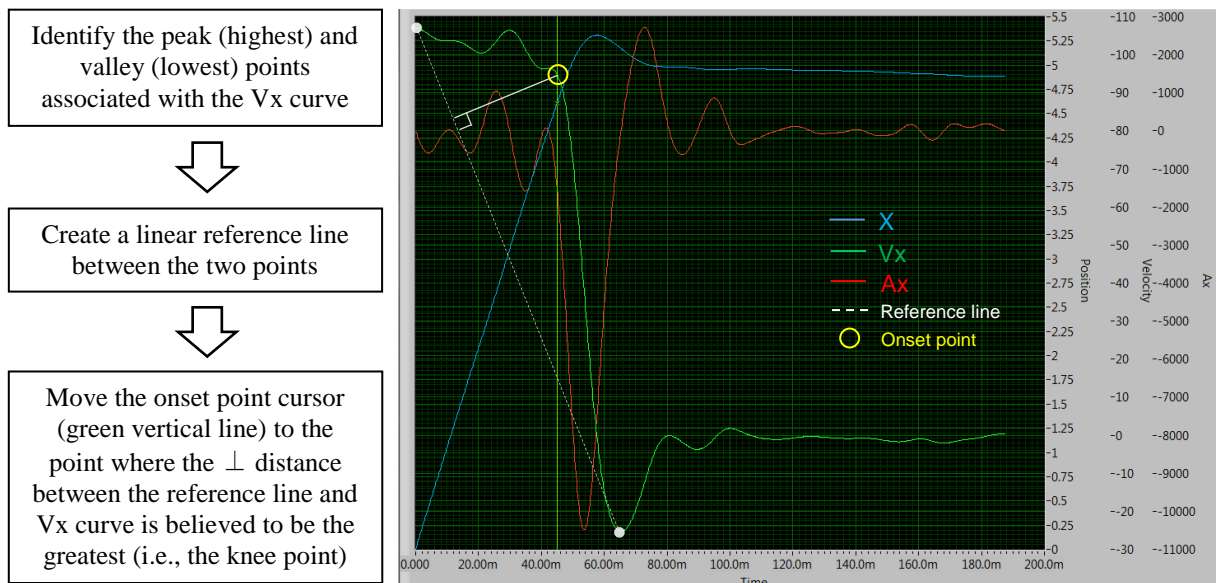
Figure 21. Onset point analysis procedures showing the graphical representation of the displacement (X), velocity (Vx), and acceleration (Ax) curves along the proximal-distal axis.

<u>3.4.1. Statistical Analysis</u>

All of the statistical tests were executed using SPSS 24 (IBM SPSS Statistics, IBM Corporation, Somers, NY, USA). Preliminary data screening was performed for each data set to identify any erroneous values (e.g., miss-keyed or unrealistic values) and potential outliers.

Purpose 1: quantify planar (2D) displacement and velocity of, and the amount of shock attenuated by, the soft tissues of the forearm following a forward fall impact;

Mean peak marker displacements and velocities were obtained by taking the average of the three impact trials from the SLU marker design in the proximal-distal and anterior-posterior directions for the marker selected in each region. Mean peak accelerations at the designated proximal and distal markers near the elbow and wrist joint (see Figure 20) were used to quantify the impact shock attenuated by the forearm soft tissues.

Purpose 2: assess if there are differences in soft tissue motion and impact shock attenuation due to sex, or as a function of the region of the forearm measured;

Two-Way Mixed Analyses of Variance (ANOVA) with sex (female, male) as the between-subject factor and forearm region (1–8) as the within-subject factor were used to examine any mean differences in the dependent measures of soft tissue displacement and velocity (from the SLU marker design trials) due to passive soft tissue movement of the forearm. Both Mauchly's Test of Sphericity and Levene's Test for Equality of Variance were used to assess the variance assumptions of the within-subject factors and between-subject factor. Post Hoc tests for pairwise comparisons were performed for any

significant main effects that were found, and if any significant interactions were revealed, simple effects tests were conducted as well. Differences in the shock attenuation capacity of the forearm soft tissue between females and males were assessed using Independent Samples T-tests. Normality of all dependent variables was assessed using Shapiro-Wilk tests and Q-Q Plots, respectively.

Purpose 3: identify the relationship between the displacement, velocity, and shock attenuation capacity of the forearm soft tissues and their individual tissue masses (BMC, FM, LM, and WM);

Pearson correlation analyses were performed to determine the relationship between the magnitudes of individual tissue masses (BMC, FM, LM, and WM) and the displacement, velocity, and shock attenuation capacity of the soft tissues in the forearm from the SLU marker design trials.

Purpose 4: determine if a stacked, non-uniform (SNU) marker design (non-uniform, ~0.5 cm diameter black dots overlaid on top of a grid of contrasting ~1 cm diameter white dots; 2 cm inter-marker distance) produces significantly different kinematic results and improves automated marker tracking across different skin pigmentations compared to the single layer, uniform (SLU) marker design (grid of uniform, 0.5 cm diameter black dots; 2 cm inter-marker distance) previously established by Brydges et al. (2015).

Three-Way Mixed ANOVAs (between-subject factor: skin pigmentation (light, dark); within-subject factor: marker design (SLU, SNU); within-subject factor forearm region (1–8)) were also performed to examine if the dependent measures of soft tissue

displacement and velocity differed between the light and dark skin pigmentation groups depending on the marker design applied to the skin and/or the region of the forearm being tracked. Appropriate statistical tests (as stated above) were used to assess the variance assumptions for each factor and to identify any significant findings as well.

In addition to the aforementioned statistical analyses, the reliability of the torso-release apparatus was also examined using Repeated Measures ANOVAs and Intraclass Correlation Coefficients (ICCs), as per Burkhart and Andrews (2010a), to compare the peak impact reaction forces recorded across each of the six trials. Good to excellent reliability was accepted for ICCs greater than 0.75 (Portney & Watkins, 2000). To determine if participants impacted their right and left hands similarly during the impact protocol, Independent Samples T-tests were performed to compare the peak impact forces as well (Burkhart & Andrews, 2010a). An alpha of 0.05 was implemented for all statistical comparisons.

4. RESULTS

During preliminary data screening of the dependent variables obtained in relation to forearm soft tissue motion, any potential outliers (z-score > 3.29) were examined to determine the source of their variability. Outliers that were the result of data entry or measurement error were simply corrected to the appropriate value. The value of any remaining outliers was visually verified against the automated motion tracking in ProAnalyst® to ensure that they were representative of genuine soft tissue motion, and therefore, were kept in the data analysis. For example, two participants demonstrated consistently high proximal and posterior displacement values, respectively, across all regions. However, since these values corresponded to the actual soft tissue motion in their forearm, their data were included in the analyses. Alternatively, two separate participants revealed relatively extreme outliers with respect to anterior soft tissue displacement. After video analysis, it was determined that these values were not due to authentic soft tissue motion, but rather a violation of the impact protocol guidelines as the upper extremity showed elbow flexion following impact. As a result, this caused significant inferior motion of the forearm, which contributed to the production of these high measures of anterior displacement. Consequently, their data were excluded from all subsequent analyses.

No statistically significant differences were found for the mean peak impact reaction forces (IRFs) across all six impact trials for each marker design (i.e., impact trials 1–3: SLU; impact trials 4–6: SNU) and between left and right hands ($p > 0.05$) (Table 5). Moreover, all ICCs were greater than 0.75, suggesting excellent reliability between impact trials for the torso-release apparatus.

Overall, participants impacted each force plate with an average force of approximately 600 N, which translated to an impact force of approximately 90% BW (Table 5 and 6). Males had higher mean peak IRFs than females, impacting the force plates with an average force just above 100% BW compared to just below 80% BW for females (Table 6). These values were deemed to be physiologically safe as they were in accordance with the results from prior studies that simulated forward fall impacts while utilizing a stiff-arm landing (DeGoede & Aston-Miller, 2002; Robinovitch & Chiu, 1998), and were also well below critical impact levels previously shown to induce structural harm to the distal radius in vitro (Burkhart et al., 2012a; Greenwald et al., 1998; Troy & Grabiner, 2007b).

Table 5. Mean (±SD) overall, female, and male peak IRFs (N) across the six trials for each hand. ICC values are included for between trials. No significant differences were found for any variable.

Overall	Trial 1		Trial 2		Trial 3		Trial 4		Trial 5		Trial 6		Mean	ICC
R	618.9	(215.0)	620.7	(225.6)	618.7	(229.4)	612.6	(215.4)	610.2	(223.6)	609.0	(223.7)	615.0	0.994
L	607.3	(216.7)	616.0	(212.1)	613.1	(213.0)	601.8	(203.7)	598.1	(224.3)	630.2	(219.5)	611.1	0.984
Female														
R	493.5	(96.2)	486.5	(104.8)	487.1	(112.1)	483.2	(85.5)	476.2	(105.6)	477.1	(104.4)	483.9	0.985
L	472.0	(118.3)	489.4	(127.2)	483.6	(117.3)	479.4	(112.8)	462.6	(119.2)	495.2	(116.4)	480.4	0.976
Male														
R	807.0	(207.8)	821.8	(208.7)	816.1	(220.1)	806.6	(206.4)	811.1	(202.8)	806.9	(209.5)	811.6	0.995
L	810.2	(165.1)	805.8	(167.7)	807.2	(172.7)	785.4	(168.7)	801.2	(188.8)	832.8	(177.4)	807.1	0.979

Note: Trial 1–3 = SLU marker design; Trial 4–6 = SNU marker design

Note: SD = standard deviation; IRF = impact reaction force; ICC = intraclass correlation coefficient; R = right hand; L= left hand

Table 6. Mean (±SD) overall, female, and male peak normalized IRFs as a percentage (%) of BW across the six trials for each hand. ICC values are included for between trials. No significant differences were found for any variable.

Overall	Trial 1		Trial 2		Trial 3		Trial 4		Trial 5		Trial 6		Mean	ICC
R	90.6	(23.4)	90.6	(24.6)	90.2	(25.0)	89.5	(23.0)	88.9	(24.2)	88.7	(23.9)	89.7	0.989
L	88.6	(24.1)	90.1	(24.3)	89.8	(24.5)	88.1	(22.6)	87.0	(24.7)	92.2	(24.9)	89.3	0.972
Female														
R	80.1	(15.8)	78.8	(15.5)	78.7	(16.4)	78.3	(13.4)	76.9	(15.3)	77.0	(14.5)	78.3	0.983
L	76.3	(18.0)	79.1	(18.8)	78.5	(19.5)	78.0	(19.1)	74.9	(18.2)	80.4	(19.5)	77.9	0.973
Male														
R	106.3	(24.8)	108.3	(25.5)	107.5	(26.3)	106.2	(24.7)	106.7	(24.5)	106.2	(25.0)	106.9	0.994
L	106.9	(20.5)	106.7	(22.7)	106.7	(21.8)	103.3	(19.1)	105.3	(22.2)	109.9	(22.0)	106.5	0.975

Note: Trial 1–3 = SLU marker design; Trial 4–6 = SNU marker design
Note: SD = standard deviation; IRF = impact reaction force; BW = body weight; ICC = intraclass correlation coefficient; R = right hand; L= left hand

4.1. Purpose 1

*Quantify planar (2D) displacement and velocity of, and the amount of shock
attenuated by, the soft tissues of the forearm following a forward fall impact.*

4.1.1. Soft Tissue Displacement

Overall, the greatest amount of forearm soft tissue displacement occurred in
region 8 following impact, where the distal displacement reached a mean peak magnitude
of 1.47 cm (Table 7). In contrast, the least amount of soft tissue displacement overall
occurred proximally in region 2 with a mean peak magnitude of only 0.02 cm.
Individually, females (1.52 cm) and males (1.39 cm) also experienced the greatest
amount displacement in region 8 as the soft tissue moved in the distal direction toward
the wrist. The least amount of soft tissue displacement for each sex was found in the
proximal direction (0.01 cm), however, this occurred in region 2 for females and in
region 8 for males, respectively. With respect to the anterior and posterior directions, the
greatest amount of overall displacement occurred anteriorly in region 7 with a mean peak
magnitude of 1.32 cm, whereas the overall posterior soft tissue displacement was very
low (≤ 0.08 cm) across all regions. These findings were reflected across both sexes as the
greatest anterior movement of forearm soft tissue was observed in region 7 for females
(1.29 cm) and males (1.36 cm).

Predominantly in the distal and anterior directions, a general trend of consistently
increasing displacements was observed, moving proximally in the forearm (i.e., from 0%,
25%, 50%, 75%), when the posterior (1, 3, 5, 7) and anterior (2, 4, 6, 8) regions of the
forearm are viewed separately (Table 7).

Table 7. Mean (±SD) overall, female, and male peak soft tissue displacement (cm) in the proximal, distal, anterior and posterior directions for each of the eight regions.

	Regions															
Overall	**1**		**2**		**3**		**4**		**5**		**6**		**7**		**8**	
Distal	0.64	(0.12)	0.75	(0.14)	1.11	(0.20)	1.21	(0.22)	1.12	(0.21)	1.31	(0.23)	1.10	(0.20)	1.47	(0.24)
Proximal	0.05	(0.08)	0.02	(0.06)	0.09	(0.13)	0.03	(0.08)	0.10	(0.14)	0.05	(0.10)	0.05	(0.11)	0.03	(0.11)
Anterior	0.24	(0.13)	0.23	(0.12)	0.55	(0.15)	0.49	(0.19)	0.95	(0.32)	0.82	(0.37)	1.32	(0.45)	1.09	(0.51)
Posterior	0.08	(0.08)	0.07	(0.10)	0.05	(0.09	0.06	(0.09)	0.05	(0.10)	0.06	(0.11)	0.06	(0.12)	0.07	(0.13)
Female																
Distal	0.67	(0.12)	0.78	(0.15)	1.14	(0.15)	1.29	(0.17)	1.16	(0.17)	1.37	(0.18)	1.12	(0.18)	1.52	(0.18)
Proximal	0.03	(0.05)	0.01	(0.03)	0.11	(0.15)	0.03	(0.09)	0.13	(0.15)	0.07	(0.11)	0.07	(0.12)	0.05	(0.13)
Anterior	0.18	(0.08)	0.18	(0.08)	0.52	(0.16)	0.47	(0.19)	0.91	(0.28)	0.77	(0.35)	1.29	(0.46)	1.07	(0.51)
Posterior	0.09	(0.09)	0.06	(0.10)	0.05	(0.09)	0.06	(0.10)	0.06	(0.12)	0.06	(0.13)	0.07	(0.14)	0.08	(0.15)
Male																
Distal	0.61	(0.13)	0.71	(0.11)	1.05	(0.25)	1.10	(0.24)	1.07	(0.26)	1.23	(0.28)	1.06	(0.23)	1.39	(0.30)
Proximal	0.07	(0.11)	0.04	(0.09)	0.05	(0.09)	0.03	(0.07)	0.05	(0.10)	0.02	(0.06)	0.03	(0.08)	0.01	(0.03)
Anterior	0.33	(0.13)	0.30	(0.13)	0.60	(0.14)	0.53	(0.19)	1.00	(0.38)	0.90	(0.40)	1.36	(0.45)	1.13	(0.53)
Posterior	0.07	(0.08)	0.07	(0.09)	0.05	(0.09)	0.06	(0.09)	0.04	(0.08)	0.05	(0.08)	0.04	(0.08)	0.06	(0.11)

Forearm soft tissue velocities in the distal direction demonstrated the greatest magnitudes overall across all regions ($\geq$ 90.9 cm/s): the greatest distal velocity occurred in region 7 with a mean peak value of 112.8 cm/s; the smallest soft tissue velocities overall occurred in the posterior direction ($\leq$ 27.6 cm/s) (Table 8). In agreement with these overall results, females and males both experienced the greatest mean peak velocities when the soft tissue moved distally after impact; region 7 had the greatest velocities (female: 110.3 cm/s; male: 116.6 cm/s).

Region 7 also possessed the greatest mean peak velocity in the anterior direction for females and males with magnitudes of 63.8 cm/s and 57.3 cm/s, respectively. Alternatively, proximal velocities were found to be the greatest closer to the wrist in region 3 for females (61.2 cm/s) and males (68.9 cm/s). Consistent with the trends observed for soft tissue displacement, when examining the posterior and anterior regions of the forearm as separate entities, a pattern of increasing velocities was observed, mostly in the distal and anterior directions, when moving proximally up the forearm toward the elbow (Table 8).

Table 8. Mean (±SD) overall, female, and male peak soft tissue velocity (cm/s) in the proximal, distal, anterior and posterior directions for each of the eight regions.

							Regions									
Overall	**1**		**2**		**3**		**4**		**5**		**6**		**7**		**8**	
Distal	90.9	(13.6)	99.4	(13.1)	103.8	(13.9)	106.2	(13.4)	108.4	(15.8)	107.3	(14.1)	112.8	(16.2)	109.9	(14.1)
Proximal	33.8	(10.2)	31.2	(10.9)	64.3	(14.1)	55.6	(9.4)	59.1	(12.9)	59.0	(10.0)	48.4	(13.3)	61.1	(12.0)
Anterior	34.6	(10.0)	36.1	(10.4)	43.7	(9.7)	42.6	(10.2)	56.5	(13.3)	48.6	(12.5)	61.2	(14.9)	49.3	(13.6)
Posterior	16.9	(8.6)	13.9	(7.0)	15.7	(7.6)	15.6	(7.8)	24.2	(11.1)	18.5	(8.4)	27.6	(11.9)	19.0	(9.8)
Female																
Distal	88.9	(13.4)	96.6	(12.8)	100.6	(12.4)	103.4	(12.6)	105.5	(14.4)	104.3	(13.1)	110.3	(14.7)	107.6	(13.4)
Proximal	32.7	(10.3)	29.7	(9.7)	61.2	(11.5)	55.3	(6.9)	57.0	(9.8)	57.5	(7.8)	45.9	(11.0)	59.8	(10.9)
Anterior	32.1	(8.5)	34.3	(9.5)	42.8	(10.4)	43.2	(10.7)	58.9	(12.9)	48.3	(13.0)	63.8	(15.7)	49.3	(15.5)
Posterior	20.3	(8.7)	15.6	(7.0)	15.1	(6.1)	16.8	(7.7)	25.9	(10.4)	18.0	(7.3)	30.4	(11.3)	19.8	(8.8)
Male																
Distal	94.0	(14.0)	103.6	(12.9)	108.7	(15.2)	110.3	(14.0)	112.9	(17.4)	111.7	(14.9)	116.6	(18.4)	113.4	(15.0)
Proximal	35.4	(10.2)	33.4	(12.5)	68.9	(16.6)	56.0	(12.5)	62.2	(16.6)	61.4	(12.7)	52.0	(15.9)	62.9	(13.8)
Anterior	38.4	(11.3)	38.8	(11.5)	44.9	(8.8)	41.7	(9.7)	52.9	(13.5)	49.1	(12.3)	57.3	(13.2)	49.3	(10.9)
Posterior	11.8	(5.5)	11.3	(6.4)	16.6	(9.6)	13.9	(8.0)	21.5	(11.9)	19.1	(10.1)	23.4	(12.1)	17.8	(11.5)

4.1.3. Soft Tissue Shock Attenuation

An overall lack of shock attenuation was demonstrated in the soft tissues of the
forearm following forward fall impacts, as the magnitudes of mean peak accelerations
were found to increase by approximately 76% moving from the distal accelerations near
the wrist (9385.8 cm/s^2) to the proximal accelerations near the elbow (16298.9 cm/s^2);
this trend was consistent for both females and males (Table 9). Shock attenuation
measures are later normalized to tissue mass (BMC, FM, LM, and WM) in section 4.2.7.
Sex and Soft Tissue Shock Attenuation.

Table 9. Mean (±SD) overall, female, and male peak soft tissue distal and proximal accelerations
(cm/s^2) of the forearm and un-normalized calculations of shock attenuation (%).

| | Peak Accelerations | | | | Shock Attenuation | |
	Distal		Proximal		Un-normalized	
Overall	9385.8	(2322.0)	16298.9	(3894.9)	-76.1	(24.8)
Female	9108.9	(2132.7)	15956.7	(3589.7)	-76.3	(17.5)
Male	9801.0	(2621.3)	16812.2	(4427.3)	-75.8	(33.9)

4.2. Purpose 2

Assess if there are differences in soft tissue motion and impact shock attenuation
due to sex, or as a function of the region of the forearm measured.

All dependent variables concerning soft tissue displacement and velocity were
approximately normally distributed, as assessed by Shapiro-Wilk's test ($p > 0.05$) and
Q-Q Plots, with the exception of mean peak proximal and posterior displacement.
During automated tracking of the forearm soft tissue motion, it was discovered that the
majority of markers did not return past the onset point in these two directions (below
Figure 22 demonstrates this motion pathway in the proximal-distal axis). As a result,

73

zero values were commonly produced for these peak displacement outputs, which lead to very positively skewed distributions. Although the two-way mixed ANOVA is fairly robust to deviations from normality, two additional variables assessing the rebound distance of the marker in each of these directions (i.e., the distance that the marker traveled in the proximal and posterior direction from the peak displacement in the distal and anterior direction, respectively) were also analyzed to help compensate for these violations.
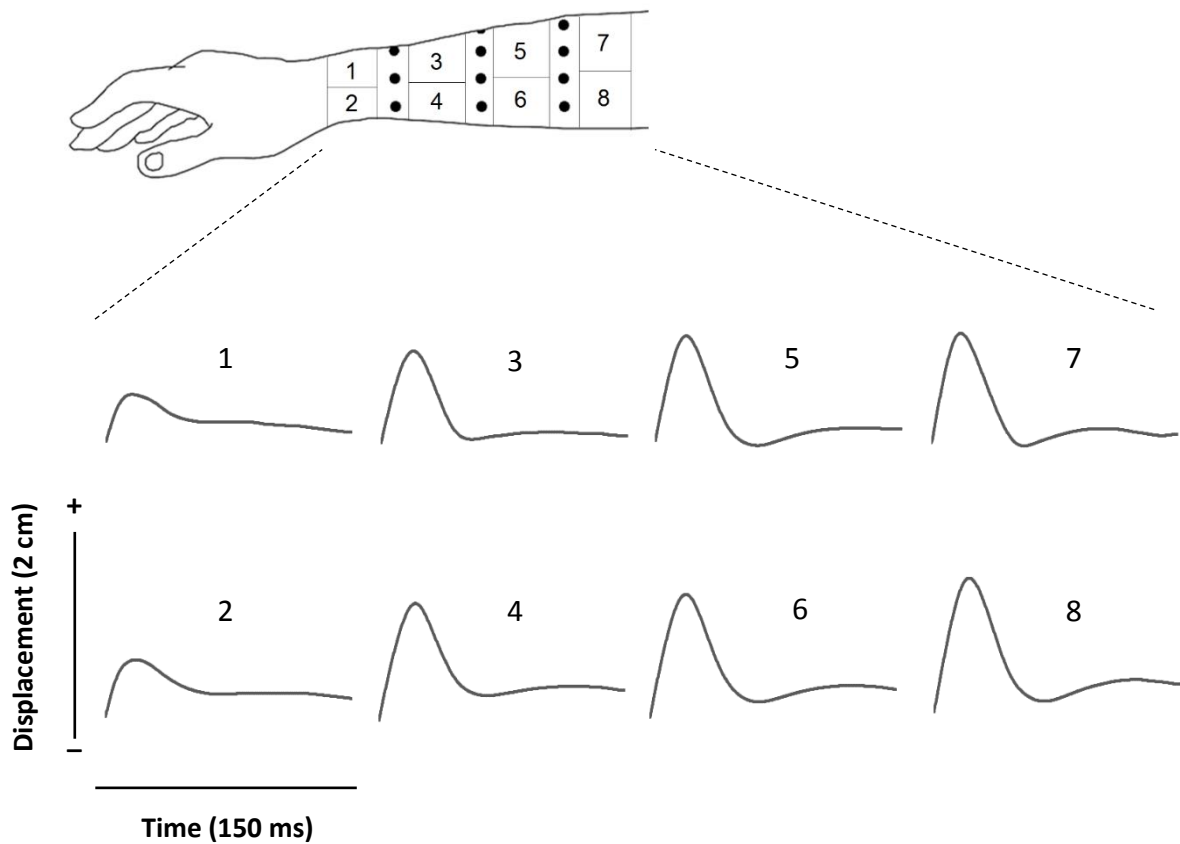
Figure 22. Sample displacement curves (proximal-distal axis) for each of the eight regions across the forearm for a single trial from one participant. The curves from each region have been aligned in time and displacement in order to show the relative differences.

74

It should be noted that the variances of the dependent variables between females and males for all regions of the forearm were homogeneous ($p > 0.05$), apart from proximal displacement in regions 1 and 2, anterior displacement in region 1, and posterior rebound distance in region 6 and 8. Within these regions, the variances for the males was found to be approximately double that of the females, consistently. Mauchly's Test of Sphericity was found to be significant ($p \leq 0.05$) for each dependent variable, therefore, corrected Greenhouse-Geisser estimates were used for all the following analyses.

4.2.1. Sex and Soft Tissue Displacement

There were no significant main effects of Sex for mean peak displacement in the distal [$F(1, 28) = 2.707$, $p = 0.111$, partial $\eta^2 = 0.088$], proximal [$F(1, 28) = 0.461$, $p = 0.503$, partial $\eta^2 = 0.016$], anterior [$F(1, 28) = 1.030$, $p = 0.319$, partial $\eta^2 = 0.035$], or posterior [$F(1, 28) = 0.109$, $p = 0.744$, partial $\eta^2 = 0.004$] directions. No significant differences were found between females and males for mean peak posterior rebound distance [$F(1, 28) = 0.009$, $p = 0.926$, partial $\eta^2 = 0.000$], however, a significant main effect of Sex was present for proximal rebound distance [$F(1, 28) = 8.123$, $p = 0.008$, partial $\eta^2 = 0.225$], in which the soft tissue of females on average rebounded approximately 22% further than males (Figure 23).
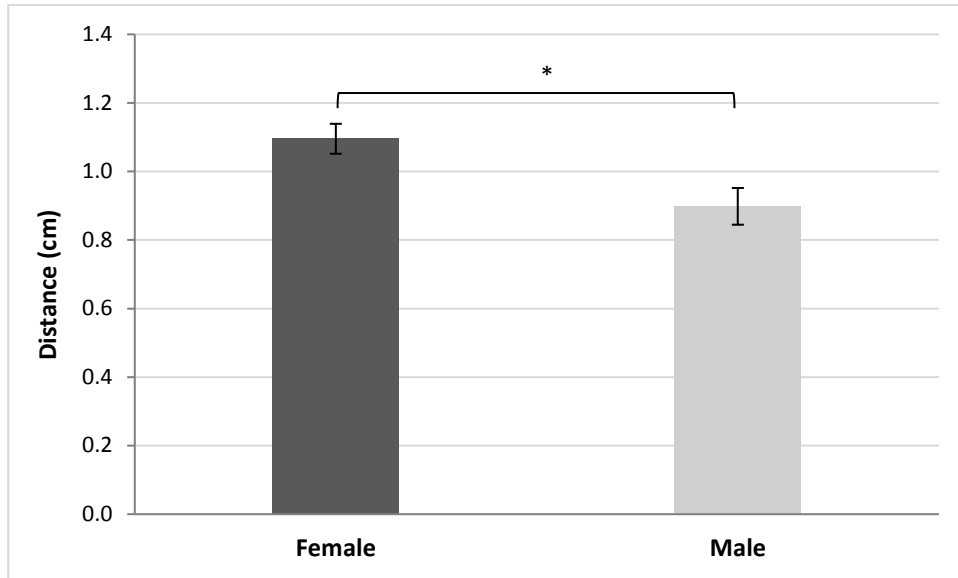
Figure 23. Mean (SE) peak soft tissue rebound distance in the proximal direction between females and males.

4.2.2. Region and Soft Tissue Displacement

A significant main effect of Region was found for mean peak distal [$F(2.588, 72.473) = 203.974$, $p = 0.000$, partial $\eta^2 = 0.879$] (Figure 24) and proximal [$F(2.640, 73.911) = 5.825$, $p = 0.002$, partial $\eta^2 = 0.175$] (Figure 25) displacement. Moving from more distal (i.e., near the wrist) to proximal (i.e., near the elbow) regions of the forearm, moderate increases in distal soft tissue displacement were observed (e.g., compared to region 1, there was 75% more displacement in region 5 and 128% in region 8, respectively). Significant consecutive increases in distal soft tissue displacement were seen across all anterior regions of the forearm (2, 4, 6, and 8) ($p \leq 0.05$), whereas the posterior regions only showed one significant increase in distal soft tissue displacement from region 1 to regions 3, 5, and 7 ($p \leq 0.05$). On average, the distal displacement in the anterior regions of the forearm was 19% greater than the posterior regions. Mean peak

soft tissue displacements in the proximal direction had very low magnitudes, averaging less than 0.10 cm for all regions. As a result, mean peak tissue displacement distally was found to be over 21 times greater in magnitude than proximally. Region 5 demonstrated the largest proximal displacement of any region (0.09 cm), which was significantly greater than regions 4, 6, 7, and 8 ($p \leq 0.05$).
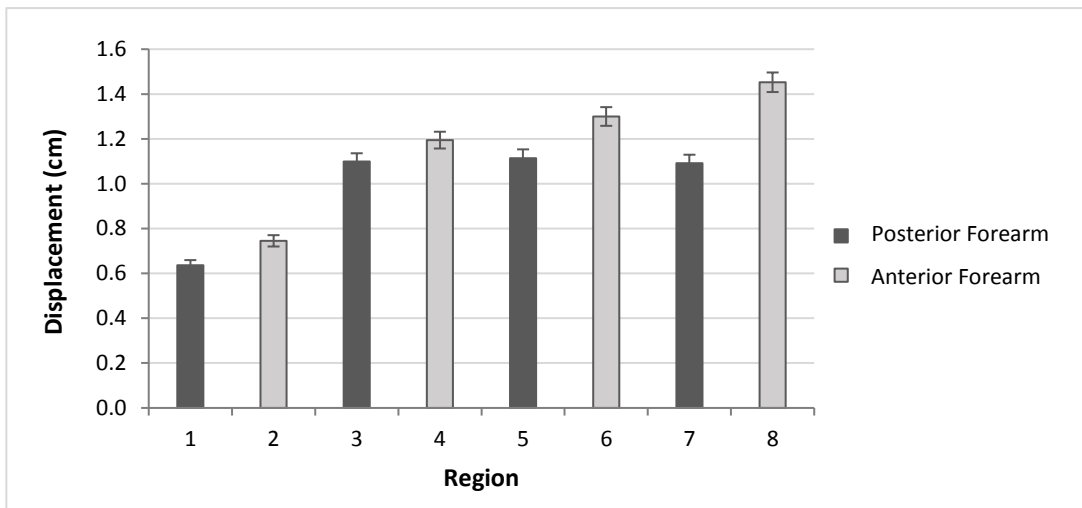
Figure 24. Mean (SE) peak soft tissue displacement in the distal direction for each region.
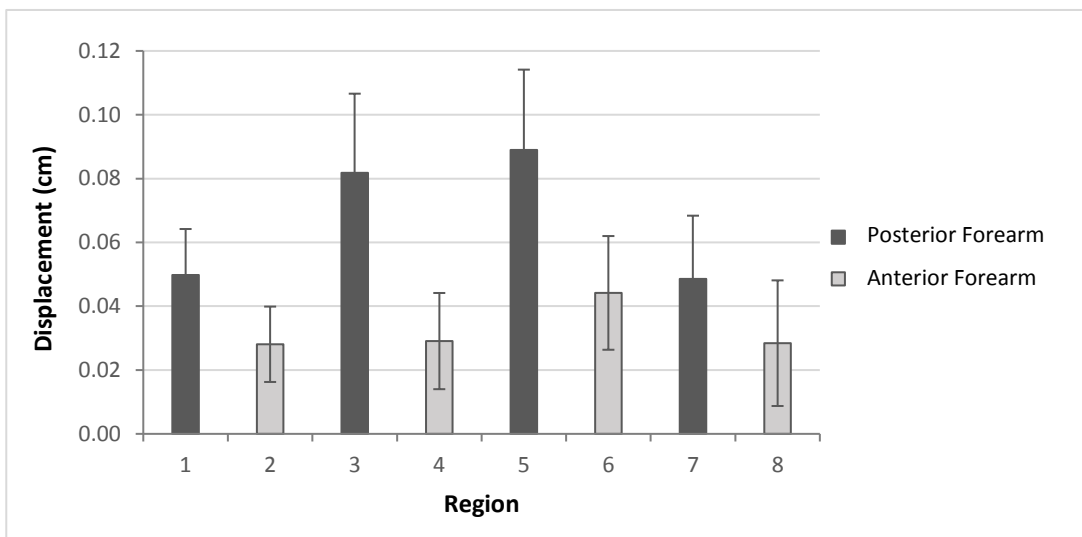
Figure 25. Mean (SE) peak soft tissue displacement in the proximal direction for each region.

A significant main effect of Region was found for mean peak soft tissue displacement in the anterior direction [$F(1.563, 43.776) = 107.967$, p = 0.000, partial η^2 = 0.794] (Figure 26), but not for the posterior direction [$F(2.261, 63.294) = 1.686$, p = 0.190, partial η^2 = 0.057]. Significant increases were observed in anterior soft tissue displacement for anterior and posterior regions of the forearm, separately, moving distally to proximally (p ≤ 0.05). Unlike the moderate increases seen with soft tissue motion in the distal direction, the increases in anterior displacement were notably steeper. Comparing displacements between anterior and posterior regions showed no significant differences for multiple pairs (p > 0.05); this included, regions 1 and 2, regions 3 and 4, as well as regions 5 and 8. However, on average, the soft tissue in the proximal regions of the forearm had 16% greater anterior displacement than the anterior regions. Region 7 had the greatest anterior displacement (1.32 cm); a value that was significantly higher than all other remaining regions (p ≤ 0.05).
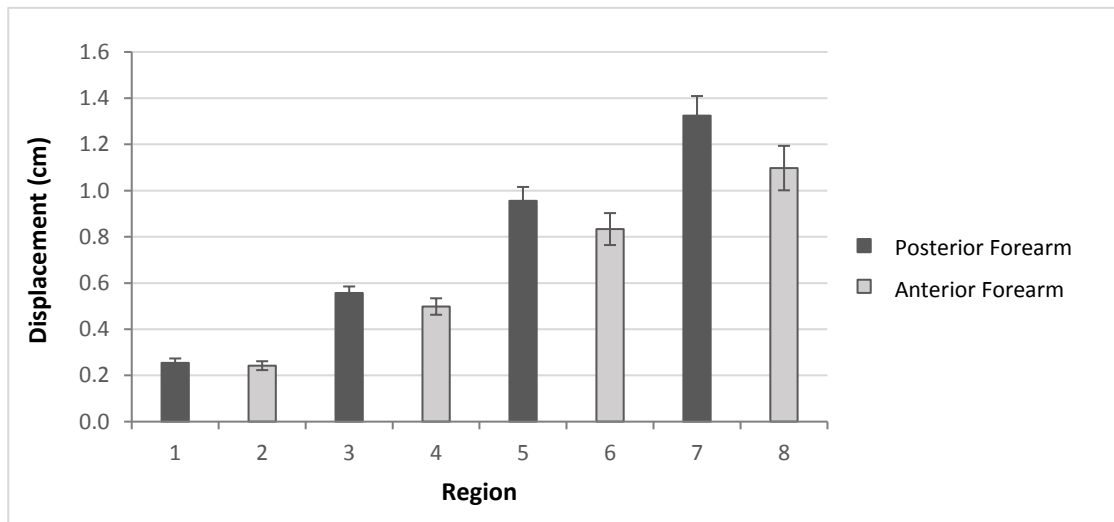
Figure 26. Mean (SE) peak soft tissue displacement in the anterior direction for each region.

With respect to the mean peak rebound distance of the forearm soft tissue, significant main effects of Region were found for both distance traveled in the proximal [$F(3.111, 87.115) = 129.623$, p = 0.000, partial $\eta^2 = 0.822$] (Figure 27) and posterior [$F(2.334, 65.362) = 44.412$, p = 0.000, partial $\eta^2 = 0.613$] directions (Figure 28). For mean peak proximal rebound distance, distal regions near the wrist (1 and 2) demonstrated significantly lower rebound values, on average traveling nearly less than half the distance of regions 3 through 8. The intermediate regions (i.e., 3–6) did not significantly differ in proximal rebound distances back toward the elbow (p > 0.05), ranging from 1.04 (region 4) to 1.19 cm (region 6), while the soft tissue rebound distance of region 8 (1.27 cm) was the significantly greatest value across all regions (p ≤ 0.05).
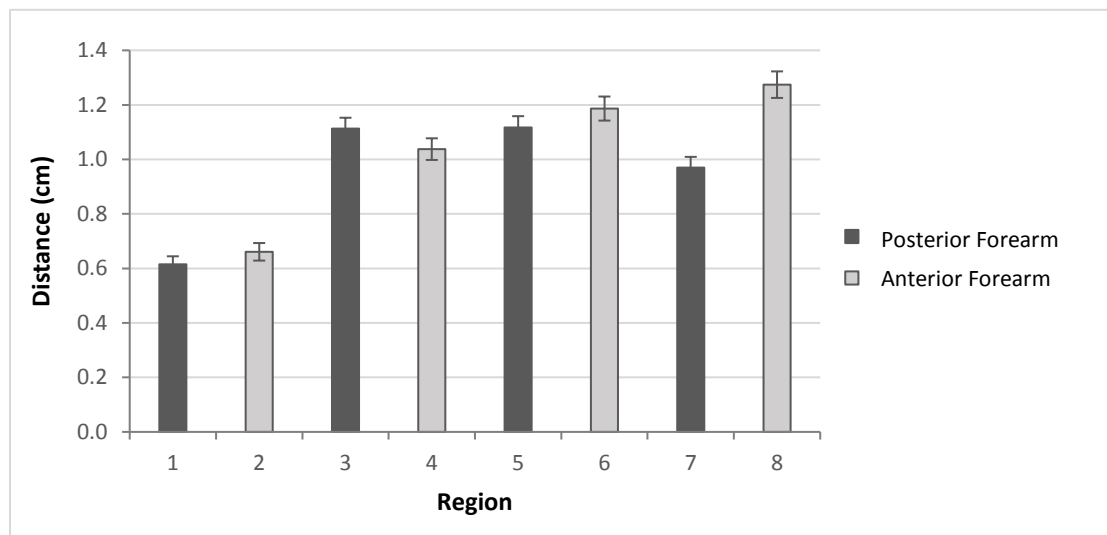
Figure 27. Mean (SE) peak soft tissue rebound distance in the proximal direction for each region.

Similar to the mean peak rebound distance in the proximal direction, regions 1 and 2 were found to have significantly lower posterior rebound distances compared to the remaining proximal regions (i.e., 3–8) of the forearm (p ≤ 0.05). Furthermore, although

79

the differences between the following pairs of regions were not significant (with the exception of region 5 and 6), when analyzing the posterior and anterior regions of the forearm within each zone (i.e., 0%, 25%, 50%, and 75) the posterior regions, in general, rebounded a greater distance compared to anterior regions.
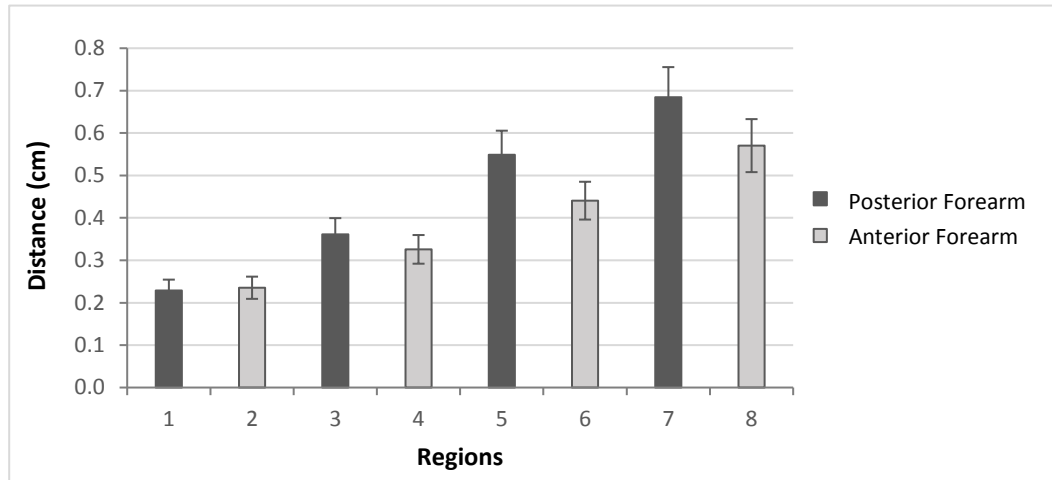
Figure 28. Mean (SE) peak soft tissue rebound distance in the posterior direction for each region.

4.2.3. Sex, Region, and Soft Tissue Displacement

A significant interaction effect between Sex and Region was present for mean peak proximal soft tissue displacement [$F(2.640, 73.911) = 4.201$, p $= 0.011$, partial $\eta^2 = 0.130$] (Figure 29), but not for displacement in the distal direction [$F(2.588, 72.473) = 1.279$, p $= 0.288$, partial $\eta^2 = 0.044$]. Analysis of the simple main effects showed that there were no significant differences for Sex on the proximal displacement of soft tissue across all regions of the forearm (p > 0.05). There was a statistically significant simple main effect of Region on proximal displacement for females [$F(2.167, 36.846) = 7.497$, p $= 0.001$, partial $\eta^2 = 0.306$], however, this result was not shared for males [$F(1.843,$

80

20.270) = 3.511, p = 0.052, partial η^2 = 0.242]. For females, there were significant differences in the mean peak proximal displacement between two region comparisons (p ≤ 0.05), including: region 3 (0.11 cm) and region 7 (0.07 cm), and region 5 (0.13 cm) compared to region 6 (0.07 cm) and region 7 (0.07 cm). Soft tissue displacement in the proximal direction did not significantly differ in any region for males (p > 0.05).
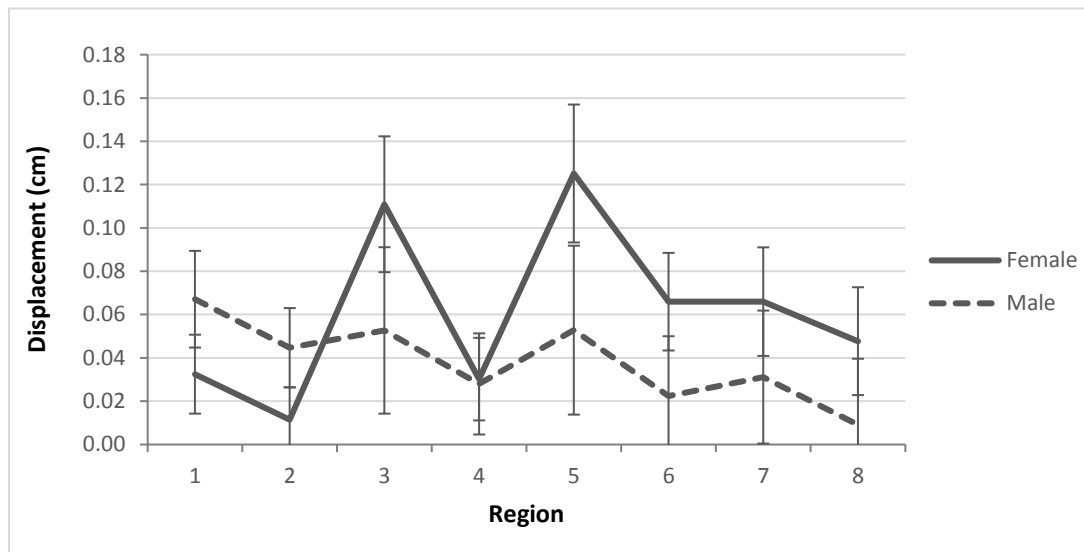
Figure 29. Interaction effect of Sex and Region (1-8) on proximal displacement.

While there were no significant interactions in the anterior [$F(1.563, 43.776)$ = 0.225, p = 0.744, partial η^2 = 0.008] or [$F(2.261, 63.294)$ = 0.004, p = 0.422, partial η^2 = 0.031] and posterior directions for mean peak soft tissue displacement, a significant interaction effect was revealed between Sex and Region for proximal peak mean rebound distance [$F(3.111, 87.115)$ = 6.724, p = 0.000, partial η^2 = 0.194] (Figure 30). An analysis of simple main effects found significant differences in proximal rebound distance between sexes, wherein females had significantly more soft tissue rebound proximally toward the elbow joint for regions 3 through 8 (p ≤ 0.05). Statistically

significant simple main effects of region on proximal rebound distance were also found

for both females [$F(3.256, 55.360) = 108.691$, p = 0.000, partial $\eta^2 = 0.865$] and males

[$F(2.521, 27.735) = 40.026$, p = 0.000, partial $\eta^2 = 0.784$]. Both sexes demonstrated

similar patterns across the regions of the forearm, in which region 1 (female: 0.62 cm;

male: 0.61 cm) and region 2 (female: 0.69 cm; male: 0.63 cm) had significantly smaller

values than the remaining regions. More specifically, females and males both had

significant differences between five different region comparisons; three of which they

had in common. No significant interaction was found for posterior mean peak rebound

distance [$F(2.334, 65.362) = 1.921$, p = 0.148, partial $\eta^2 = 0.064$].
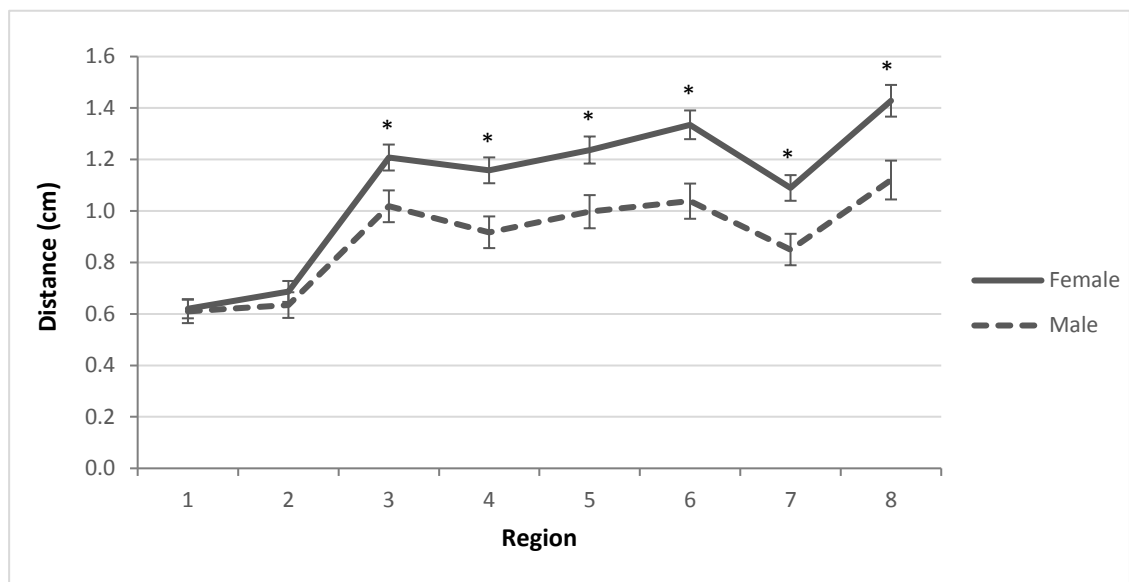
Figure 30. Interaction effect of Sex and Region (1-8) on proximal rebound distance (* = statistically significant at p ≤ 0.05).

4.2.4. Sex and Soft Tissue Velocity

There were no significant main effects of Sex for mean peak velocity in any of the directions analyzed (distal [$F(1, 28) = 1.787$, p = 0.192, partial $\eta^2 = 0.060$], proximal [$F(1, 28) = 1.235$, p = 0.276, partial $\eta^2 = 0.042$], anterior [$F(1, 28) = 0.000$, p = 0.993, partial $\eta^2 = 0.000$], and posterior [$F(1, 28) = 1.857$, p = 0.184, partial $\eta^2 = 0.062$]).

4.2.5. Region and Soft Tissue Velocity

A significant main effect of Region was found for mean peak velocity in the distal [$F(1.655, 46.351) = 71.817$, p = 0.000, partial $\eta^2 = 0.719$] (Figure 31) and proximal [$F(4.107, 115.001) = 114.332$, p = 0.000, partial $\eta^2 = 0.803$] (Figure 32) directions. Velocity in the distal direction demonstrated very gradual increases from distal to proximal zones of the forearm for posterior and anterior regions, respectively. Distal soft tissue velocities for all regions were significantly greater than regions 1 (91.4 cm/s) and 2 (100.1 cm/s), while the velocity occurring in region 7 (113.4 cm/s) was the fastest overall (p ≤ 0.05). No significant differences in distal velocity were observed between region 2 and 3, region 4, 5, and 6, as well as region 5 and 8 (p > 0.05). Overall, the velocities achieved during distal soft tissue movement toward the wrist and hand were the greatest in magnitude compared to all other directions.
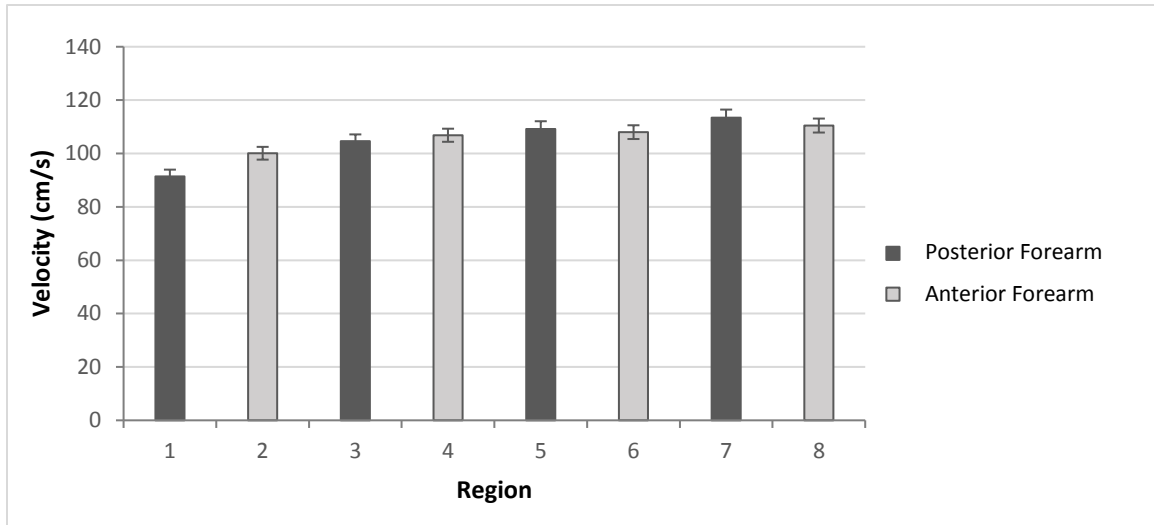
Figure 31. Mean (SE) peak soft tissue velocity in the distal direction for each region.

The mean peak soft tissue velocities in the proximal direction demonstrated a significantly sharp increase, more than doubling in magnitude, from 31.5 cm/s to 65.1 cm/s when moving proximally from the 0% zone (regions 1 and 2) to the 25% zone (regions 3 and 4) ($p \leq 0.05$). This transition was consistent throughout the remaining proximal regions, as all intermediate and distal regions (i.e., 3–8) were found to be significantly greater than regions 1 and 2 ($p \leq 0.05$). The largest proximal velocity of these regions was found in region 3 (significantly greater than ($p \leq 0.05$) regions 4–7), while the slowest was found in region 7 (significantly less than ($p \leq 0.05$) regions 4–8). Furthermore, from the 25% to 75% (regions 7 and 8) zones of the forearm, proximal velocity in the posterior regions incrementally decreased a total of 25% from region 3 to region 7 and, in contrast, anterior regions began to slowly increase by 10% from region 4 to region 8.
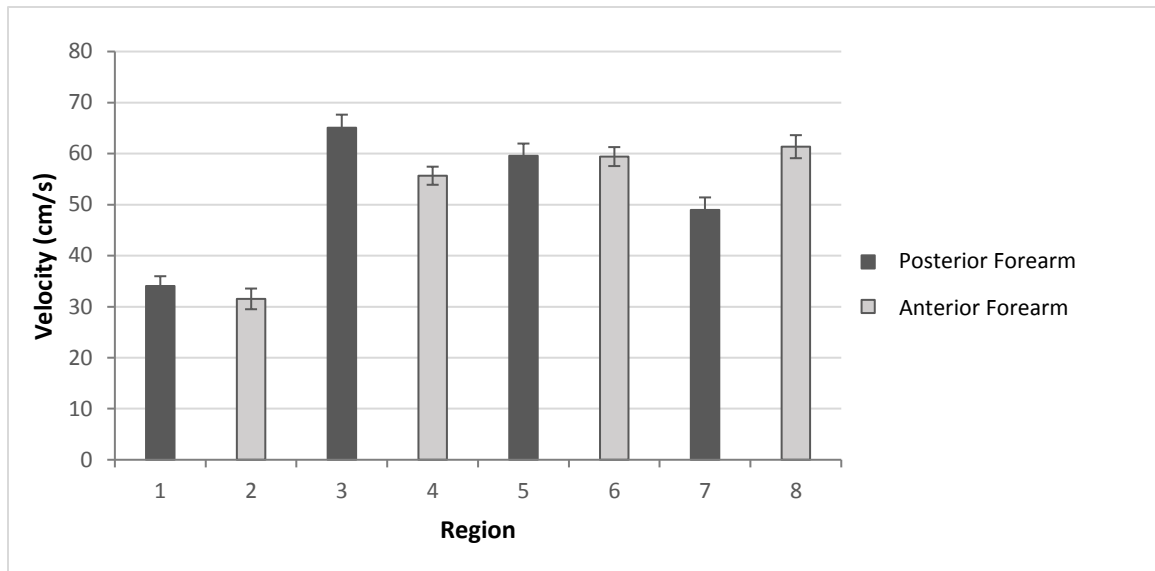
Figure 32. Mean (SE) peak soft tissue velocity in the proximal direction for each region.

Significant main effects of Region were also observed for mean peak velocity in the anterior [$F(2.556, 71.566) = 45.792$, p = 0.000, partial $\eta^2 = 0.621$] (Figure 33) and posterior [$F(3.504, 98.105) = 13.805$, p = 0.000, partial $\eta^2 = 0.330$] (Figure 34) directions. Following the same progression as soft tissue velocities in the distal and proximal directions, anterior velocities in regions 3 through 8 were significantly greater than those distal velocities near the wrist (i.e., regions 1 and 2) (p ≤ 0.05). Moreover, a distinct pattern emerged when comparing anterior velocities across the anterior and posterior regions of the forearm, in which the velocities of the posterior regions were increasingly faster than those of the anterior regions within the same zone moving proximally (e.g., 25% zone: + 3%; 50% zone: + 15%; 75% zone: + 23%); this trend compares favourably to the findings from both mean peak anterior displacement as well as mean posterior rebound distance. The greatest velocities in the anterior direction were

found in region 5 (55.9 cm/s) and region 7 (60.6 cm/s), which did not differ significantly in magnitude (p > 0.05).
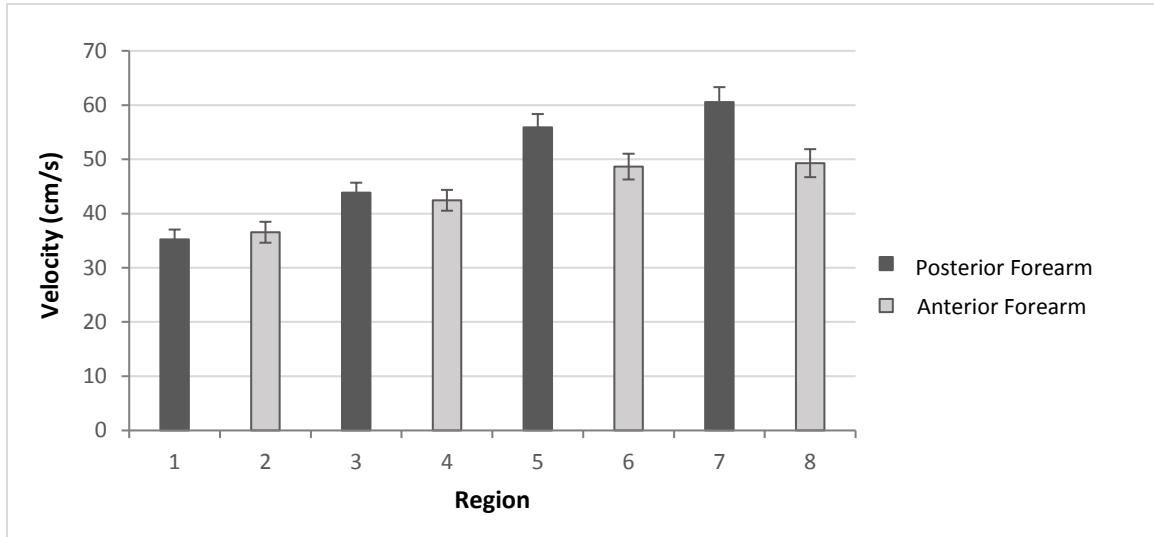

Figure 33. Mean (SE) peak soft tissue velocity in the anterior direction for each region.

For mean peak velocities in the posterior direction, no significant differences in magnitude were observed for the designated soft tissue regions located in the distal half of the forearm (i.e., regions 1–4). Conversely, significant differences in the proximal half of the forearm (i.e., regions 5–8) showed significantly greater values of posterior velocity for region 5 (23.7 cm/s) compared to all other regions, with the exception of region 8, and region 7 (26.9 cm/s).
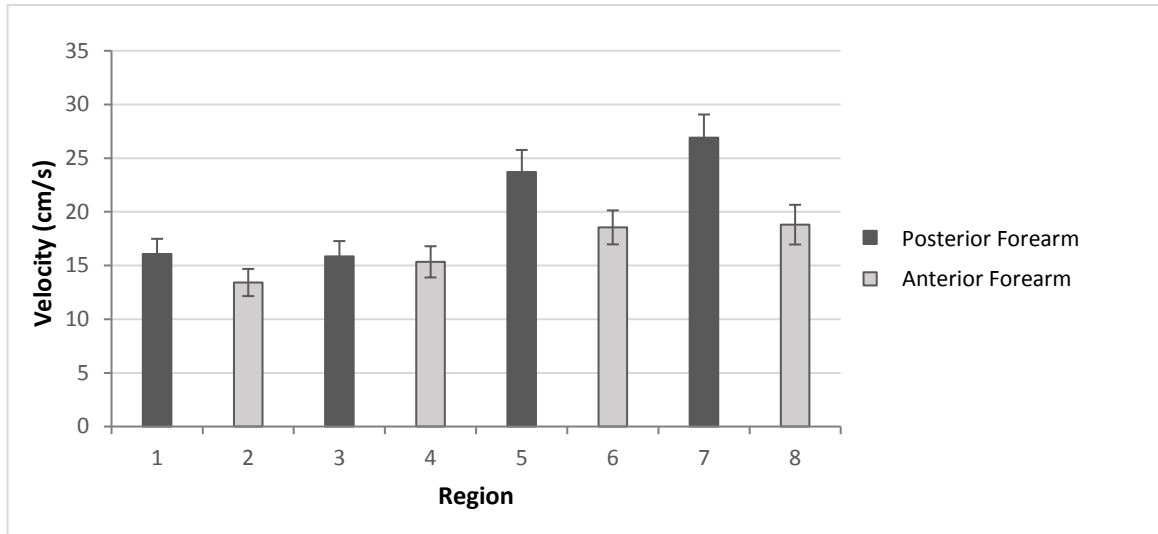
Figure 34. Mean (SE) peak soft tissue velocity in the posterior direction for each region.

4.2.6. Sex, Region, and Soft Tissue Velocity

Of the four soft tissue velocity directions analyzed, only one significant interaction effect existed between Sex and Region for mean peak anterior velocity [$F(2.556, 71.566) = 3.023$, p = 0.043, partial $\eta^2 = 0.097$] (Figure 35); no significant interactions were found for velocities in the distal [$F(1.655, 46.351) = 0.356$, p = 0.662, partial $\eta^2 = 0.013$], proximal [$F(4.107, 115.001) = 0.831$, p = 0.511, partial $\eta^2 = 0.029$], or posterior [$F(3.504, 98.105) = 2.006$, p = 0.108, partial $\eta^2 = 0.067$] directions. Resultant analysis of the simple main effects revealed that there were no significant differences for Sex on anterior soft tissue velocities across any of the forearm regions (p > 0.05). However, a statistically significant simple main effect of Region on anterior velocity was found for both females [$F(2.295, 39.011) = 40.543$, $p = 0.000$, partial $\eta^2 = 0.705$] and males [$F(2.574, 28.316) = 13.041$, $p = .000$, partial $\eta^2 = 0.542$]. Further investigation of the simple main effects of Region showed that there were significant

87

differences between three different region comparisons for females and males, with only one region comparison being shared between both sexes; regions 5 and 7 were found to have significantly greater anterior velocities for females (region 5: 58.9 cm/s; region 7: 63.8 cm/s) and males (region 5: 52.9 cm/s; region 7: 57.3 cm/s) ($p \leq 0.05$). Only for females was the anterior velocity of the soft tissue in distal regions (1 and 2) also found to be significantly lower than the more proximal regions (3 through 8).
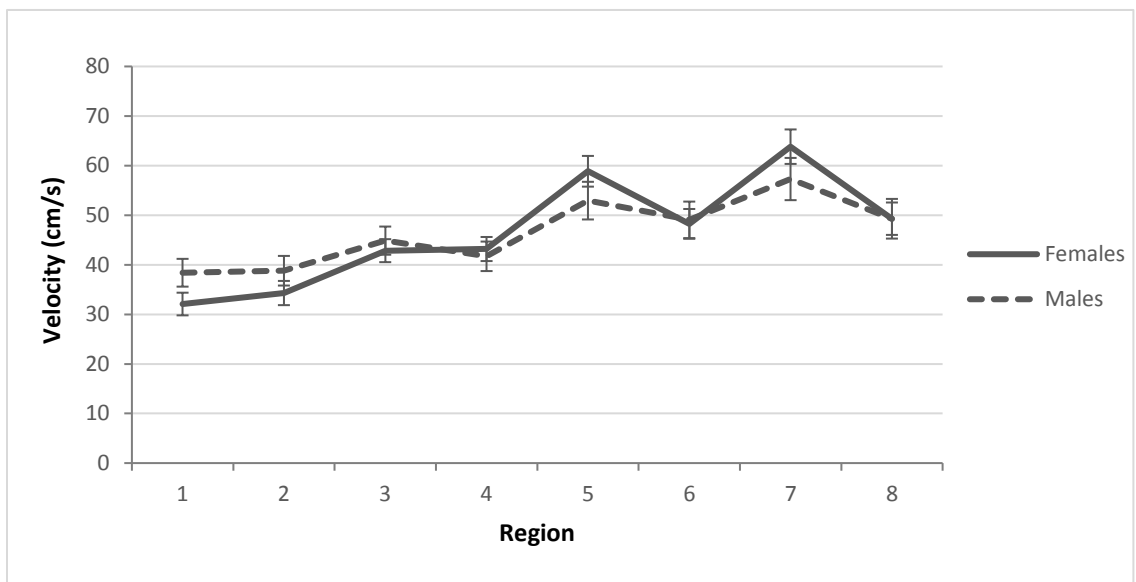
Figure 35. Interaction effect of Sex and Region (1-8) on anterior velocity.

4.2.7. Sex and Soft Tissue Shock Attenuation

Measures of un-normalized shock attenuation for each level of sex were normally distributed, as assessed by both Q-Q Plots and Shapiro-Wilk's test ($p > 0.05$). Levene's test for equality of variances was significant ($p = 0.026$), and therefore, statistical significance was reported using the adjusted scores for when equal variances was not assumed. Ultimately, it was found that the mean difference in un-normalized shock

attenuation responses between females (-76.3 ± 17.5%) and males (-75.8 ± 33.9%) was

not significant [$t(14.947) = -0.046$, p = 0.964], as was calculated by the acceleration ratio

from Equation 2. Accordingly, no significant mean differences for mean peak proximal

and distal accelerations were found between sexes as well (p > 0.05).

In an attempt to further investigate if shock attenuation responses differed

between females and males, shock attenuation was normalized to tissue mass, as per

Schinkel-Ivy et al. (2012), by dividing the shock attenuation values by each of the four

tissue mass magnitudes estimated for the forearm (i.e., BMC, FM, LM, WM). Shock

attenuation measures normalized to tissue mass were normally distributed for each level

of sex, as determined by Q-Q Plots and Shapiro-Wilk's test (p ≤ 0.05), with the exception

of shock attenuation normalized to fat mass. As a result of this violation, the Mann-

Whitney U test was run as a non-parametric alternative to confirm the statistical scores

from the Independent Samples T-test for this measure. The variances of all normalized

shock attenuation measures between females and males were homogeneous (p ≤ 0.05).

Significant differences between females and males were observed for shock attenuation

responses normalized to BMC [$t(28) = -3.101$, p = 0.004], LM [$t(28) = -3.873$, p =

0.001], and WM [$t(28) = -3.305$, p = 0.003], in which females demonstrated a greater

susceptibility to a lack of impact shock attenuation compared to males per gram of tissue.

No statistically significant difference between sexes was found for shock attenuation

normalized to FM [$t(28) = 1.322$, p = 0.196].

4.3. Purpose 3

Identify the relationship between the displacement, velocity, and shock

attenuation capacity of the forearm soft tissues and their individual tissue masses (BMC,

FM, LM, and WM).

4.3.1. Participant Tissue Masses

On average, the tissue mass estimations for the forearm determined that females

had approximately 43% more FM than males, whereas males were found to have 44%,

57%, and 45% greater BMC, LM, and WM, respectively, compared to females (Table

10).

Table 10. Mean (±SD) bone mass (g), fat mass (g), lean mass (g), and wobbling mass (g) of all participants estimated using the tissue mass prediction equations from Arthurs et al. (2009).

Participants	Bone Mass (g)		Fat Mass (g)		Lean Mass (g)		Wobbling Mass (g)	
Overall (n=30)	75.1	(18.3)	88.2	(42.4)	1058.6	(282.7)	1177.2	(278.6)
Female (n=18)	64.0	(11.3)	100.2	(44.7)	861.8	(147.3)	999.0	(169.1)
Male (n=12)	91.9	(13.2)	70.2	(32.4)	1353.8	(148.3)	1444.5	(174.8)

4.3.2. Displacement (Distal) Correlations

For females, significant positive correlations were found between FM and the

distal displacement of soft tissue in the (anterior) forearm regions of 4, 6, and 8, in

addition to the mean distal displacement ($p \leq 0.05$) (Table 11). A significant positive

correlation also existed between WM and the magnitude of distal soft tissue displacement

in region 6 ($p \leq 0.05$). No significant relationships ($p > 0.05$) were found for males

between the displacement of forearm soft tissue in the distal direction and any of the

forearm tissue masses (BMC, FM, LM, and WM) (Table 12).

90

Table 11. Pearson correlations (r-values) between female distal soft tissue displacement (cm) in each region (1-8), as well as the entire forearm (mean), and specific tissue masses: bone mineral content (BMC), fat mass (FM), lean mass (LM), and wobbling mass (WM).

	1	2	3	4	5	6	7	8	Mean
BMC	0.220	-0.021	-0.014	0.051	0.107	0.268	0.101	0.169	0.130
FM	0.254	0.303	0.295	**0.518***	0.334	**0.604***	0.316	**0.517***	**0.473***
LM	0.275	0.024	0.009	0.041	0.167	0.282	0.169	0.186	0.169
WM	0.349	0.162	0.147	0.262	0.294	**0.479***	0.289	0.363	0.348

*= Correlation is significant at the 0.05 level (2-tailed).

Table 12. Pearson correlations (r-values) between male distal soft tissue displacement (cm) in each region (1-8), as well as the entire forearm (mean), and specific tissue masses: bone mineral content (BMC), fat mass (FM), lean mass (LM), and wobbling mass (WM).

	1	2	3	4	5	6	7	8	Mean
BMC	-0.247	-0.370	-0.045	-0.019	-0.158	-0.023	-0.118	-0.051	-0.106
FM	0.168	0.206	0.198	0.234	0.097	0.253	0.128	0.237	0.207
LM	-0.312	-0.402	-0.171	-0.098	-0.261	-0.131	-0.204	-0.177	-0.212
WM	-0.166	-0.203	-0.129	-0.045	-0.223	-0.086	-0.165	-0.114	-0.144

4.3.3. Displacement (Proximal) Correlations

Females had significant positive correlations between BMC and proximal forearm soft tissue displacement in regions 1 and 2, as well as FM and proximal displacement in the intermediates regions 3 and 5 (p ≤ 0.05) (Table 13). Males had significant positive correlations between FM and the proximal soft tissue displacement in more distally located regions of the forearm (i.e., regions 6 and 8) (p ≤ 0.05) (Table 14).

Table 13. Pearson correlations (r-values) between female proximal soft tissue displacement (cm) in each region (1-8), as well as the entire forearm (mean), and specific tissue masses: bone mineral content (BMC), fat mass (FM), lean mass (LM), and wobbling mass (WM).

	1	2	3	4	5	6	7	8	Mean
BMC	**0.576***	**0.481***	0.366	0.368	0.418	0.361	0.406	0.413	0.434
FM	0.278	0.325	**0.537***	0.339	**0.515***	0.416	0.437	0.353	0.461
LM	0.416	0.397	0.261	0.287	0.256	0.196	0.287	0.288	0.296
WM	0.458	0.447	0.408	0.356	0.410	0.319	0.399	0.372	0.417

*= Correlation is significant at the 0.05 level (2-tailed).

Table 14. Pearson correlations (r-values) between male proximal soft tissue displacement (cm) in each region (1-8), as well as the entire forearm (mean), and specific tissue masses: bone mineral content (BMC), fat mass (FM), lean mass (LM), and wobbling mass (WM).

	1	2	3	4	5	6	7	8	Mean
BMC	0.030	0.051	0.025	-0.010	0.079	-0.060	-0.021	-0.069	0.018
FM	-0.267	-0.408	-0.386	-0.513	-0.330	**-0.582***	-0.537	**-0.590***	-0.435
LM	0.113	0.146	0.121	0.064	0.186	-0.008	0.047	-0.021	0.104
WM	0.011	0.002	-0.009	-0.105	0.067	-0.193	-0.128	-0.208	-0.044

*= Correlation is significant at the 0.05 level (2-tailed).

4.3.4. Rebound Distance (Proximal) Correlations

For females, multiple significant positive correlations were found across each of the four tissue masses and proximal rebound distance of the forearm soft tissues. Specifically, FM and WM were significantly positively correlated to soft tissue rebound distance in the proximal direction for all regions of the forearm, including the mean values, with the sole exception of LM and proximal rebound distance for region 2 (p ≤ 0.05) (Table 15). Both BMC and LM also had significant positive correlations with proximal soft tissue rebound distance for females with region 1, 5, 7, along with the mean and regions 1 and 7, respectively (p ≤ 0.05). In contrast to females, there were no significant relationships between the rebound distance of the soft tissues in the proximal direction and any of the forearm tissue masses (BMC, FM, LM, and WM) for male participants (Table 16).

Table 15. Pearson correlations (r-values) between female proximal soft tissue rebound distance (cm) in each region (1-8), as well as the entire forearm (mean), and specific tissue masses: bone mineral content (BMC), fat mass (FM), lean mass (LM), and wobbling mass (WM).

	1	2	3	4	5	6	7	8	Mean
BMC	**0.648***	0.295	0.406	0.423	**0.491***	0.464	**0.513***	0.422	**0.517***
FM	**0.472***	**0.543***	**0.765***	**0.759***	**0.757***	**0.736***	**0.732***	**0.629***	**0.776***
LM	**0.572***	0.274	0.310	0.321	0.392	0.354	**0.470***	0.335	0.424
WM	**0.668***	0.441	**0.548***	**0.567***	**0.628***	**.572***	**0.678***	**0.518***	**0.655***

*= Correlation is significant at the 0.05 level (2-tailed).

Table 16. Pearson correlations (r-values) between male proximal soft tissue rebound distance (cm) in each region (1-8), as well as the entire forearm (mean), and specific tissue masses: bone mineral content (BMC), fat mass (FM), lean mass (LM), and wobbling mass (WM).

	1	2	3	4	5	6	7	8	Mean
BMC	-0.162	0.003	0.119	0.330	0.088	0.327	0.052	0.409	0.191
FM	0.035	0.021	0.155	0.319	0.075	0.312	-0.139	0.426	0.189
LM	-0.153	0.019	0.028	0.284	0.052	0.243	0.086	0.293	0.140
WM	-0.088	0.021	0.010	0.262	0.023	0.207	-0.007	0.282	0.116

4.3.5. Displacement (Anterior) Correlations

With respect to anterior soft tissue displacement for females, only a single significant positive correlation was found with FM in region 4 ($p \leq 0.05$) (Table 17). For males, significant negative relationships were present between BMC and anterior displacement for regions 3 through 8 and the mean ($p \leq 0.05$). Additionally, males had significant negative correlations between LM and anterior soft tissue displacement in regions 3, 5, 6, and all regions together (i.e., the mean), and between WM and region 5 (Table 18).

Table 17. Pearson correlations (r-values) between female anterior soft tissue displacement (cm) in each region (1-8), as well as the entire forearm (mean), and specific tissue masses: bone mineral content (BMC), fat mass (FM), lean mass (LM), and wobbling mass (WM).

	1	2	3	4	5	6	7	8	Mean
BMC	0.080	0.103	-0.109	0.195	0.152	0.089	0.221	0.194	0.163
FM	0.176	0.308	0.365	**0.573**[*]	0.433	0.351	0.323	0.456	0.437
LM	0.093	0.139	-0.202	0.113	0.013	-0.077	0.049	0.030	0.012
WM	0.122	0.213	-0.069	0.299	0.155	0.069	0.184	0.205	0.173

*= Correlation is significant at the 0.05 level (2-tailed).

Table 18. Pearson correlations (r-values) between male anterior soft tissue displacement (cm) in each region (1-8), as well as the entire forearm (mean), and specific tissue masses: bone mineral content (BMC), fat mass (FM), lean mass (LM), and wobbling mass (WM).

	1	2	3	4	5	6	7	8	Mean
BMC	-0.355	-0.435	**-0.653***	**-0.577***	**-0.760***	**-0.640***	**-0.625***	**-0.600***	**-0.669***
FM	0.169	0.135	-0.071	-0.126	-0.376	-0.190	-0.129	-0.074	-0.143
LM	-0.383	-0.505	**-0.651***	-0.561	**-0.717***	**-0.585***	-0.562	-0.558	**-0.632***
WM	-0.254	-0.360	-0.509	-0.463	**-0.655***	-0.470	-0.413	-0.420	-0.501

*= Correlation is significant at the 0.05 level (2-tailed).

4.3.6. Displacement (Posterior) Correlations

For both females and males, no significant relationships were found between posterior soft tissue displacement and any of the forearm soft tissue masses (BMC, FM, LM, and WM) (Tables 19 and 20).

Table 19. Pearson correlations (r-values) between female posterior soft tissue displacement (cm) in each region (1-8), as well as the entire forearm (mean), and specific tissue masses: bone mineral content (BMC), fat mass (FM), lean mass (LM), and wobbling mass (WM).

	1	2	3	4	5	6	7	8	Mean
BMC	-0.004	-0.130	-0.250	-0.252	-0.338	-0.279	-0.379	-0.254	-0.261
FM	-0.153	-0.274	-0.282	-0.349	-0.221	-0.375	-0.249	-0.394	-0.307
LM	0.090	0.000	-0.114	-0.120	-0.213	-0.147	-0.252	-0.109	-0.126
WM	0.046	-0.065	-0.182	-0.213	-0.256	-0.251	-0.296	-0.222	-0.203

Table 20. Pearson correlations (r-values) between male posterior soft tissue displacement (cm) in each region (1-8), as well as the entire forearm (mean), and specific tissue masses: bone mineral content (BMC), fat mass (FM), lean mass (LM), and wobbling mass (WM).

	1	2	3	4	5	6	7	8	Mean
BMC	0.248	0.267	0.294	0.304	0.331	0.314	0.347	0.291	0.320
FM	0.022	-0.036	0.103	0.000	0.178	0.222	0.186	0.170	0.112
LM	0.314	0.327	0.380	0.393	0.414	0.395	0.408	0.382	0.403
WM	0.243	0.234	0.329	0.326	0.421	0.423	0.393	0.415	0.374

4.3.7. Rebound Distance (Posterior) Correlations

Same as the findings for posterior displacement, both females and males had no

significant relationships between posterior soft tissue rebound distance and any of the

forearm soft tissue masses (BMC, FM, LM, and WM) (Tables 21 and 22).

Table 21. Pearson correlations (r-values) between female posterior soft tissue rebound distance (cm) in each region (1-8), as well as the entire forearm (mean), and specific tissue masses: bone mineral content (BMC), fat mass (FM), lean mass (LM), and wobbling mass (WM).

	1	2	3	4	5	6	7	8	Mean
BMC	0.133	-0.081	-0.186	0.054	-0.136	-0.188	-0.061	-0.020	-0.083
FM	-0.134	-0.103	-0.117	0.108	-0.120	-0.116	-0.051	0.078	-0.059
LM	0.312	0.111	-0.046	0.203	-0.005	-0.067	-0.001	0.127	0.064
WM	0.233	0.080	-0.087	0.221	-0.065	-0.084	0.018	0.157	0.048

Table 22. Pearson correlations (r-values) between male posterior soft tissue rebound distance (cm) in each region (1-8), as well as the entire forearm (mean), and specific tissue masses: bone mineral content (BMC), fat mass (FM), lean mass (LM), and wobbling mass (WM)

	1	2	3	4	5	6	7	8	Mean
BMC	0.103	0.182	0.223	0.080	0.079	0.025	0.167	0.086	0.119
FM	0.154	0.227	0.085	0.016	-0.022	0.064	0.091	0.188	0.099
LM	0.131	0.178	0.261	0.118	0.127	0.100	0.247	0.153	0.175
WM	0.124	0.178	0.189	0.054	0.048	0.080	0.210	0.169	0.141

4.3.8. Velocity (Distal) Correlations

No significant relationships existed between distal soft tissue velocity and any of

the forearm soft tissue masses for females and males (BMC, FM, LM, and WM) (Table

23 and 24).

Table 23. Pearson correlations (r-values) between female distal soft tissue velocity (cm/s) in each region (1-8), as well as the entire forearm (mean), and specific tissue masses: bone mineral content (BMC), fat mass (FM), lean mass (LM), and wobbling mass (WM).

	1	2	3	4	5	6	7	8	Mean
BMC	0.154	0.072	0.097	0.094	0.099	0.107	0.088	0.128	0.108
FM	0.345	0.365	0.345	0.261	0.387	0.269	0.330	0.403	0.350
LM	0.094	0.009	0.050	0.020	0.050	0.034	0.038	0.068	0.047
WM	0.217	0.156	0.167	0.121	0.184	0.137	0.156	0.213	0.175

Table 24. Pearson correlations (r-values) between male distal soft tissue velocity (cm/s) in each region (1-8), as well as the entire forearm (mean), and specific tissue masses: bone mineral content (BMC), fat mass (FM), lean mass (LM), and wobbling mass (WM).

	1	2	3	4	5	6	7	8	Mean
BMC	-0.386	-0.422	-0.326	-0.301	-0.265	-0.265	-0.268	-0.268	-0.324
FM	-0.347	-0.448	-0.482	-0.470	-0.444	-0.462	-0.393	-0.428	-0.455
LM	-0.421	-0.442	-0.332	-0.306	-0.261	-0.249	-0.272	-0.252	-0.327
WM	-0.421	-0.482	-0.437	-0.426	-0.372	-0.369	-0.362	-0.359	-0.420

4.3.9. Velocity (Proximal) Correlations

For females, significant positive correlations were found between proximal soft tissue velocity in region 1 and BMC, LM, as well as WM ($p \leq 0.05$) (Table 25). Significant positive correlations between WM and proximal velocity of the forearm soft tissues were also seen in regions 5, 7, and the mean of all regions together ($p \leq 0.05$) (Table 25). In comparison, there were no significant relationships for males between the velocity of soft tissues in the proximal direction and any of the forearm tissue masses (BMC, FM, LM, and WM) (Table 26).

Table 25. Pearson correlations (r-values) between female proximal soft tissue velocity (cm/s) in each region (1-8), as well as the entire forearm (mean), and specific tissue masses: bone mineral content (BMC), fat mass (FM), lean mass (LM), and wobbling mass (WM).

	1	2	3	4	5	6	7	8	Mean
BMC	**0.601***	0.172	0.425	0.355	0.453	0.278	0.437	0.181	0.443
FM	0.343	0.305	0.173	0.167	0.249	0.214	0.360	0.056	0.284
LM	**0.559***	0.179	0.430	0.353	0.466	0.280	0.389	0.184	0.433
WM	**0.599***	0.269	0.436	0.377	**0.483***	0.307	**0.481***	0.175	**0.477***

*= Correlation is significant at the 0.05 level (2-tailed).

Table 26. Pearson correlations (r-values) between male proximal soft tissue velocity (cm/s) in each region (1-8), as well as the entire forearm (mean), and specific tissue masses: bone mineral content (BMC), fat mass (FM), lean mass (LM), and wobbling mass (WM).

	1	2	3	4	5	6	7	8	Mean
BMC	-0.103	-0.043	-0.056	-0.044	-0.041	-0.029	-0.010	-0.016	-0.045
FM	-0.099	-0.070	-0.265	-0.195	-0.319	-0.332	-0.443	-0.242	-0.287
LM	-0.037	0.034	-0.052	-0.016	-0.013	-0.018	0.083	-0.033	-0.006
WM	0.027	0.097	-0.118	-0.052	-0.112	-0.150	-0.040	-0.108	-0.070

4.3.10. Velocity (Anterior) Correlations

Two significant positive correlations were found for females between the anterior velocity of forearm soft tissues and FM in regions 2 and 4 ($p \leq 0.05$) (Table 27). Males exhibited multiple significant negative correlations between anterior soft tissue velocity and the forearm tissue masses. Excluding FM, the magnitude of the anterior velocities in regions 1, 2, 4, 6, and the respective tissue mass mean values, were significantly negatively correlated with BMC, LM, and WM; region 3 showed significant negative correlations between anterior velocity across all tissue masses (BMC, FM, LM, and WM) ($p \leq 0.05$) (Table 28). Distal regions of the forearm (regions 7 and 8) also had significant negative correlations between anterior soft tissue velocity and BMC, while region 5 had one significant negative correlation with WM ($p \leq 0.05$).

Table 27. Pearson correlations (r-values) between female anterior soft tissue velocity (cm/s) in each region (1-8), as well as the entire forearm (mean), and specific tissue masses: bone mineral content (BMC), fat mass (FM), lean mass (LM), and wobbling mass (WM).

	1	2	3	4	5	6	7	8	Mean
BMC	0.012	-0.034	-0.167	-0.171	0.013	-0.205	-0.021	-0.202	-0.119
FM	0.331	**0.593**[*]	0.434	**0.502**[*]	0.380	0.137	0.254	0.085	0.372
LM	0.018	-0.054	-0.204	-0.260	-0.141	-0.285	-0.210	-0.287	-0.227
WM	0.141	0.163	-0.042	-0.055	-0.008	-0.203	-0.088	-0.226	-0.072

*= Correlation is significant at the 0.05 level (2-tailed).

Table 28. Pearson correlations (r-values) between male anterior soft tissue velocity (cm/s) in each region (1-8), as well as the entire forearm (mean), and specific tissue masses: bone mineral content (BMC), fat mass (FM), lean mass (LM), and wobbling mass (WM).

	1	2	3	4	5	6	7	8	Mean
BMC	**-0.628**[*]	**-0.636**[*]	**-0.623**[*]	**-0.713**[*]	-0.557	**-0.745**[*]	**-0.655**[*]	**-0.591**[*]	**-0.751**[*]
FM	-0.309	-0.292	**-0.643**[*]	-0.462	-0.469	-0.526	-0.467	-0.245	-0.495
LM	**-0.671**[*]	**-0.718**[*]	**-0.606**[*]	**-0.716**[*]	-0.542	**-0.650**[*]	-0.547	-0.502	**-0.720**[*]
WM	**-0.632**[*]	**-0.668**[*]	**-0.669**[*]	**-0.687**[*]	**-0.600**[*]	**-0.603**[*]	-0.513	-0.417	**-0.695**[*]

*= Correlation is significant at the 0.05 level (2-tailed).

4.3.11. Velocity (Posterior) Correlations

For females, significant positive correlations were present between both FM and WM and posterior soft tissue velocity in region 4 ($p \leq 0.05$) (Table 29). There were no significant relationships for males between the velocity of soft tissue in the posterior direction and any of the forearm tissue masses (BMC, FM, LM, and WM) (Table 30).

Table 29. Pearson correlations (r-values) between female posterior soft tissue velocity (cm/s) in each region (1-8), as well as the entire forearm (mean), and specific tissue masses: bone mineral content (BMC), fat mass (FM), lean mass (LM), and wobbling mass (WM).

	1	2	3	4	5	6	7	8	Mean
BMC	-0.047	-0.061	-0.067	0.438	-0.179	-0.170	0.009	-0.320	-0.086
FM	0.189	0.182	-0.055	**0.681**[*]	-0.055	-0.339	-0.088	0.143	0.117
LM	-0.017	0.039	0.063	0.452	-0.128	-0.157	0.006	-0.192	-0.003
WM	0.067	0.127	0.008	**0.658**[*]	-0.165	-0.253	-0.020	-0.134	0.037

*= Correlation is significant at the 0.05 level (2-tailed).

Table 30. Pearson correlations (r-values) between male posterior soft tissue velocity (cm/s) in each region (1-8), as well as the entire forearm (mean), and specific tissue masses: bone mineral content (BMC), fat mass (FM), lean mass (LM), and wobbling mass (WM).

	1	2	3	4	5	6	7	8	Mean
BMC	-0.498	-0.311	0.342	0.279	0.084	0.071	0.271	0.087	0.105
FM	-0.474	-0.212	0.185	0.078	-0.270	-0.002	-0.018	0.009	-0.076
LM	-0.444	-0.318	0.320	0.192	0.080	0.070	0.323	0.173	0.120
WM	-0.428	-0.281	0.286	0.131	-0.048	0.067	0.244	0.163	0.071

4.3.12. Shock Attenuation Correlations

Females showed no significant relationships between any of the forearm soft tissue masses (BMC, FM, LM, and WM) and shock attenuation, as well as distal and proximal accelerations (Table 31). For males, there were significant negative correlations between BMC, LM, and WM in the forearm and the un-normalized shock attenuation response ($p \leq 0.05$) (Table 32). A significant negative correlation was also present for males between distal acceleration and WM ($p \leq 0.05$).

Table 31. Pearson correlations (r-values) between female soft tissue peak acceleration (cm/s^2), as well as un-normalized shock attenuation, and specific tissue masses: bone mineral content (BMC), fat mass (FM), lean mass (LM), and wobbling mass (WM).

	Peak Acceleration		Shock Attenuation
	Distal	Proximal	Un-normalized
BMC	0.124	0.117	0.050
FM	0.283	0.302	0.025
LM	-0.044	-0.009	-0.066
WM	0.069	0.095	-0.025

Table 32. Pearson correlations (r-values) between male soft tissue peak acceleration (cm/s^2), as well as un-normalized shock attenuation, and specific tissue masses: bone mineral content (BMC), fat mass (FM), lean mass (LM), and wobbling mass (WM).

	Acceleration		Shock Attenuation
	Distal	Proximal	Un-normalized
BMC	-0.556	-0.229	**-0.602**[*]
FM	-0.506	-0.356	-0.340
LM	-0.568	-0.214	**-0.639**[*]
WM	**-.601**[*]	-0.259	**-0.640**[*]

[*]= Correlation is significant at the 0.05 level (2-tailed).

4.4. Purpose 4

Determine if a stacked, non-uniform (SNU) marker design (non-uniform, ~0.5 cm diameter black dots overlaid on top of a grid of contrasting ~1 cm diameter white dots; 2 cm inter-marker distance) produces significantly different kinematic results and improves automated marker tracking across different skin pigmentations compared to the single layer, uniform (SLU) marker design (grid of uniform, 0.5 cm diameter black dots; 2 cm inter-marker distance) previously established by Brydges et al. (2015).

Assessment of normality using Shapiro-Wilk's test and Q-Q Plots revealed similar results to Purpose 2, wherein the distributions of the dependent variables for mean peak displacement in the proximal and posterior directions were very positively skewed. Moderate deviations from normality were also observed for other dependent variables due to the inclusion of potential outliers; however, as stated previously, these values were verified to represent authentic soft tissue motion, and thus were kept in the analyses.

Variances of the dependent variables between light and dark skin pigmentation groups for each marker design across all forearm regions were determined to be homogeneous ($p > 0.05$), except proximal displacement of the SLU markers in region 4, proximal rebound distance and posterior velocity of the SNU markers in region 2, and posterior velocity of the SNU markers in region 8. Mauchly's Test of Sphericity was significant ($p \leq 0.05$) for each dependent variable, therefore, corrected Greenhouse-Geisser estimates were applied for all of the following analyses.

4.4.1. Marker Design, Skin Pigmentation, and Region on Soft Tissue Displacement

There was no statistically significant three-way interactions between Skin Pigmentation, Marker Design, and Region for mean peak displacement of forearm soft tissue in any of the four directions analysed [distal: $F(2.748, 76.938) = 2.374$, p = 0.082, partial $\eta^2 = 0.078$; proximal: $F(2.845, 79.669) = 1.080$, p = 0.360, partial $\eta^2 = 0.037$; anterior: $F(1.115, 31.220) = 1.442$, p = 0.242, partial $\eta^2 = 0.049$; and posterior: $F(1.944, 54.428) = 0.891$, p = 0.414, partial $\eta^2 = 0.031$]. Two-way interactions between Skin Pigmentation and Region were not significant for all directions of soft tissue displacement (p > 0.05), with the exception of anterior displacement [$F(1.461, 40.915) = 3.689$, p = 0.047, partial $\eta^2 = 0.116$]. Simple main effects showed that anterior soft tissue displacements across skin pigmentations only significantly differed in region 7 (p ≤ 0.05); therefore, it can be concluded that, in general, the displacements of forearm soft tissue were found to be similar between light and dark skin pigmentation groups.

Statistically significant two-way interactions were present for distal soft tissue displacement between Marker Design and Region [$F(2.748, 76.938) = 5.657$, p = 0.002 partial $\eta^2 = 0.168$] (Figure 36), and between Marker Design and Skin Pigmentation [$F(1.000, 28.000) = 4.530$, p = 0.042, partial $\eta^2 = 0.139$] (Figure 37). Analysis of simple main effects showed that the distal displacement for the SLU marker design was significantly greater than the SNU marker design for regions 2 through 8 (p ≤ 0.05), and that the difference between the mean distal displacements for the SLU and SNU marker designs was significantly higher for the dark skin pigmentation group (p ≤ 0.05), but not the light skin pigmentation group (p > 0.05).
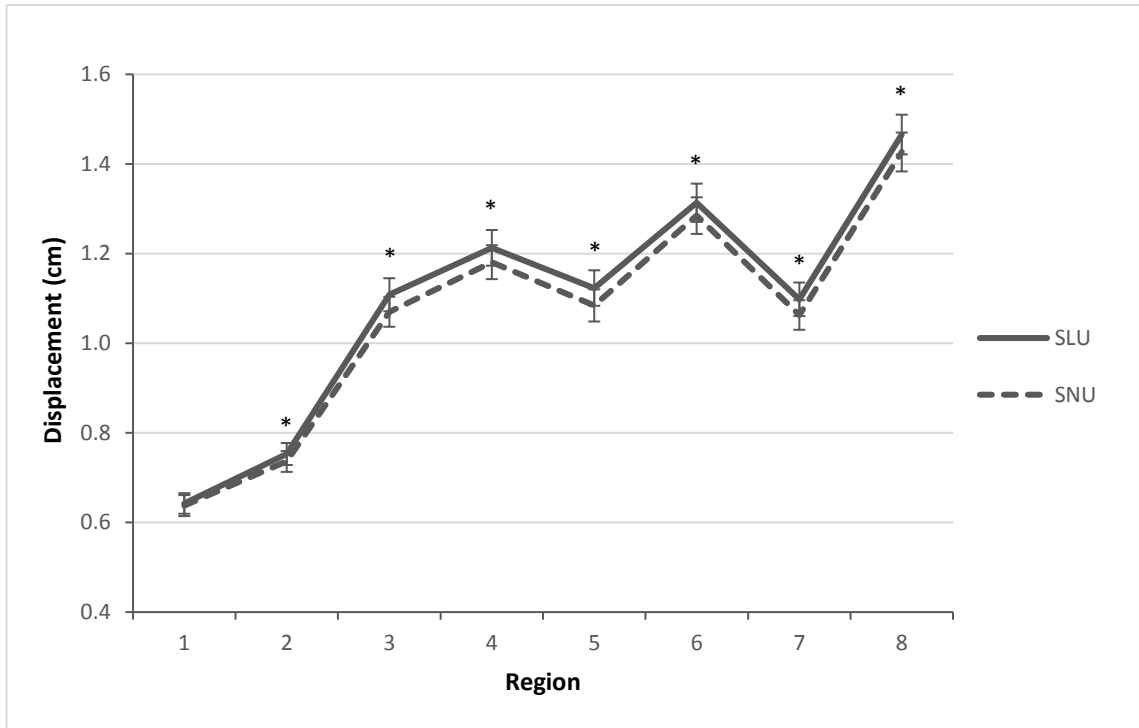
Figure 36. Interaction effect of Marker Design (SLU, SNU) and Region (1-8) on distal displacement (* = statistically significant at $p \leq 0.05$).

Figure 37. Interaction effect of Marker Design (SLU, SNU) and Skin Pigmentation (light, dark) on distal displacement (* = statistically significant at $p \leq 0.05$).

For proximal soft tissue displacement, no statistically significant two-way interaction was found between Marker Design and Region [$F(2.845, 79.669) = 1.309$, p = 0.277, partial $\eta^2 = 0.045$]. However, there was a statistically significant two-way interaction present for proximal displacement between Marker Design and Skin Pigmentation [$F(1.000, 28.000) = 5.554$, p = 0.026, partial $\eta^2 = 0.166$] where, on average, the SLU marker design recorded 34% higher magnitudes of proximal displacement than the SNU marker design for the light skin pigmentation group, while SLU marker design recorded proximal displacements that were 25% lower than the SNU marker design for the dark skin pigmentation group (Figure 38). With respect to soft tissue displacement in the anterior and posterior directions, no significant two-way interactions were found between Marker Design and Region [anterior: $F(1.115, 31.220) = 0.526$, p = 0.493, partial $\eta^2 = 0.018$; posterior: $F(1.944, 54.428) = 2.892$, p = 0.65, partial $\eta^2 = 0.094$] or Marker Design and Skin Pigmentation [anterior: $F(1.000, 28.000) = 1.004$, p = 0.325, partial $\eta^2 = 0.03$; posterior: $F(1.000, 28.000) = 0.897$, p = 0.352, partial $\eta^2 = 0.031$].

Figure 38. Interaction effect of Marker Design (SLU, SNU) and Skin Pigmentation (light, dark) on proximal displacement.

4.4.2. Marker Design, Skin Pigmentation, and Region on Soft Tissue Rebound Distance

There was a statistically significant three-way interaction between Marker Design, Skin Pigmentation, and Region on proximal soft tissue rebound distance [$F(3.850, 107.796) = 2.919$, p $= 0.026$, partial $\eta^2 = 0.094$]. Statistically significant simple two-way interactions were found between Marker Design and Region for both light [$F(3.887, 54.423) = 3.388$, p $= 0.016$, partial $\eta^2 = 0.195$] and dark [$F(3.185, 44.597) = 4.918$, p $= 0.004$, partial $\eta^2 = 0.260$] skin pigmentation groups. An analysis of simple main effects of marker design for the light skin pigmentation group revealed significantly greater magnitudes of proximal rebound distance for the SLU marker design compared to the SNU marker design for regions 1, 2, 3, 5, 6, and 8 (Figure 39), while the dark skin pigmentation group showed significantly greater proximal rebound distance across regions 3 through 8 (p ≤ 0.05) (Figure 40). No significant two-way interactions existed for soft tissue rebound distance in the posterior direction between Marker Design and Region [$F(1.571, 43.977) = 0.873$, p $= 0.401$, partial $\eta^2 = 0.030$], as well as Marker Design and Skin Pigmentation [$F(1.000, 28.000) = 0.382$, p $= 0.541$, partial $\eta^2 = 0.013$].
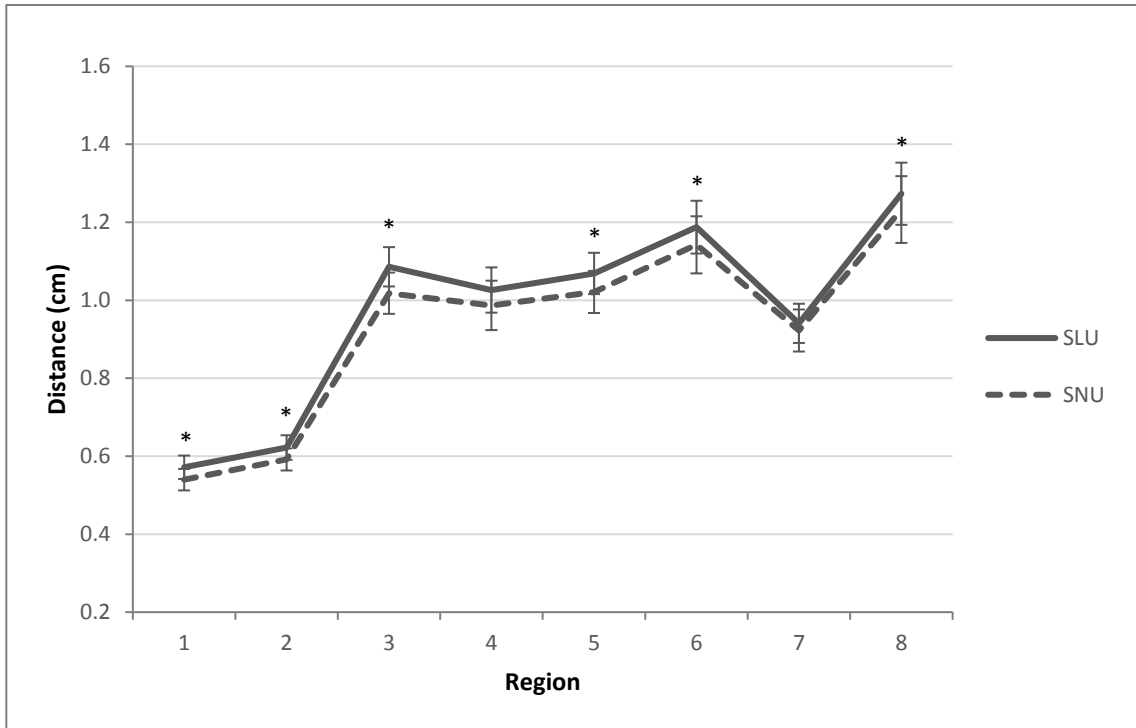
Figure 39. Interaction effect of Marker Design (SLU, SNU) and Region (1-8) on proximal rebound distance for the light skin pigmentation group (* = statistically significant at p ≤ 0.05).
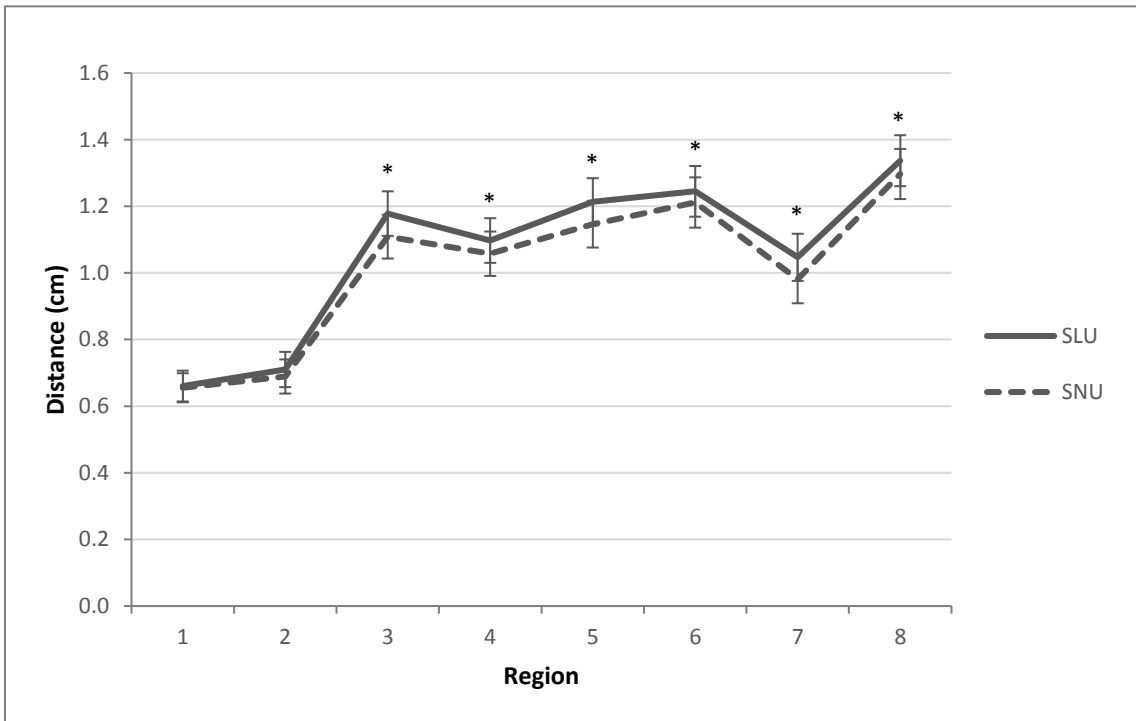
Figure 40. Interaction effect of Marker Design (SLU, SNU) and Region (1-8) on proximal rebound distance for the dark skin pigmentation group (* = statistically significant at p ≤ 0.05).
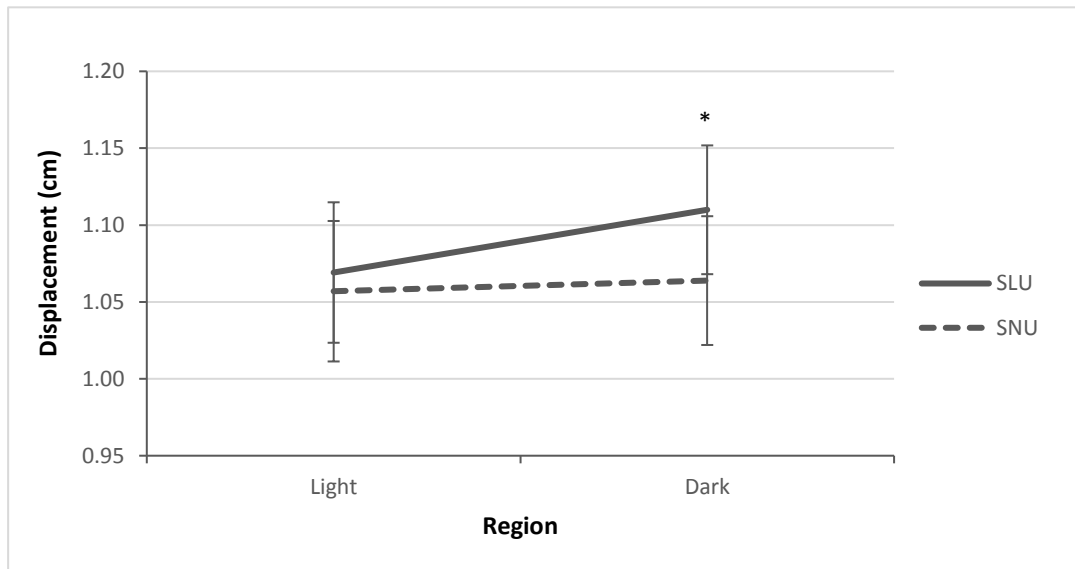
4.4.3. Marker Design, Skin Pigmentation, and Region on Soft Tissue Velocity

No statistically significant three-way interactions between Skin Pigmentation, Marker Design, and Region were present for mean peak velocity of forearm soft tissue in any of the four directions analysed [distal: $F(2.746, 76.896) = 1.096$, p = 0.353, partial η^2 = 0.038; proximal: $F(4.794, 134.245) = 1.191$, p = 0.317, partial η^2 = 0.041; anterior: $F(3.432, 96.106) = 0.632$, p = 0.617, partial η^2 = 0.022; and posterior: $F(3.740, 104.713)$ = 1.132, p = 0.345, partial η^2 = 0.039]. Moreover, no two-way interactions between Skin Pigmentation and Region were significant for all directions of soft tissue velocity analysed (p > 0.05). As a result, the magnitudes of forearm soft tissue velocities were found to be similar between light and dark skin pigmentation groups.

Statistically significant two-way interactions were found between Marker Design and Region for soft tissue velocities in the distal [$F(2.746, 76.896) = 5.409$, p = 0.003, partial η^2 = 0.162] (Figure 41) and proximal [$F(4.794, 134.245) = 3.389$, p = 0.007, partial η^2 = 0.108] directions (Figure 42), but not between Marker Design and Skin Pigmentation [distal velocity: $F(1.000, 28.000) = 2.156$, p = 0.153, partial η^2 = 0.071; proximal velocity: $F(1.000, 28.000) = 0.093$, p = 0.763, partial η^2 = 0.003]. Analysis of the simple main effects found significant differences for magnitudes of distal velocity between marker designs across all regions of the forearm (1-8) (p ≤ 0.05), in which SLU marker design provided 2.5% greater values for distal velocity, on average, compared to the SNU marker design. For proximal velocity, the simple main effects also found that the SLU marker design had significantly greater magnitudes (by 3.0% on average (p ≤ 0.05)) than the SNU marker design across the distal and intermediate regions of 2, 3, 4, 5, and 6.
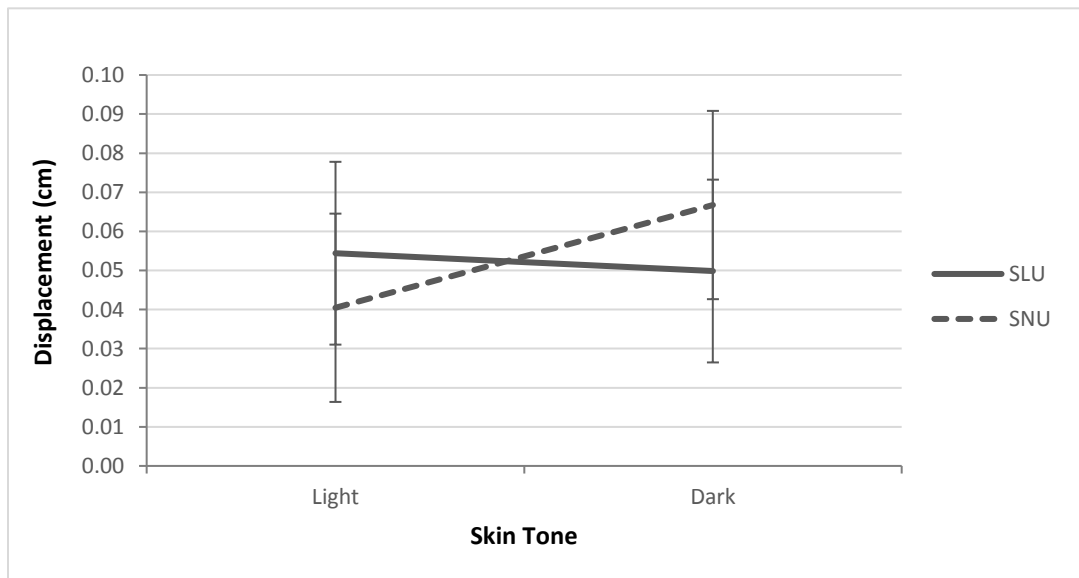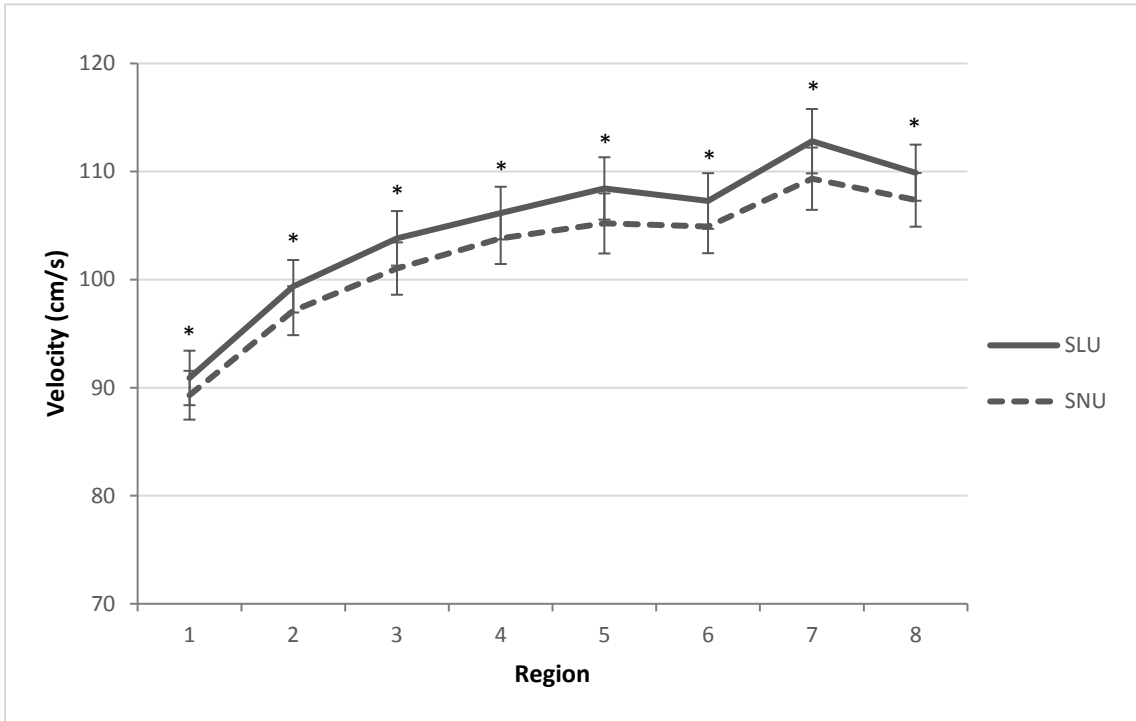
Figure 41. Interaction effect of Marker Design (SLU, SNU) and Region (1-8) on distal velocity (* = statistically significant at p ≤ 0.05).
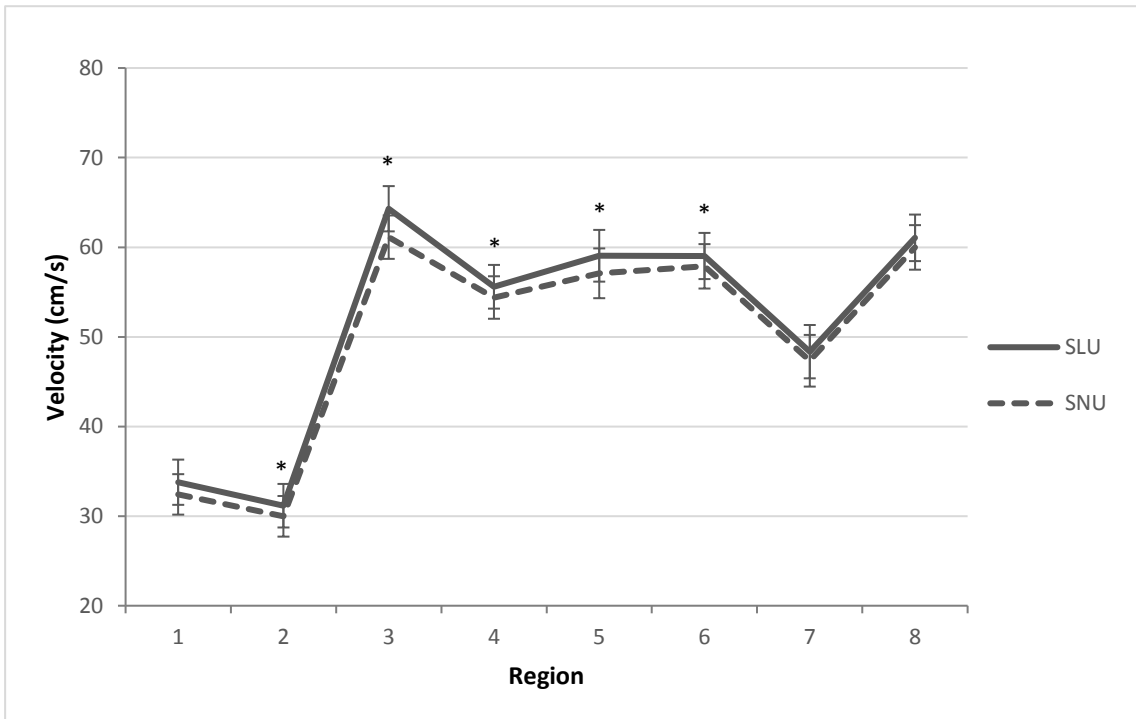
Figure 42. Interaction effect of Marker Design (SLU, SNU) and Region (1-8) on proximal velocity (* = statistically significant at p ≤ 0.05).

In the anterior-posterior direction, there was a statistically significant two-way interaction for anterior soft tissue velocity between Marker Design and Region [$F(3.432, 96.106) = 2.756$, p = 0.040, partial $\eta^2 = 0.090$] (Figure 43), while there was no interaction between Marker Design and Skin Pigmentation [$F(1.000, 28.000) = 1.159$, p = 0.291, partial $\eta^2 = 0.040$]. An analysis of the simple main effects showed that significant differences in anterior velocity between marker designs existed for intermediate and distal regions (3, 5, 6, and 7) of the forearm (p ≤ 0.05). For the significant differences highlighted, the SLU marker design once again had significantly higher values compared to the SNU marker design (p ≤ 0.05). No statistically significant two-way interactions were found for soft tissue velocity in the posterior direction between Marker Design and Region [$F(3.740, 104.713) = 1.200$, p = 0.315, partial $\eta^2 = 0.041$] and Marker Design and Skin Pigmentation [$F(1.000, 28.000) = 0.072$, p = 0.791, partial $\eta^2 = 0.003$], respectively.
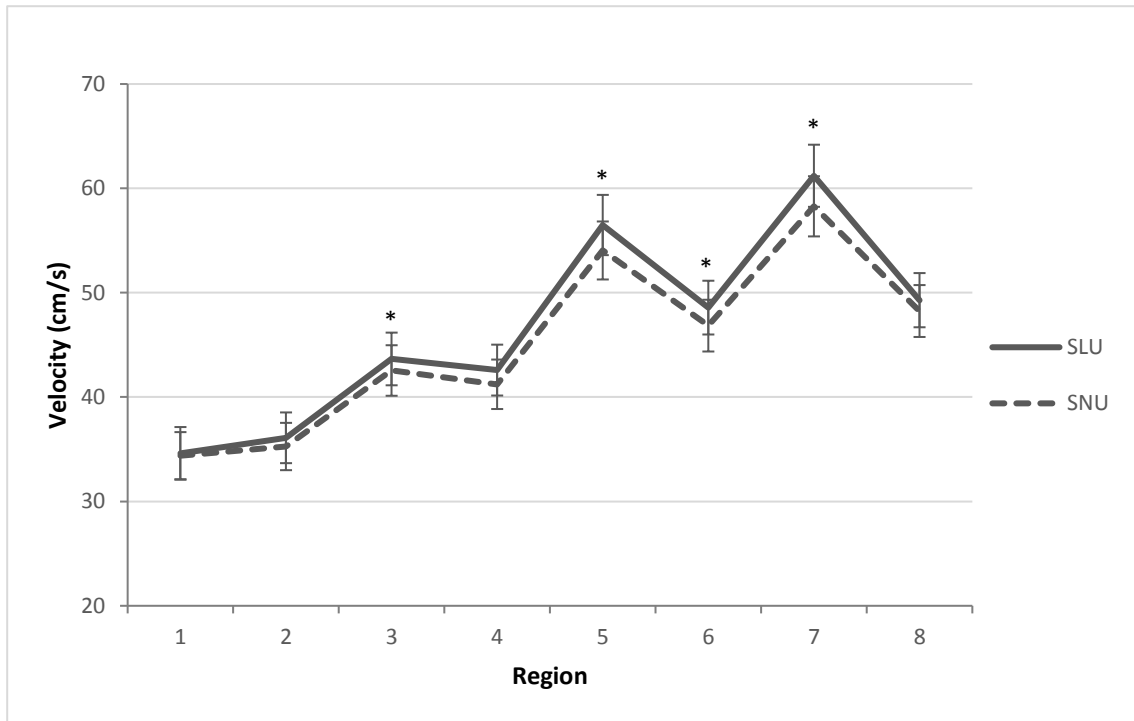
Figure 43. Interaction effect of Marker Design (SLU, SNU) and Region (1-8) on anterior velocity (* = statistically significant at p ≤ 0.05).

4.4.4. Improvements to Automated Motion Tracking

With respect to the automated motion tracking process performed in ProAnalyst®, one case occurred in which the defined region surrounding a SLU marker which was selected to be tracked jumped to an adjacent marker mid-way through the automated tracking process; no tracking discrepancies occurred with the SNU markers. Furthermore, for markers located near the anterior and posterior edges of the forearm, SLU markers were found to be more susceptible to marker drop out compared to the SNU markers, especially on the anterior edge where minor shadowing underneath the forearm reduced the contrast. Similarly, higher rates of marker drop out were also observed for SLU markers located distally and posteriorly in the 0% region of the forearm, as the automated tracking of the smaller sized (0.5 cm diameter) SLU markers was more easily lost where the skin would get compressed near the wrist joint due to hyperextension; the larger size (~1 cm diameter) of the SNU markers proved to be slightly more resilient to this issue.

In an attempt to resolve the automated tracking issues associated with some of these markers, minor adjustments were made in ProAnalyst® to improve the size and position of the defined search region around the marker, and to establish slightly stricter search parameters (e.g., increased threshold tolerance). However, tracking loss was still observed. In spite of this, it should be noted that only one marker was needed from each region to determine the soft tissue displacement and velocity, and therefore, marker drop out did not appreciably affect the results overall.

5. DISCUSSION

5.1. Purpose 1

Quantify planar (2D) displacement and velocity of, and the amount of shock attenuated by, the soft tissues of the forearm following a forward fall impact.

Following impact, the greatest soft tissue displacements recorded for the forearm occurred in the distal direction toward the hand and wrist, and increased in magnitude moving from distal to proximal regions of the forearm. Mean peak distal displacements ranged from a minimum of 0.64 cm in region 1 (distal) to a maximum of 1.47 cm in region 8 (proximal). Compared to mean marker motion (across all markers) for the shank (1.8) and thigh (3.2 cm) following a heel strike task (Pain and Challis, 2006), these values are understandably lower because of the smaller amount of soft tissue in the upper compared to the lower extremities. With respect to soft tissue motion in the forearm, Pain and Challis (2002) reported a mean change in marker displacement along the long axis of the forearm of 1.7 cm. While this value compares more favourably to the results reported here, differences in the study designs may explain why the results are not closer in magnitude. For example, Pain and Challis (2002) employed an active downward striking task to apply impacts to the hand, where initial contact was made at the proximal end (i.e., heel) of the palm and not the fingers, as was seen by a number of participants in the current study.

Previous studies that have measured soft tissue motion using skin surface markers, specifically in relation to STA, have traditionally only analyzed marker displacements (Fuller et al., 1997; Manal et al., 2003; Wrbaškić & Dowling, 2007). As a result, limited information exists in the literature to date regarding soft tissue velocities.

In the current study, the greatest mean peak velocity recorded for forearm soft tissue motion occurred in the distal direction, with a magnitude of 112.8 cm/s. This value is higher than the maximum velocities reported for breast tissue movement in the vertical direction of 92.0 cm/s and 93.1 cm/s while running (Scurr et al., 2010) and performing a two-step star jump (Bridgman et al., 2010), respectively. The mean peak distal velocity of leg soft tissue motion following horizontal pendulum impacts (95.2 cm/s) was similar to that of breast tissue, but reached a much higher magnitude of 137.5 cm/s for vertical drop tests (Brydges et al., 2015), surpassing the forearm soft tissue velocities found in this study. The contribution of gravity to leg soft tissue motion during the vertical drop tests may help to explain the higher tissue velocities for the leg, compared to the forearm values reported here.

Measures of shock attenuation in the forearm soft tissue following forward fall impacts (calculated using the acceleration ratio in Equation 2) highlighted a 76% increase in mean peak accelerations between the distal and proximal ends of the forearm. This indicates that impact shock was not attenuated, but amplified across the soft tissues of the forearm. This finding directly opposes previous research, wherein soft tissues were found to mitigate the effects of impact on the body through shock attenuation (Cole et al., 2006; Gittoes et al., 2006; Pain & Challis, 2001; Pain & Challis, 2002; Pain & Challis, 2006). Potential reasons for this outcome can be linked to the locations from which the acceleration responses were acquired. For instance, surface mounted accelerometers are commonly used to directly measure acceleration responses in the body, where it is recommended that accelerometers are affixed firmly to the body segment at or near underlying rigid bony landmarks within the region of interest (Voloshin, 2000). In

comparison, limitations in the current study with respect to the camera angle and marker drop out resulting from the planar experimental setup made it impossible to acquire accelerations at the wrist and elbow that exactly replicated the distal and proximal bony landmark locations used in previous studies investigating forward fall impacts to the distal upper extremity (Burkhart & Andrews, 2010a, 2010b). Consequently, the peak accelerations recorded in this study, especially those near the elbow, are more representative of the motion of the soft tissue at these locations, rather than the accelerations of the underlying bone. Therefore, the shock attenuation values reported here are not representative of what have been reported previously during impacts (Dufek et al., 2009; García-Pérez et al., 2014; Mercer et al., 2003).

5.2. Purpose 2

Assess if there are differences in soft tissue motion and impact shock attenuation due to sex, or as a function of the region of the forearm measured.

5.2.1. Forearm Region and Tissue Movement

Overall, significant differences were observed with respect to soft tissue movement as a function of the region of the forearm measured. A notable trend occurred along the proximal-distal axis: the soft tissues demonstrated the largest changes in mean peak displacement and velocity from the 0% zone (wrist) to the 25% zone, before generally continuing to increase more gradually in magnitude until the 75% zone (elbow). For example, distal displacement had an average step increase of 66% between the 0% zone (0.70 cm) and 25% zone (1.16 cm), while proximal velocity showed an

112

increase of nearly 85% (from 32.5 cm/s to 59.9 cm/s) between these same regions. The sharp increases observed in this section of the distal forearm could be due to the change in tissue composition occurring here. For example, the tendons of the forearm muscles (i.e., tough bands of fibrous connective tissue) that taper near the wrist, begin to transition into their more prominent muscle bellies in this location. This may have affected the movement of the overlying soft tissues to a greater extent than in other regions of the forearm, where the tissue composition is more uniform. Consequently, this particular region of the forearm may be an important part of the distal upper extremity to consider when analysing the shock attenuation capacity of the body following a fall on the hand of an outstretched arm, especially given the high incidence of distal radius fractures occurring at or near this location (Nellans et al., 2012).

In general, the greatest magnitudes of displaced soft tissue occurred distally and anteriorly, and increased from distal to more proximal regions of the forearm. More specifically, soft tissue displacement in the distal direction was found to be approximately 19% greater on average for the anterior regions of the forearm, while displacements in the anterior direction were 16% greater for the posterior regions. These findings are most likely due to the greater amounts of soft tissue distributed proximally and anteriorly in the forearm, supporting the hypothesis previously made.

Some unanticipated results were observed for peak proximal and posterior displacements due to the fact that the motion pathway of the selected markers, and thus the underlying soft tissues, often did not move back past the point at which impact was estimated to have occurred. This response is in contrast to the underdamped soft tissue response seen by Pain and Challis (2002), where the markers on the anterior forearm

113

were found to continue their downward (or distal) motion immediately after impact from the vertical palm strikes, move back upward (proximal) past the final stationary position, and then experience two further small oscillations before coming to rest. The response seen in the current study produced very low overall magnitudes of peak displacement in the proximal (≤ 0.10 cm) and posterior (≤ 0.08 cm) directions. Although these peak values demonstrated the amount that the forearm soft tissues displaced proximally or posteriorly after impact, they did not necessarily provide tangible information regarding the actual distance the soft tissues traveled in these given directions. Thus, the proximal and posterior rebound distances were also quantified to highlight how far the soft tissues recovered from their peak displacements in the distal and anterior directions, respectively.

The rebound distance magnitudes were also shown to increase from distal to proximal, where more soft tissue is distributed in the forearm. Specifically, it was found that the soft tissues rebounded proximally about 93% of the magnitude of the peak distal displacements for both distal (1–4) and proximal (5–8) regions of the forearm, but only rebounded in the posterior direction up to 80% and 54% of the peak anterior displacement for distal and proximal regions, respectively. These finding may be attributed to a variety of factors. For example, palm deformation against the force plate was not factored in as part of the measured marker motion from the point of impact, which was determined by Pain and Challis (2002) to add 3.5 mm in displacement. In addition, even slight elbow flexion during impact could have contributed to small inferior rotations of the forearm about the hand and wrist, and therefore, hinder the ability of the motion tracking software to track posterior displacement of the soft tissues compared to

the downward motion of the entire forearm, especially for those markers located in distal regions closer to the elbow (i.e., farthest from the axis of rotation).

The trends in mean peak soft tissue velocities were similar to those for displacements. Overall, the velocities in each direction increased in magnitude moving distally to proximally along the forearm, with the greatest peak velocities occurring in the distal direction across all regions. For velocities along the anterior-posterior axis, when the proximal forearm (i.e., 50% and 75% zones) was divided into anterior and posterior regions, the posterior regions of the forearm (5 and 7) were found to have consistently higher velocity magnitudes than the respective anterior regions (6 and 8) within the same zone. These findings are collectively supported by the fact that the greatest mean peak velocities in the distal (112.8 cm/s), anterior (61.2 cm/s), and posterior (27.6 cm/s) directions were recorded in region 7; the most proximally located region of the posterior forearm. Considering the position of the hand and forearm during a forward fall impact, the results observed for the soft tissue velocities could be related to the contractile state of certain muscles in the forearm. For example, with the hand hyperextended at the wrist, the extensor muscles located in the posterior compartment of the forearm are shortened, and thus, fairly stiff during impact. Thus, as suggested by Burkhart and Andrews (2010b), this increased stiffness could contribute to greater transmission of the impact force through the forearm soft tissues, which may help explain the higher velocities observed in this study for the posterior compared to the anterior aspect of the forearm as the shock wave propagates proximally.

In summary, it is evident that regional differences do exist in the response of forearm soft tissues to forward fall impacts on the hand of an outstretched arm. Given

that current WM biomechanical models include very simplified soft tissue components, with respect to their shape and motion characteristics (Gittoes et al., 2006; Gruber et al., 1998; Pain and Challis, 2006), further examination of the relative motions of soft tissue elements within individual segments appears necessary so that the biofiely of future biomechanical modeling efforts can be improved.

5.2.2. Sex and Tissue Movement

No significant differences in soft tissue displacement and velocity were found between sexes (with the sole exception of proximal rebound distance), suggesting that forearm soft tissue motion associated with forward fall impacts was not driven by tissue composition (despite clear differences in soft and rigid tissue masses between sexes), but rather more due to the distribution of soft tissues in the forearm. This result did not support the hypothesis that males would have greater soft tissue displacements and velocities due to greater amounts of WM in their arms compared to females (Mazess et al., 1990). However, when the ratios of FM and LM to the total WM (FM+LM) in the forearm were compared between sexes for the participants in the current study, they were discovered to be reasonably similar (females: 10% FM, 86% LM; males: 5% FM, 94% LM). Although this finding does lend further support for the relative importance of tissue distribution rather than tissue composition, it contradicts the significant differences in the percentage composition of muscle and fat between female and male forearms previously reported by Maughan et al. (1984). The fact that participants in the current study were recruited from a population known to be moderately physically active could have contributed to a reduction in the differences in forearm tissue ratios seen between the

116

sexes. Thus, more research should be conducted on populations of various physical activity levels to better understand if the lack of differences observed in soft tissue kinematics of the distal upper extremity between females and males is a valid result, or a product of the population from which the sample of participants was recruited for this study.

With respect to the proximal rebound distance, the average motion of the forearm soft tissue as it traveled back towards the elbow joint was about 25% higher for females than males across the intermediate and distal regions (3–8). A possible reason for this result may be attributable to differences in the soft tissue thickness of the palm between the sexes. Formed predominantly by the thenar and hypothenar eminences of the hand, the palmar heel pad for males may be thicker than that of females; similar to what has been shown for the heel pad of the foot (Prichasuk, 1994). This anatomical difference would help to absorb more impact shock at the hand for males as the palm compresses and contribute to reduced proximal motion of the forearm soft tissues. However, to date, soft tissue thickness over the palm has only been quantified by ultrasound for young women (Choi & Robinovitch, 2011). Therefore, more research is required to substantiate this claim.

5.2.3. Sex and Shock Attenuation

With respect to the capacity of the forearm to attenuate impact shock following forward fall impacts, no differences in un-normalized shock attenuation measures and mean peak proximal and distal accelerations were observed between females and males. However, when normalized to the individual forearm tissue masses (BMC, FM, LM, and

117

WM), significant differences were observed for shock attenuation measures normalized to BMC, LM, and WM. On average, males experienced significantly lower magnitudes of increased shock per gram of tissue (i.e., less of an increase from distal to proximal peak accelerations per gram of tissue) than females. This mirrored the normalized peak acceleration responses at the tibia following heel impacts between sexes reported by Schinkel-Ivy et al. (2012), supporting the notion that these tissue masses potentially have a more important role in attenuating shock in the body for males compared to females.

5.3. Purpose 3

Identify the relationship between the displacement, velocity, and shock attenuation capacity of the forearm soft tissues and their individual tissue masses (BMC FM, LM, and WM).

5.3.1. Tissue Masses and Movement

Overall, moderately strong relationships were found between the magnitudes of BMC, FM, LM, and WM and the kinematics associated with the motion of the forearm soft tissues after impact. These relationships were different for females and males in several ways. For example, females had significant positive relationships predominantly with BMC, FM, and WM for soft tissue motion occurring in the proximal-distal direction, whereas males had significant negative relationships with BMC, LM, and WM for soft tissue motion occurring almost exclusively in the anterior direction; no significant relationships were found in the posterior direction for both sexes. Although interesting to see such stark contrasts between the tissue mass correlations for females and males, these results demonstrate that the magnitudes of soft and rigid tissue masses alone cannot

explain the lack of sex differences previously observed in the present study for the soft tissue kinematics of the forearm.

Since the relationships for each tissue type were also varied across different forearm regions, no distinct patterns were revealed from which to draw more definitive conclusions on the roles that these tissue masses may have played with respect to region-specific marker motion within the forearm. However, when assessing intra-segmental marker motion of the forearm as a whole, it is clear that FM and WM are strongly associated with proximal rebound distance for females, as significant positive relationships were found across all the regions for the forearm (except region 2 for WM). This indicates that the higher amounts of FM in the forearms of females compared to males (Maughan et al., 1984) is likely a key contributor to greater magnitudes of soft tissue rebound proximally toward the elbow.

Schinkel-Ivy et al. (2012) showed that the mass of passive structures in the body (i.e., soft and rigid tissues) influence the acceleration responses, and thus the shock attenuation capacity, of the lower extremity following foot impacts. Specifically, it was suggested that increases in absolute tissue masses decreased acceleration responses measured at the proximal tibia, where BMC and LM had the strongest (negative) relationships with peak acceleration. In the current study, it was hypothesized that similar trends would be observed in the distal upper extremity for forward fall impacts to the hands. However, this was found to only be the case for males, as the correlations across all tissue masses (BMC, FM, LM, and WM) and peak distal and proximal accelerations were negative; no statistically significant relationships were noted for females.

It appears that a meaningful link does exist between the magnitudes of specific rigid and soft tissue masses and the kinematics related to the soft tissue configuration of the forearm, to a different extent for females and males. Consequently, the results presented here clearly support the importance of including this information in the development of future WM models in order to reflect the unique behaviour of the surrounding soft tissues between the sexes. Furthermore, given that there are no known previous studies in the literature that have taken into account the role of different forearm tissue masses (BMC, FM, LM, WM) on soft tissue displacement or velocity, and only the contribution of active mechanisms of shock attenuation (e.g., muscle activation and joint angle) have been investigated for hand impacts (Burkhart & Andrews, 2010b; DeGoede & Ashton-Miller, 2002; Pain & Challis, 2002), further research in this area for upper extremity impacts is necessary.

Forearm tissue mass estimates in the current study were determined using upper extremity prediction equations developed by Arthurs et al. (2009), where anthropometric measurements such as skin fold thicknesses, breadths, circumferences, and lengths were used as inputs. Although there is always the potential for error when performing anthropometric measurements, the investigator was previously trained in the proper execution of these measurements in which good to excellent between- and within-measurer reliability was established (Burkhart et al., 2008). The following equations were also validated against DXA scans from which segmental tissue masses for the hand, forearm, and arm were determined from custom regions of interest that were found to be replicated with excellent reliability (Burkhart et al., 2009). In addition, the general physical and age profiles of the sample of participants used in this study closely matched

those used by Arthurs et al. (2009) to develop the prediction equations initially. For these

reasons, errors associated with taking anthropometric measurements were not believed to

be a major limitation of this research. However, an important consideration to take into

account when interpreting the results of the current study is that these equations only

produce tissue mass estimates of the entire segment of interest. Region-specific tissue

mass composition of the forearm is still required in order to provide better insight into the

differential soft tissue mass motion seen in this investigation.

5.4. Purpose 4

Determine if a stacked, non-uniform (SNU) marker design (non-uniform, ~0.5 cm

diameter black dots overlaid on top of a grid of contrasting ~1 cm diameter white dots; 2

cm inter-marker distance) produces significantly different kinematic results and improves

automated marker tracking across different skin pigmentations compared to the single

layer, uniform (SLU) marker design (grid of uniform, 0.5 cm diameter black dots; 2 cm

inter-marker distance) previously established by Brydges et al. (2015).

5.4.1. Skin Pigmentation and Tissue Movement

Motion of the soft tissues of the forearm was found to be very similar overall

between the light and dark skin pigmentation groups. This is highlighted by the fact that

no interaction effects were present between skin pigmentation and the regions of the

forearm for any of the kinematic variables assessed (apart from anterior soft tissue

displacement across skin pigmentations in region 7). This demonstrates that the

participants in this study were matched relatively well in terms of age and physical

121

characteristics (i.e., height and body mass) for each skin pigmentation group (light: 9F, 6M; dark: 9F, 6M), thereby limiting the effects of individual differences on the following comparisons.

5.4.2. Marker Design, Skin Pigmentation, and Tissue Movement

While significant differences in soft tissue kinematics were observed between the two massless surface marker designs as a function of both skin pigmentation and forearm region, the magnitudes of, and consequently meaningful influence of these statistical differences for the automated tracking of soft tissue motion, were negligible.

With respect to differences in mean peak soft tissue displacement, only values along the proximal-distal axis were affected; no discrepancies were found anteriorly and posteriorly. For the light skin pigmentation group, the displacement of the soft tissues in the distal direction showed no differences between the two marker designs, while the magnitudes of distal displacement for the SLU marker design was, on average, 0.05 cm greater in regions 2 through 8 than the SNU marker design for the dark skin pigmentation group. Mean peak proximal soft tissue displacement demonstrated opposite trends for each skin pigmentation group across all regions, as the SLU marker design resulted in higher magnitudes of proximal displacement for the light group, and lower proximal displacements for the dark group, when compared to the SNU marker design. However, the proximal soft tissue displacement magnitudes on average were very low (< 0.07 mm).

Similar to displacement, only the mean soft tissue rebound distance in the proximal direction showed significant differences between marker designs. For both skin pigmentation groups, the mean proximal rebound distances were found to be higher in

magnitude for the SLU marker design than the SNU marker design for six of the eight regions of the forearm. Nevertheless, these differences were exceptionally small at 0.04 cm and 0.05 cm on average for the light and dark skin pigmentation groups, respectively.

The SLU and SNU marker designs affected the mean peak soft tissue velocities in the distal, proximal, and anterior directions the same for each skin pigmentation; the SLU marker design had significantly higher values compared to the SNU marker design. Average increases in velocity for each of the highlighted directions were approximately 2.6 cm/s distally (regions 1–8), 1.7 cm/s proximally (regions 2, 3, 4, 5, and 6), as well as 2.0 cm/s anteriorly (regions 3, 5, 6, and 7). These increases correspond to a collective increase of less than 3%.

In general, for instances when the soft tissue kinematics differed between the two marker designs, the SLU marker design was found to consistently produce greater values than the SNU marker design (excluding proximal soft tissue displacement for the dark skin pigmentation group). As alluded to earlier, the magnitudes of these differences were very small overall, and therefore, could be argued to be functionally irrelevant when comparing the precision of motion tracking using the two marker designs. Moreover, it is likely that these differences are related to slight variations in the position of the defined rectangular regions used in ProAnalyst® to track selected markers, as the difference in marker size (SNU markers: ~1 cm diameter; SLU markers: 0.5 cm diameter), combined with the free-hand application of the SNU markers on the forearm, could have easily led to minor differences in the geometric centre of the defined tracking region between marker designs, despite the vigilance of the investigator to apply the SNU markers directly over top of the SLU markers.

Additionally, the overall effect of each marker design was very similar between skin pigmentation groups, suggesting that the automated tracking of forearm soft tissue motion was not significantly influenced by the different markers and different skin pigmentations, thus not supporting the original hypothesis, especially with respect to the proposed benefits of the enhanced marker contrast of the SNU design. However, an important consideration for the current study is that the majority of participants in the dark skin pigmentation group (i.e., 11 of 15) were categorized as Type IV based on their results from the Fitzpatrick Skin Type Questionnaire. Since this category borders the division between the two skin pigmentation groups (light: Type I–III; dark: Type IV–VI), the need for markers with enhanced contrast may not have been necessary for accurate motion tracking. Also, because a major section of the questionnaire is subjective to the reader's perception of how well they tan, of those 11 participants, some may have been falsely categorized into the dark skin pigmentation group, when they should have been included in the light skin pigmentation group instead. Therefore, the validity of this questionnaire for categorizing skin pigmentations needs to be addressed if it is to be used to determine contrast requirements for soft tissue motion capture, as done in this study.

Only one case occurred throughout all video analyses where the automated motion tracking software had difficulties differentiating between separate SLU markers, whereas no tracking disputes occurred with the SNU markers. Consequently, as hypothesized, the increased shape variations of the SNU marker design did have a beneficial effect on the automated motion tracking; although, it could be argued that this result is not as significant as what has been reported for other non-contact motion tracking methods, such as DIC (Crammond et al., 2013; Haddadi and Belhabib, 2008).

Furthermore, improvements to both frame rate and resolution of the captured video in the current study (5000 frames/s, 1024 x 800 pixels^2 resolution) may help explain the lack of marker discrepancies observed in the SLU design compared to previous work by Brydges et al. (2015), where the same massless marker approach was used to capture soft tissue motion of the leg following heel impacts but with different collection parameters (1000 frames/s, 640×480 pixels^2 resolution).

Ultimately, since the overall effectiveness of each marker design was found to be functionally equivalent, either marker set could theoretically be used to accurately and reliably track soft tissue motion, assuming adequate motion capture equipment and automatic tracking software are utilized. However, if the practicality of the two marker designs is taken into account, application of the SLU marker design would arguably be considered the superior approach. This is because, compared to the SNU marker design, the SLU marker design is more time- and cost-effective since it only requires one layer to be applied to the area of interest with a single permanent black marker, rather than multiple layers that need additional time to properly dry and are applied with two expensive specialty black and white water-based paint markers.

5.5. Limitations

The present study was not without its limitations. With respect to the modified torso-release apparatus used to apply forward fall impacts to the hands, the final orientation of the forearm at impact ended up being relatively horizontal. In combination with the effects of gravity, this would likely pull the soft tissues towards the ground (i.e., anteriorly), possibly contributing to the limited response in the proximal and posterior

directions observed in this study. Moreover, despite the efforts of the investigator to prevent the participant from anticipating the initiation of the forward fall simulation, an audible noise was produced when the quick release devise was engaged. This may have given participants advanced warning of the impending release.

Small discrepancies in the inter-marker distance (2 cm) may have occurred when the SLU marker design was applied using the flat stencil over the rounded surface of the participants' forearms. These discrepancies may have translated into calibration errors in ProAnalyst®. However, these errors were minimised by selecting calibration points from the straightest row of markers located on the proximal forearm, away from the compressed tissues near the wrist. In addition, despite its importance in attenuating impact shock for the distal upper extremity, compression of the palm region was not measured in the current study. While this may have affected the results to some degree, it was not feasible to measure palm deformation, in a similar fashion as Brydges et al. (2015) measured heel pad deformation, because of the lack of space for marker placement on the hand.

The motion of the rigid tissue (i.e., bone) was not directly measured in the present study. As a result, the relative motion of the soft tissue could not be entirely isolated. In other words, the intra-segmental marker motion may have been influenced, to a certain extent, by the whole limb motion of the forearm (Pain & Challis, 2002). The impact of this limitation was minimised by carefully instructing the participants to maintain their upper extremity posture during data collection. In addition, inspection of the data prior to analysis did not reveal appreciable forearm motion separate from the motion of the soft tissue.

Due to the age parameters of the tissue mass prediction equations that were used to estimate individual soft and rigid tissue masses in the forearm (Arthurs et al., 2009), all participants in the current study were between 17 and 30 years of age. Consequently, the generalizability of the following results is limited to a younger adult population. Significant changes in body composition, such as sarcopenia (i.e., skeletal muscle atrophy) (Baumgartner et al., 1998), and progressive declines of skin elasticity (Luebberding et al., 2014; Sumino et al., 2004) have been found to occur with age, which would undoubtedly influence the impact response of the forearm soft tissues. In addition, since participants were also recruited from a moderately active population, potential differences in athleticism may have contributed to some of the variation observed between participants with respect to the total number of impact trials needed to achieve the three consistent impacts per marker design. For example, two trained dancers participated in the study and were both able to complete the impact trials efficiently without the need for additional feedback, which could be justified by the advanced proprioceptive capabilities they learned to control their body movements. However, it should be noted that the total number of recorded impact trials executed did not exceed more than six forward fall impacts per marker design.

Finally, as stated by Brydges et al. (2015) for the leg, an assumption of using massless surface markers on the skin to quantify soft tissue movement following impact, is that the superficial soft tissues (i.e., skin) move synchronously with the underlying deep soft tissues (i.e., muscle and fat), and therefore, produce identical impact responses relative to bone. This assumption could not be tested in the current study, given the superficial, and non-invasive nature of the approaches used.

6. FUTURE DIRECTIONS

6.1. Muscle Activation and Joint Angles

Significant relationships were found in this study between different tissue masses (i.e., BMC, FM, LM, and WM), which offers support to the notion that tissue composition does, to some extent, contribute to the impact response of the forearm soft tissues. Although participants were asked to maintain a relaxed state during the impact trials with their arms extended at the elbows, muscle activation levels and elbow joint angle were not directly controlled for in this thesis.

Muscle activation levels have been shown to play an important role with regards to impact shock attenuation, as the mechanical changes that occur with varying muscle activation, such as changes to structural stiffness (Cholewicki & McGill, 1995), can affect the energy absorbing capability of soft tissues (Pain & Challis, 2002). For example, Burkhart and Andrews (2010b) demonstrated that increases in the activation of forearm muscles (the extensor carpi ulnaris and flexor carpi ulnaris) resulted in increased transmission of impact shock waves through the forearm. Moreover, with respect to the influence of varying elbow angles when arresting a forward fall, a 0.9 percent/degree decrease in impact force as elbow flexion increased has been reported (DeGoede et al., 2002). Therefore, these factors need to be controlled for in future research efforts if the passive impact response of the forearm soft tissues alone is to be quantified properly. However, quantifying these measures without the use of devices which need to be externally affixed to the skin (e.g., electromyography, electrogoniometers, etc.), is a challenge which could not be met during the current study. Methods requiring external

fixation will disrupt the natural physiological motion of the underlying soft tissues, as documented previously for the leg (Stefanczyk et al., 2013).

6.2. Forward Fall Impact Simulations

The modified torso release apparatus used in the current study offered a cost-effective and flexible approach to simulate forward fall hand impacts consistently, while accommodating for the configuration of the high speed camera and lighting equipment. Despite the advantages of this particular impact method, the orientation of the body at impact did not truly represent that which would be witnessed during a forward fall (Hsiao & Robinovitch, 1998; O'Neill et al., 1994). Future research investigating the response of forearm soft tissues to forward fall impacts should therefore strive to validate the findings of the current study using impact methods that better simulate the kinetics and kinematics of real world fall events.

The PULARIS fall simulation method developed by Burkhart et al. (2012) incorporates many of these real world parameters into its design, allowing it to accurately simulate the non-stationary, multi-directional movements indicative of the body positions and impact loads experienced during an actual forward fall. Although this impact method is relatively complex compared to the approach used here, measuring the soft tissue response in the distal upper extremity using PULARIS could advance our understanding of the injury mechanisms surrounding forward falls by providing more realistic information of how the soft tissues mitigate the response to these harmful impact events.

6.3. Three-Dimensional Motion Capture

Forearm soft tissue motion was only measured in 2D in the current study. As with the previous study by Brydges et al. (2015) for the leg, planar analysis of the forearm was deemed to be an appropriate first step towards understanding soft tissue motion relative to the underlying bone resulting from an impact event. It was evident during video analysis that there was some soft tissue motion occurring outside of the plane recorded. For example, soft tissues located in the more proximal regions were seen to twist to some degree around the long axis of forearm. In addition, very prominent undulations of the soft tissues were observed in the posterior regions of the proximal forearm near the elbow. Most of this motion is believed to be due to the muscles constituting the forearm extensors, which collectively originate on or near to the lateral epicondyle of the humerus (e.g., brachioradialis, extensor carpi ulnaris). This out-of-plane motion is consistent with soft tissue motion that has been previously recorded during 3D analyses (Akbarshahi et al., 2010; Manal et al., 2003; Mills et al., 2011; Stagni et al., 2005)

Therefore, 3D analysis would be a logical next step to advance the scope of the approach used here, and to fully understand the effect that soft tissue motion has on the propagation and attenuation of impact forces in the forearm. Furthermore, 3D DIC (Blenkinsopp et al., 2012; Ito et al., 2015; Omkar et al., 2013) should also be considered as an alternate non-contact method, with which full-field surface displacement and strain maps of the distal upper extremity could be acquired.

6.4. Massless Surface Markers

The two types of massless surface marker designs (SLU and SNU) used in the present study were each found to effectively track soft tissue motion, with only very minor differences. Therefore, attempting to establish which marker design is superior for soft tissue motion tracking purposes is difficult. The water-based paint markers utilized for the SNU design did demonstrate some cracking after 20 to 30 minutes of wear, although this was well past the time needed to complete the impact trials. Nevertheless, future studies looking to replicate this marker design should be conscious of this, if soft tissue motion tracking is needed over an extended period of time. With respect to the SLU marker design, it may be beneficial for future research to investigate the effect of different coloured permanent markers on soft tissue motion measurement. For instance, metallic coloured markers (e.g., silver) may possess enough reflective properties to act as retro-reflective markers, which could be useful with other motion capture techniques, such as optoelectronic camera systems.

6.5. Wrist Guards and Compliant Safety Flooring

Future applications of this research could potentially extend into multiple areas associated with fall injury prevention strategies. For example, wrist guards have been shown to be effective at reducing impact-induced accelerations at the wrist and elbow by almost 50% (Burkhart & Andrews 2010a). It would be interesting to determine the extent to which wrist guard use also influences the impact response of the underlying soft tissues, especially for the sport of snowboarding, where research efforts are currently working towards assessing the functionality and efficacy of snowboarding wrist

131

protectors for the development of a harmonized ISO-standard (Brügger & Michel, 2015; Michel et al., 2013). Consequently, the relative novelty of this soft tissue motion research could offer an interesting perspective for improving the design parameters of wrist protectors in snowboarding (in addition to other sports), which has not yet been considered otherwise. Furthermore, to date, the effects of energy-absorbing flooring systems have only been assessed for hip impacts (Laing & Robinovitch, 2009). Considering the negative implications that forward fall-related injuries to the distal upper extremity have on our healthcare systems (Bonafede et al., 2013; Kilgore et al., 2009; Stevens et al., 2006), future research investigating the shock attenuating capacity of compliant safety flooring systems to forward fall impacts, and how safety floors modify the motion of the forearm soft tissues, appears warranted. The positive implications of this work are considerable across a variety of high-risk environments where forward fall impacts are common (e.g., nursing homes, playgrounds, gymnasiums).

6.6. Force-Time Analyses

Although not assessed in the current study, analysis of the collected force-time data could offer valuable information regarding the contributions of the hand impact forces to the forearm soft tissue motion observed. Similar to Burkhart et al. (2012a), force-time curves could be used to calculate additional measures such as impulse, impulse duration, and load rate for each of the three force components recorded during the forward fall simulation (F_x, F_y, F_z), and therefore, determine how the impact response of the forearm in vivo compares to that of the distal radius in vitro. Moreover, pairing the forearm soft tissue motion data with the respective force-time profiles will provide a

better understanding of the shock attenuation response of the distal upper extremity at critical moments (e.g., F_{imp} and F_{brk}) during forward fall impacts (Chiu & Robinovitch, 1998; DeGoede & Ashton-Miller, 2002; Hwang et al., 2006; Kim & Ashton-Miller, 2003). Therefore, future studies extending from this research should aim to establish the link between the kinematics and the kinetics associated with the forearm soft tissue response following a forward fall on the hand of an outstretched arm.

7. CONCLUSIONS

The results of this study can be summarized as follows:

- To the best knowledge of the author, the present study is the first to quantify displacements and velocities associated with forearm soft tissue motion following forward fall impacts using high speed motion capture and automated motion tracking software (ProAnalyst®).

- The amount of shock attenuated by the soft tissues of the forearm could not be accurately determined. However, the magnitude of peak soft tissue acceleration responses increased by approximately 76% from distal (9385.8 cm/s²) to the proximal (16298.9 cm/s²) ends of the forearm segment overall.

- On average, the greatest mean peak soft tissue displacements and velocities in the forearm occurred in the distal direction towards the hand and wrist after impact with magnitudes of 1.09 cm and 104.8 cm/s, respectively.

- Overall, regions of the forearm with greater amounts of total wobbling mass (i.e., the proximal forearm) experienced greater mean peak soft tissue displacements and velocities. On average, the soft tissues of the anterior forearm displaced distally 19% further than posterior regions, while the tissues of the posterior forearm displaced anteriorly 16% further than anterior regions; region 7 had the greatest peak soft tissue velocities in both the distal (112.8 cm/s) and anterior (61.2 cm/s) directions.

- Although females demonstrated greater mean peak distal soft tissue displacements (females: 0.67–1.52 cm; males: 0.61–1.39 cm), and males had greater mean peak distal soft tissue velocities (females: 88.9–110.3 cm/s; males: 94.0–116.6 cm/s), the kinematic response of the forearm soft tissues to forward fall impacts did not significantly differ between the sexes (p > 0.05) (with the exception of the rebound distances). This suggests that there may not be meaningful differences in the distribution of soft tissue in the forearm between females and males, despite differences in forearm tissue composition.

- The lack of significant trial effects across any of the impact reaction force data presented for the modified torso-release apparatus (p > 0.05), and extremely high ICCs (≥ 0.972) reflects the excellent reliability of this approach for simulating forward falls.

- The magnitudes of some rigid and soft tissue masses within the forearm (BMC, FM, LM, and WM) had significant correlations with the magnitudes of soft tissue displacements and velocities after impact (p ≤ 0.05). Females had significant positive relationships primarily with BMC, FM, and WM for soft tissue motion along the proximal-distal axis (r = 0.470 to 0.776), while males had significant negative relationships with BMC, LM, and WM for soft tissue motion almost exclusively in the anterior direction (r = -0.577 to -0.760). These results provide an interesting perspective on the roles that specific tissues may play in the

mitigation of impact shock in the distal upper extremity between sexes; an insight that has not yet been reported in the literature.

- In general, for the significant differences in the soft tissue kinematics observed between the two marker designs tested, the SLU marker design consistently provide higher values than the SNU marker design, regardless of skin pigmentation ($p \leq 0.05$). However, the actual magnitudes of these differences were found to be exceptionally small; for example, with respect to proximal soft tissue rebound distance, the average difference between the two marker designs was ≤ 0.05 cm for both the light and dark skin pigmentation group. Thus, the resultant impact of these statistical differences on the soft tissue motion kinematics were deemed to be functionally irrelevant for motion capture purposes.

- Enhanced marker contrast and shape variation of the SNU marker design did not appreciably improve the automated motion tracking process compared to the SLU design. Apart from correcting one case of faulty marker tracking and slightly reducing drop out and loss of tracking for those markers located on the anterior and posterior edges of the forearm, the SNU and SLU marker designs were equally effective for tracking soft tissue motion. Therefore, when considering the practicality of the two marker designs, the SLU marker pattern would be the more reasonable option.

- The results presented in this thesis provide valuable information about how the soft tissues of the forearm respond to impacts consistent with forward falls on the hand of an outstretched arm and, as a result, how shock propagates through the distal upper extremity. This information will advance our understanding of the associated injury mechanisms and hopefully help drive the development of improved biomechanical models which are able to better predict the risk of injury associated with forward fall impact events.

REFERENCES

Abanto-Bueno J, Lambros J. Investigation of crack growth in functionally graded materials using digital image correlation. Eng Fract Mech. 2002; 69: 1695-711.

Akbarshahi M, Schache A, Fernandez J, Baker R, Banks S, Pandy M. Non-invasive assessment of soft-tissue artifact and its effect on knee joint kinematics during functional activity. J Biomech. 2010; 43: 1292-301.

Alexander EJ, Andriacchi TP. Correcting for deformation in skin-based marker systems. J Biomech. 2001; 34(3): 355-61.

Alsakarneh A, Quinn B, Kelly G, Barrett J. Modelling and simulation of the coefficient of restitution of the sliotar in hurling. Sports Biomech. 2012; 11(3): 342-57.

Audysho R, Smith R, Altenhof W, Patel K. Aluminum foam core density and geometry influences on the deformation mechanisms of foam filled braided tubular structures in tension. Mater Design. 2014; 54: 394-413.

Arthurs KL, Andrews DM. Upper extremity soft and rigid tissue mass prediction using segment anthropometric measures and DXA. J Biomech. 2009; 42(3): 389-94.

Backman D, Jodoin A, Poon C, Mendis Y. The use of digital image correlation to verify the behavior of fiber metal laminate cylinders under torsional loading. J ASTM Int. 2006; 3(5): 1-9.

Ball KA. Kinematic comparison of the preferred and non-preferred foot punt kick. J Sport Sci. 2011; 29(14): 1545-52.

Barranger Y, Doumalin P, Dupré JC, Germaneau A. Digital image correlation accuracy: influence of kind of speckle and recording setup. EPJ Web of Conferences. 2010; 6; 31002.

Baumgartner RN. Body composition in healthy aging. Ann N Y Acad Sci. 2000; 904: 437-48.

Baumgartner RN, Koehler KM, Gallagher D, Romero L, Heymsfield SB, Ross RR, et al. Epidemiology of sarcopenia among the elderly in New Mexico. Am J Epidemiol. 1998; 147(8): 755-63.

Bennett SW, Lanovaz JL, Muir GD. The biomechanics of locomotor compensation after peripheral nerve lesion in the rat. Behav Brain Res. 2012; 229(2): 391-400.

Betts SC, Miller TH, Gupta R. Location of the neutral axis in wood beams: A preliminary study. Wood Mater Sci Eng. 2010; 5(3-4): 173-80.

Bewerse C, Gall KR, McFarland GJ, Zhu PP, Brinson LC. Local and global strains and strain ratios in shape memory alloys using digital image correlation. Mater Sci Eng. 2013; A(568): 134-42.

Blenkinsopp R, Harland A, Price D, Lucas T, Roberts J. A method to measure dynamic dorsal foot surface shape and deformation during linear running using digital image correlation. Procedia Eng. 2012; 34: 266-71.

Bonafede M, Espindle D, Bower AG. The direct and indirect costs of long bone fractures in a working age US population. J Med Econ. 2013; 16(1):169-78.

Bridgman C, Scurr J, White J, Hedger W, Galbraith H. Three-dimensional kinematics of the breast during a two-step star jump. J Appl Biomech. 2010; 26(4): 465-72.

Brizuela GG, Llana SS, Ferrandis RR, Garcia-Belenguer AC. The influence of basketball shoes with increased ankle support on shock attenuation and performance in running and jumping. J Sports Sci. 1997; 15(5): 505-15.

Bruck HA, McNeill SR, Sutton MA, Peters III WH. Digital image correlation using Newton-Raphson method of partial differential correction. Exp Mech. 1989; 29(3): 261-7.

Brügger O, Michel FI. Development of a ISO-standard for wrist protection in snowboarding: history, presence, future. Conference: ISO 20320 Meeting. San Vito di Catore, Italy, March 2015.

Brydges EA, Burkhart TA, Altenhof WJ, Andrews DM. Leg soft tissue position and velocity data from skin markers can be obtained with good to acceptable reliability following heel impacts. J Sports Sci. 2015; 33(15): 1606.

Burkhart TA, Andrews DM, Dunning CE. Failure characteristics of the isolated distal radius in in response to dynamic impact loading. J Orthop Res. 2012a; 30(6): 885.

Burkhart TA, Andrews DM. The effectiveness of wrist guards for reducing wrist and elbow accelerations resulting from simulated forward falls. J Appl Biomech. 2010a; 26(3): 281-92.

Burkhart TA, Andrews DM. Activation level of extensor carpi ulnaris affects wrist and elbow acceleration responses following simulated forward falls. J Eletromyogr Kines. 2010b; 20: 1203-10.

Burkhart TA, Arthurs KL, Andrews DM. Reliability of upper and lower extremity anthropometric measurements and the effect on tissue mass predictions. J Biomech. 2008; 41(7): 1604-10.

Burkhart TA, Arthurs KL, Andrews DM. Manual segmentation of DXA scan images results in reliable upper and lower extremity soft and rigid tissue mass estimates. J Biomech. 2009; 42(8): 1138-42.

Burkhart TA, Clarke D, Andrews DM. Reliability of impact forces, hip angles and velocities during simulated forward falls using a novel Propelled Upper Limb fall ARrest Impact System (PULARIS). J Biomech Eng. 2012b; 134(1): 011001.

Burkhart TA, Quenneville CE, Dunning CE, Andrews DM. Development and validation of a distal radius finite element model to simulate impact loading indicative of a forward fall. Proc IMechE Part H: J Engineering in Medicine. 2014; 228(3): 258-71.

Canadian Ski Council. Canadian skier and snowboarder facts and stats, 2012-2013. Collingwood, ON: Canadian Ski Council; 2014. [cited 2017 Apr 14]. Available from: https://www.skicanada.org/wp-content/uploads/2014/08/CSC-2012-13-Facts-Stats-August-7-2014_final.doc.pdf

Cappello A, Cappozzo A, La Palombara PF, Lucchetti L, Leardini A. Multiple anatomical landmark calibration for optimal bone pose estimation. Hum Mov Sci. 1997; 16(2-3): 259-74.

Cappello A, Stagni R, Fantozzi S, Leardini A. Soft tissue artifact compensation in knee kinematics by double anatomical landmark calibration: performance of a novel method during selected motor tasks. IEEE Trans Biomed Eng. 2005; 52(6): 992-8.

Cappozzo A, Catani F, Leardini A, Benedetti MG, Croce UD. Position and orientation in space of bones during movement: experimental artefacts. Clin Biomech. 1996; (2): 90-100.

Centers for Disease Control and Prevention. (October, 1994). The National Institute for Occupational Safety and Health (NIOSH): International Chemical Safety Cards (ICSC): Zinc Powder. Retrieved from http://www.cdc.gov/niosh/ipcsneng/neng1205.html

Chiu J, Robinovitch SN. Prediction of upper extremity impact forces during falls on the outstretched hand. J Biomech. 1998; 31(12): 1169-76.

Choi WJ, Kaur H, Robinovitch SN. Measurement of the effect of playground surface materials on hand impact forces during upper limb fall arrests. J Appl Biomech. 2014; (2): 276-81.

Choi WJ, Robinovitch SN. Pressure distribution over the palm region during forward falls on the outstretched hands. J Biomech. 2011; 44(3): 532-39.

Choi S, Shah SP. Measurement of deformations on concrete subjected to compression using image correlation. Exp Mech. 1997; 37: 307-13.

Cholewicki J, McGill SM. Relationship between muscle force and stiffness in the whole mammalian muscle. J Biomech Eng. 1995; 117(3): 339-42.

Chu JJ, Caldwell GE. Stiffness and damping response associated with shock attenuation in downhill running. J Appl Biomech, 2004; 20(3): 291-308.

Chu V, Fong D, Chan Y, Yung P, Fung K, Chan K. Differentiation of ankle sprain motion and common sporting motion by ankle inversion velocity. J Biomech. 2010; 43(10): 2035-8.

Cole GK, Nigg BM, van den Bogert AJ, Gerritsen KGM. Lower extremity joint loading during impact in running. Clin Biomech. 1996; 11(4): 181-93.

Cooper KE, Edholm OG, Mottram RF. The blood flow in skin and muscle of the human forearm. J Physiol. 1955; 128(2): 258-67.

Coventry E, O'Connor KM, Hart BA, Earl JE, Ebersole KT. The effect of lower extremity fatigue on shock attenuation during single-leg landing. Clin Biomech. 2006; 21(10): 1090-7.

Cowley KC, MacNeil BJ, Chopek JW, Sutherland S, Schmidt BJ. Neurochemical excitation of thoracic propriospinal neurons improves hindlimb stepping in adult rats with spinal cord lesions. Exp Neurol. 2015; 264: 174-87.

Crammond G, Boyd SW, Dulieu-Barton JM. Speckle pattern quality assessment for digital image correlation. Opt Lasers Eng. 2013; 51(12): 1368-78.

Daniels SR, Khoury PR, Morrison JA. The utility of body mass index as a measure of body fatness in children and adolescents: Differences by race and gender. Pediatrics. 1997; 99(6): 804-7.

DeGoede KM, Ashton-Miller JA, Schultz AB, Alexander NB. Biomechanical factors affecting the peak hand reaction force during the bimanual arrest of a moving mass. J Biomech Eng. 2002; 124(1): 107-12.

DeGoede KM, Ashton-Miller JA. Fall arrest strategy affects peak hand impact force in a forward fall. J Biomech. 2002; 35(6): 843-8.

Dufek JS, Bates BT. Biomechanical factors associated with injury during landing in jump sports. Am J Sports Med. 1991; 12: 326-37.

Dufek JS, Mercer JA, Griffin JR. The effects of speed and surface compliance on shock attenuation characteristics for male and female runners. J Appl Biomech. 2009; 25(3): 219-28.

Facchinello Y, Brailovski V, Petit Y, Brummund M, Tremblay J, Mac-Thiong JM. Biomechanical assessment of the stabilization capacity of monolithic spinal rods with different flexural stiffness and anchoring arrangement. Clin Biomech. 2015; 30: 1026-35.

Fitzpatrick TB. The validity and practicality of sun reactive skin types I through VI. Arch Dermatol. 1988: 124(6): 869-71.

Fuller J, Liu L, Murphy M, Mann R. A comparison of lower-extremity skeletal kinematics measured using skin- and pin-mounted markers. Hum Mov Sci. 1997; 16(2-3): 219-42.

Flynn C, Taberner A, Nielsen P. Mechanical characterisation of in vivo human skin using a 3D force-sensitive micro-robot and finite element analysis. Biomech Model Mechanobiol. 2011; 10(1): 27-38.

García-Pérez JA, Pérez-Soriano P, Belloch SL, Lucas-Cuevas AG, Sánchez-Zuriaga D. Effects of treadmill running and fatigue on impact acceleration in distance running. Sport Biomech. 2014; 13(3): 259-66.

Gao B, Zheng N. Investigation of soft tissue movement during level walking: translations and rotations of skin markers. J Biomech, 2008; 41(15): 3189-95.

Gao B, Conrad BP, Zheng N. Comparison of skin error reduction techniques for skeletal motion analysis. J Biomech. 2007; 40(Suppl. 2): pS551.

Gerhardt LC, Schmidt J, Sanz-Herrera JA, Baaijens FPT, Ansari T, Peters GWM, Oomens CWJ. A novel method for visualising and quantifying through-plane skin layer deformations. J Mech Behav Biomed Mater. 2012; 14: 199-207.

Gitajn IL, Rodriguez EK. Biomechanics of Musculoskeletal Injury. In: Klika V, editor. Biomechanics in Applications. Rijeka, Croatia: InTech; 2011. p. 3-36.

Gittoes MJ, Brewin MA, Kerwin DG. Soft tissue contributions to impact forces simulated using a four-segment wobbling mass model of forefoot–heel landings. Hum Mov Sci. 2006; 25(6): 775-87.

Greenwald RM, Janes PC, Swanson SC, McDonald. Dynamic impact response of human cadaveric forearms using a wrist brace. Am J Sports Med. 1998; 26(6): 825-30.

Guo W, Bradbury KE, Reeves GK, Key TJ. Physical activity in relation to body size and composition in women in UK Biobank. Ann Epidemiol. 2015; 25(6): 406-13.

Haddadi H, Belhabib S. Use of rigid-body motion for the investigation and estimation of the measurement errors related to digital image correlation technique. Opt Lasers Eng. 2008; 46(2): 185-96.

Holden JP, Orsini JA, Lohmann Siegel K, Kepple TM, Gerber LH, Stanhope SJ. Surface movement errors in shank kinematics and knee kinetics during gait. Gait Posture. 1997; 5(3): 217-27.

Horber FF, Gruber B, Thomi F, Jensen EX, Jaeger P. Effect of sex and age on bone mass, body composition and fuel metabolism in humans. Nutrition. 1997; 13(6): 524-34.

Houck J, Yack HJ, Cuddeford T. Validity and comparisons of tibiofemoral orientations and displacement using a femoral tracking device during early to mid stance of walking. Gait Posture 2004; 19(1): 76-84.

Hsiao ET, Robinovitch SN. Common protective movements govern unexpected falls from standing height. J Biomech. 1998; 31(1): 1-9.

Hua T, Xie H, Wang S, Hu Z, Chen P, Zhang Q. Evaluation of the quality of a speckle pattern in the digital image correlation method by mean subset fluctuation. Opt Lasers Eng. 2011; 43(1): 9-13.

Hwang IK, Kim KJ, Kaufman KR, Cooney WP, An KN. Biomechanical efficiency of wrist guards as a shock isolator. J Biomech Eng. 2006; 128(2): 229-34.

Idzikowski JR, Janes PC, Abbott PJ. Upper extremity snowboarding injuries. Ten-year results from the Colorado snowboard injury survey. Am J Sports Med. 2000; 28(6): 825-32.

Ito K, Fujiwara I, Hosoda K, Nagura T, Ogihara N. Measurement of 3D foot deformation during human walking by digital image correlation method. 25th Annual Conference of the International Society of Biomechanics; 2015 July 12–16; Glasgow, UK.

Jablonski NG, Chaplin G. The evolution of human skin coloration. J Hum Evol. 2000; 39(1): 57-106.

Khatyr F, Imberdis C, Vescovo P, Varchon D, Lagarde JM. Model of the viscoelastic behaviour of skin in vivo and study of anisotropy. Skin Res Technol. 2004; 10(2): 96-103.

Kilgore ML, Morrisey MA, Becker DJ, et al. Health care expenditures associated with skeletal fractures among Medicare beneficiaries, 1999–2005. J Bone Min Res. 2009; 24: 2050-5.

Kim KJ, Ashton-Miller JA. Biomechanics of fall arrest using the upper extremity: Age differences. Clin Biomech. 2003; 18(4): 311-8.

Krishnan J. Distal radius fractures in adults. Orthopedics. 2002; 25(2): 175-9.

Kuo, MY, Tsai TY, Lin CC, Lu TW, Hsu HC, Shen WC. Influence of soft tissue artifacts on the calculated kinematics and kinetics of total knee replacements during sit-to-stand. Gait Posture. 2011; 33: 379-84.

Laing AC, Robinovitch SN. Low stiffness floors can attenuate fall-related femoral impact forces by up to 50% without substantially impairing balance in older women. Accid Anal Prev. 2009; 41(3): 642-50.

Lan L, Wang CG, Tan HF. Experiment and evaluation of wrinkling strain in a corner tensioned square membrane. Acta Mechanica Sinica. 2014; 30(3): 430-6.

Leardini A, Chiari L, Croce U, Cappozzo A. Human movement analysis using stereophotogrammetry: part 3. Soft tissue artifact assessment and compensation. Gait Posture. 2005; 21(2): 212-25.

Lecompte D, Smits A, Bossuyt S, Sol H, Vantomme J, Van Hemelrijck D, et al. Quality assessment of speckle patterns for digital image correlation. Opt Lasers Eng. 2006; 44(11): 1132-45.

Li XY, Li J, Feng DF. Diffuse axonal injury induced by simultaneous moderate linear and angular head accelerations in rats. Neurosci. 2010; 169(1): 357-69.

Libertiaux V, Pascon F, Cescotto S. Experimental verification of brain tissue in compressibility using digital image correlation. J Mech Behav Biomed Mater. 2011: 4(7): 1177-85.

Luebberding S, Krueger N, Kerscher M. Mechanical properties of human skin in vivo: a comparative evaluation in 300 men and women. Skin Res Technol. 2014; 20(2): 127-35.

Manal KK, McClay Davis II, Galinat BB, Stanhope SS. The accuracy of estimating proximal tibial translation during natural cadence walking: bone vs. skin mounted targets. Clin Biomech. 2003; 18(2): 126-31.

Marcellier H, Vescovo P, Varchon D, Vacher P, Humbert P. Optical analysis of displacement and strain fields on human skin. Skin Res Technol. 2001; 7(4): 246-53.

Maughan RJ, Abel RW, Watson JS, Weir J. Forearm composition and muscle function in trained and untrained limbs. Clin Physiol. 1986; 6(4): 389-96.

Mates SP, Forster AM, Hunston D, Rhorer R, Everett RK, Simmonds KE, Bagchi A. Identifying the dynamic compressive stiffness of a prospective biomimetic elastomer by an inverse method. J Mech Behav Biomed Mater. 2012; 14: 89-100.

Maurel ML, Fitzgerald LG, Miles AW, Giddins GEB. Biomechanical study of the efficacy of a new design of wrist guard. Clin Biomech. 2013; 28(5): 509-13.

Mazess RB, Barden HS, Bisek, JP, Hanson J. Dual-energy x-ray absorptiometry for total-body and regional bone-mineral and soft-tissue composition. Am J Clin Nutr. 1990; 51(6): 1106-12.

Mercer JA, Bates BT, Dufek JS, Hreljac AA. Characteristics of shock attenuation during fatigued running. J Sports Sci. 2003; 21(11): 911-9.

Mercer JA, Dutek JS, Mangus BC, Rubley MD, Bhanot K, Aldridge JM. A description of shock attenuation for children running. J Athl Train. 2010; 45(3): 259-64.

Michel FI, Schmitt KU, Greenwald RM, Russell K, Simpson FI, Schulz D et al. White paper: functionality and efficacy of wrist protectors in snowboarding – towards a harmonized international standard. Sports Eng. 2013; 16(4): 197-210.

Mills C, Scurr J, Wood L. A protocol for monitoring soft tissue motion under compression garments during drop landings. J Biomech. 2011; 44(9): 1821-3.

Mirhadi S, Ashwood N, Karagkevrekis B. Review of rollerblading injuries. Trauma. 2015; 17(1): 29-32.

Moerman KM, Holt CA, Evans SL, Simms CK. Digital image correlation and finite element modelling as a method to determine mechanical properties of human soft tissue in vivo. J Biomech. 2009; 42(8): 1150-3.

Muller ME, Webber CE, Bouxsein ML. Predicting the failure load of the distal radius. Osteoporos Int. 2003; 14(4): 345-52.

Myers E, Sebeny E, Hecker A, Corcoran T, Hipp J, Greenspan S, Hayes W. Correlations between photon absorption properties and failure load of the distal radius in vitro. Calcif Tissue Int. 1991; 49(4): 292-7.

Nellans KW, Kowalski E, Chung KC. The epidemiology of distal radius fractures. Hand Clin. 2012; 28(2): 113-25.

Neto OP, Magini M. Electromiographic and kinematic characteristics of Kung Fu Yau-Man palm strike. J Electromyo and Kinesio. 2008; 18(6): 1047-52.

Nevitt MC, Cummings SR. Type of fall and risk of hip and wrist fractures: The study of osteoporotic fractures. The Study of Osteoporotic Fractures Research Group. J Am Geriatr Soc. 1993; 41(11): 1226-34.

Ní Annaidh A, Bruyère K, Destrade M, Gilchrist MD, Otténio M. Characterization of the anisotropic mechanical properties of excised human skin. J Mech Behav Biomed Mater. 2012; 5(1): 139-48.

Nigg BM, Cole GK, Bruggemann GP. Impact forces during heel-toe running. J Appl Biomech. 1995; 11(4): 407-32.

Northern Digital Inc. [Internet]. [Place unknown]: Northern Digital Inc; c2016. Optotrak Certus technical specifications; c2016 [cited 2016 May 11]. Available from: http://www.ndigital.com/msci/products/optotrak-certus/optotrak-certus-technical-specifications/

Omkar SN, Praveen GB, Singh A. Analysis of wrist extension using 3D digital image correlation. J Biomed Biotechnol. 2013; 1(1): 1-7.

O'Neill MC, Lee L-F, Demes B, Thompson NE, Larson SG, Stern JT, et al. Three-dimensional kinematics of the pelvis and hind limbs in chimpanzee (Pan troglodytes) and human bipedal walking. J Hum Evol. 2015; 86: 32-42.

O'Neill TW, Varlow J, Silman AJ, Reeve J, Reid DM, Todd C, Woolf AD. Age and sex influences on fall characteristics. Ann Rheum Dis. 1994; 53(11): 773-5.

Oskam J, Kingma J, Klasen HJ. Fracture of the distal forearm: Epidemiological developments in the period 1971-1995. Injury. 1998; 29(5): 353-5.

Özgüven HN, Berme N. An experimental and analytical study of impact forces during human jumping. J Biomech. 1988; 21: 1061-66.

Pailler-Mattei C, Bec S, Zahouani H. In vivo measurements of the elastic mechanical properties of human skin by indentation tests. Med Eng Phys. 2008; 30(5): 599-606.

Pain MT, Challis JH. Soft tissue motion during impacts: Their potential contributions to energy dissipation. J Appl Biomech. 2002; 18: 231-42.

Pain MT, Challis JH. The influence of soft tissue movement on ground reaction forces, joint torques and joint reaction forces in drop landings. J Biomech. 2006; 39(1): 119-24.

Pain MT, Challis JH. The role of the heel pad and shank soft tissue during impacts: A further response to dynamic impact loading. J Biomech. 2001; 34(3): 327-33.

Palvanen M, Kannus P, Parkkari J, Pitkäjärvi T, Pasanen M, Vuori I, Järvinen M. The injury mechanisms of osteoporotic upper extremity fractures among older adults: a controlled study of 287 consecutive patients and their 108 controls. Osteoporos Int. 2000; 11(10): 822-31.

Pan B, Lu Z, Xie H. Mean intensity gradient: An effective global parameter for quality assessment of the speckle patterns used in digital image correlation. Opt Lasers Eng. 2010; 48(4): 469-77.

Parachute. The Cost of Injury in Canada [Internet]. Toronto, ON: Parachute; 2015 [cited 2017 Apr 14]. Version No.: 2.2. Available from: http://www.parachutecanada.org/downloads/research/Cost_of_Injury-2015.pdf

Peters A, Galna B, Sangeux M, Morris M, Baker R. Quantification of soft tissue artifact in lower limb human motion analysis: a systematic review. Gait Posture. 2010; 31(1): 1-8.

Portney, LG, Watkins MP. Foundation of clinical research applications to practice. 2nd ed. New Jersey: Prentice-Hall Inc; 2000.

Prichasuk S. The heel pad in plantar heel pain. J Bone Joint Surg Br. 1994; 76(1): 140-2.

Qualisys. Super-spherical markers [Image on the Internet]. 2016a [cited 2016 Apr 15]. Available from: http://www.qualisys.com/accessories/passive-markers/super-spherical-markers/

Qualisys. Long range active marker [Image on the Internet]. 2016b [cited 2016 Apr 15]. Available from: http://www.qualisys.com/accessories/active-markers/long-range-active-marker/

Qualisys. Short range active markers [Image on the Internet]. 2016c [cited 2016 Apr 15]. Available from: http://www.qualisys.com/accessories/active-markers/short-range-active-marker/

Reu P. Hidden components of 3D-DIC: triangulation and post-processing – Part 3. Exp Tech. 2012a; 36(4): 3-5.

Reu P. Hidden Components of 3D-DIC: Interpolation and matching – Part 2. Exp Tech. 2012b; 36(3): 3-4.

Robinovitch SN, Chiu J. Surface stiffness affects impact force during a fall on the outstretched hand. J Orthop Res. 1998; 16(3): 309-13.

Ryu T, Choi HS, Chung MK. 2009. Soft tissue artifact compensation using displacement dependency between anatomical landmarks and skin markers: a preliminary study. Int J Ind Ergon. 2009; 39(1): 152-58.

Samarasinghe S, Kulasiri D. Stress intensity factor of wood from crack-tip displacement fields obtained from digital image processing. Silva Fenn. 2004; 38(3): 267-78.

Sangeux MM, Marin FF, Charleux FF, Dürselen LL, Ho Ba Tho MC. Quantification of the 3D relative movement of external marker sets vs. bones based on magnetic resonance imaging. Clin Biomech. 2006; 21(9): 984-91.

Sasaki K, Takagi M, Ida H, Yamakawa M, Ogino T. Severity of upper limb injuries in snowboarding. Arch Orthop Trauma Surg. 1999; 119(5): 292-5.

Sati M, de Guise JA, Larouche S, Drouin G. Quantitative assessment of skin-bone movement at the knee. Knee. 1996; 3(3): 121-38.

Schinkel-Ivy A, Burkhart TA, Andrews DM. Leg tissue mass composition affects tibial acceleration response following impact. J Appl Biomech. 2012; 28(1): 29-40.

Scholz, JP. Reliability and validity of the WATSMART three-dimensional optoelectronic motion analysis system. Phys Ther. 1989; 69(8): 679-89.

Schwartz M, Trost JP, Wervey R. Measurement and management of errors in quantitative gait data. Gait Posture. 2004; 20: 196-203.

Scurr JC, White JL, Hedger W. The effect of breast support on the kinematics of the breast during the running gait cycle. J Sport Sci. 2010; 28(10): 1103-9.

Shih MH, Sung WP. Application of digital image correlation method for analysing crack variation of reinforced concrete beams. Sadhana-Acad P Eng Sci. 2013; 38(4): 723-41.

Shorten MR, Winslow DS. Spectral analysis of impact shock during running. Int J Sport Biomech. 1992; 8(4): 288-304.

Silver FH, Freeman JW, DeVore D. Viscoelastic properties of human skin and processed dermis. Skin Res Technol. 2001; 7(1): 18-23.

Soderkvist I, Wedin PA. Determining the movements of the skeleton using well-configured markers. J Biomech. 1993; 26(12): 1473-77.

Stagni R, Fantozzi S, Cappello A, Leardini A. Quantification of soft tissue artefact in motion analysis by combining 3D fluoroscopy and stereophotogrammetry: a study on two subjects. Clin Biomech. 2005; 20(3): 320-9.

Staloff IA, Rafailovitch M. Measurement of skin stretch using digital image speckle correlation. Skin Res Technol. 2008a; 14(3): 298-303.

Staloff IA, Guan E, Katz S, Rafailovitch M, Sokolov A, Sokolov S. An in vivo study of the mechanical properties of facial skin and influence of aging using digital image speckle correlation. Skin Res Technol. 2008b; 14(2): 127-34.

Stefanczyk JM, Brydges EA, Burkhart TA, Altenhof WJ, Andrews DM. Surface accelerometer fixation method affects leg soft tissue motion following heel impacts. Int J Kinesiol Sports Sci. 2013; 1(3): 1-8.

Stevens JA, Corso PS, Finkelstein EA, Miller TR. The costs of fatal and non-fatal falls among older adults. Inj Prev. 2006; 12(5): 290-5.

Sturm RA, Box NF, Ramsay M. Human pigmentation genetics: the difference is only skin deep. BioEssays. 1998; 20(9): 712-21.

Südhoff I, Van Driessche S, Laporte S, de Guise JA, Skall W. Comparing three attachment systems used to determine knee kinematics during gait. Gait Posture. 2007; 25(4): 533-43.

Sumino H, Ichikawa S, Abe M, Endo Y, Ishikawa O, Kurabayashi M. Effects of aging, menopause, and hormone replacement therapy on forearm skin elasticity in women. J Am Geriatr Soc. 2004; 52(6): 945-9.

Sutton MA, Orteu J-J, Schreier HW. Image correlation for shape, motion and deformation measurements: basic concepts. Boston, MA, USA: Springer Science & Business Media; 2009.

Tadokoro T, Yamaguchi Y, Batzer J, Coelho SG, Zmudzka BZ, Miller SA, et al. Mechanisms of skin tanning in different racial/ethnic groups in response to ultraviolet radiation. J Invest Dermatol. 2005; 124(6): 1326-32.

Telfer SS, Morlan GG, Hyslop EE, Semple RR, Rafferty DD, Woodburn JJ. A novel device for improving marker placement accuracy. Gait Posture. 2010; 32(4): 536-9.

Thong HY, Jee SH, Sun CC, Boissy RE. The patterns of melanosome distribution in keratinocytes of human skin as one determining factor of skin colour. Br J Dermatol. 2003; 149(3): 498-505.

Tonkovich A, Li Z, DiCecco S, Altenhof W, Banting R, Hu H. Experimental observations of tyre deformation characteristics on heavy mining vehicles under static and quasi-static loading. J Terramech. 2012; 49(3-4): 215-31.

Tortora GJ, Nielsen MT. (2014). Principles of human anatomy (13th ed.). Hoboken, NJ: John Wiley & Sons, Inc.

Troy KL, Gavin CG, Grabiner MD. Wrist kinematics and kinetics during ground impact following a fall. 51st Annual Meeting of the Orthopaedic Research Society, 2005 Feb 20–23; Washington, DC.

Troy KL, Grabiner MD. Asymmetrical ground impact of the hands after a trip-induced fall: experimental kinematics and kinetics. Clin Biomech. 2007a; 22(10): 1088-95.

Troy KL, Grabiner MD. Off-axis loads cause failure of the distal radius at lower magnitudes than axial loads: a finite element analysis. J Biomech. 2007b; 40(8): 1670-5.

Uyen LDP, Nguyen DH, Kim EK. Mechanism of skin pigmentation. Biotechnol Bioprocess Eng. 2008; 13(4): 383-95.

Vellas BJ, Wayne SJ, Garry PJ, Baumgartner RN. A two-year longitudinal study of falls in 482 community-dwelling elderly adults. J Gerontol A Biol Sci Med Sci. 1998; 53(4): M264-74.

Voloshin A, Wosk J, Brull M. Force wave transmission through the human locomotor system. J Biomech Eng. 1981; 103(1): 48-50.

Voloshin AS. The influence of walking speed on dynamic loading of the human musculoskeletal system. Med Sci Sport Exerc. 2000; 32(6): 1156-9.

Whiting W & Zernicke R. Biomechanics of musculoskeletal injury. 2nd ed. Champaign, IL, USA: Human Kinetics; 2008.

Winter DA. Biomechanics and motor control of human movement. 2nd ed. Hoboken, NJ, USA: John Wiley and Sons Inc.; 2005.

Wolf A, Senech M. Estimating joint kinematics from skin motion observation: modelling and validation. CMBBE. 2011; 14(11): 939-46.

Wrbaškić NN, Dowling JJ. An investigation into the deformable characteristics of the human foot using fluoroscopic imaging. Clin Biomech. 2007; 22(2): 230-38.

Xcitex Inc. [Internet]. [Place unknown]: Xcitex Inc. Tutorial 113 - Quantifying motion in three dimensions with ProAnalyst®; c2007 [revised 2011; cited 2016 Apr 14]. Available from: http://www.xcitex.com/proanalyst-example-files-motion-analysis-software-applications.php

Yavari SA, vander Stok J, Weinans H, Zadpoor AA. Full-field strain measurement and fracture analysis of rat femora in compression test. J Biomech. 2013; 46(7): 1282-92.

Zhang D, Eggleton CD, Arola DD. Evaluating the mechanical behavior of arterial tissue using digital image correlation. Exp Mech. 2002; 42(4): 409-16.

Zhang D, Arola D. Applications of digital image correlation to biological tissues. J Biomed Opt. 2004; 9(4): 691-9.

Zhang S, Clowers K, Kohstall C, Yu YJ. Effects of various midsole densities of basketball shoes on impact attenuation during landing activities. J Appl Biomech. 2005; 21(1): 3-17.

APPENDICES

<u>Appendix A</u>

FITZPATRICK SKIN TYPE QUESTIONNAIRE

PART 1: Genetic Disposition

<u>Your eye color is:</u>

Light blue, light gray or light green = 0
Blue, gray or green = 1
Hazel or light brown = 2
Dark brown = 3
Brownish black = 4

<u>Your natural hair color is:</u>

Red or light blonde = 0
Blonde = 1
Dark blonde or light brown = 2
Dark brown = 3
Black = 4

<u>Your natural skin color (before sun exposure) is:</u>

Ivory white = 0
Fair or pale = 1
Fair to beige, with golden undertone = 2
Olive or light brown = 3
Dark brown or black = 4

<u>How many freckles do you have on unexposed areas of your skin?</u>

Many = 0
Several = 1
A few = 2
Very few = 3
None = 4

Total score for genetic disposition: _____

PART 2: Reaction to Extended Sun Exposure

How does your skin respond to the sun?

Always burns, blisters and peels = 0
Often burns, blisters and peels = 1
Burns moderately = 2
Burns rarely, if at all = 3
Never burns = 4

Does your skin tan?

Never – I always burn = 0
Seldom = 1
Sometimes = 2
Often = 3
Always = 4

How deeply do you tan?

Not at all or very little = 0
Lightly = 1
Moderately = 2
Deeply = 3
My skin is naturally dark = 4

How sensitive is your face to the sun?

Very sensitive = 0
Sensitive = 1
Normal = 2
Resistant = 3
Very resistant/Never had a problem = 4

Total score for reaction to sun exposure: _____

Add up your genetic disposition and sun exposure totals to find your Fitzpatrick

Skin Type: _____

Type I (scores 0 – 6)
Pale white; blonde or red hair; blue eyes; freckles — Always burns, never tans.

Type II (scores 7 – 12)
White; fair; blonde or red hair; blue, green, or hazel eyes — Usually burns, tans minimally.

Type III (scores 13 – 18)
Cream white; fair with any hair or eye color; quite common — Sometimes mild burn, tans uniformly.

Type IV (scores 19 – 24)
Moderate brown; typical Mediterranean skin tone — Rarely burns, always tans well.

Type V (scores 25 – 30)
Dark brown — Very rarely burns, tans very easily.

Type VI (scores ≥ 31)
Deeply pigmented dark brown to black — Never burns, tans very easily.

GENERAL HEALTH QUESTIONNAIRE (GHQ)

Please answer the following questions:

1. Have you had any recent trauma (e.g., sprain, strain, fracture, major bruising, stitches, etc.) to your hands, wrists, forearms, elbows, or shoulders in the past year?

    [ ] YES   [ ] NO

2. Have you had any prior surgeries to your hands, wrists, forearms, elbows, or shoulders?

    [ ] YES   [ ] NO

3. Do you suffer from arthritis, carpal tunnel syndrome, or any congenital abnormalities concerning your hands, wrists, forearms, elbows, or shoulders?

    [ ] YES   [ ] NO

4. Do you have any current health conditions that may exclude you from experiencing submaximal impacts to the palms of your hands (e.g., osteoporosis)?

    [ ] YES   [ ] NO

5. Do you have sensitive skin or any skin condition that may cause you to have an allergic reaction to the water-based body paint being applied to your forearm?

    [ ] YES   [ ] NO

6. Do you have any major scarring from a previous injury of surgery or tattoos on your dominant hand and forearm?

    [ ] YES   [ ] NO

Please note that this questionnaire will be kept confidential. If you answered 'YES' to any of these questions, or if you do not wish to disclose this information, it is your right to not answer or withdraw from the study.

DESCRIPTION OF FOREARM ANTHROPOMETRIC MEASUREMENTS

(Modified from Burkhart et al., 2008)

Measurements	Segment	Description and landmarks
Lengths (cm)	Forearm (L)	Distance between the lateral aspect of the articular capsule of the elbow joint and the lateral (radial) styloid process
Circumferences (cm)	Elbow	Distance around the epicondyles of the humerus
	Forearm (mid)	Maximal distance around the forearm midway between the articular capsule of the elbow joint and the styloids
	Styloid	Distance around the radial and ulnar styloids and overlying tissues
Breadths (cm)	Forearm (mid, M/L)	Distance across the ulna and radius and overlying tissues at the level of maximum forearm circumference
Skinfolds (mm)	Forearm (mid, M)	Vertical fold on the medial aspect of the forearm at the level of maximum circumference
	Forearm (mid, P)	Vertical fold on the posterior aspect of the forearm at the level of maximum circumference

A = anterior; P = posterior; M = medial; L = lateral; mid = between the anterior and posterior or medial and lateral aspects of a segment.

VITA AUCTORIS

NAME:	Danielle Gyemi
PLACE OF BIRTH:	Windsor, ON
YEAR OF BIRTH:	1991
EDUCATION:	Walkerville Collegiate Institute, Windsor, ON, 2009
	University of Windsor, BHK, Windsor, ON, 2014
	University of Windsor, MHK, Windsor, ON, 2017